Synthesis and Application of Nano-Sized Metal-Organic Frameworks for Nanofiltration Membranes

SHANGKUM YILDUN GOJI

Japan Advanced Institute of Science and Technology

Synthesis and Application of Nano-Sized Metal-Organic Frameworks for Nanofiltration Membranes

SHANGKUM YILDUN GOJI

Japan Advanced Institute of Science and Technology

September 2019

DOCTORAL DISSERTATION

Synthesis and Application of Nano-Sized Metal-Organic Frameworks for Nanofiltration Membranes

SHANGKUM YILDUN GOJI

Supervisor: Associate Professor (Dr.) Toshiaki Taniike

Graduate School of Advanced Science and Technology,

Japan Advanced Institute of Science and Technology

September 2019

Abstract

Metal-Organic Frameworks (MOFs) nanoparticles have emerged as a new class of hybrid materials with potential for broad range of applications. When this materials is scaled down to the nanoscale, design of the nanosized MOFs composite membranes from it show remarkable permeability and selectivity because of the presence of nanochannels in the MOFs structure. Therefore, it is possible to use MOFs nanoparticle to tackle the problems of permeability and selectivity tradeoff and fouling through hybridization of polymeric membranes with MOFs as an approaches to address these problems. Several methods have been employed to integrate MOFs into flexible polymeric membranes for nanofiltration; however, the major challenge is how to form a MOF-based selective layer on a heterogeneous support without defects. Because the nucleation and growth of these MOFs usually requires harsh thermal treatment, the combination between a MOFs and a polymeric support to form a uniform selective layer before damaging the support is severely limited. Therefore, the deposition of nanoparticles via suction filtration, where nanoparticles could fill in the pore network or be loaded on the external surface of the support membrane to form a selective layer is a novel technique.

Chapter 2 describes the strategy of depositing preformed nanoparticles onto a porous polymer support as a facile strategy to access a performant and flexible composite membrane with a semi-continuous selective layer of a metal-organic framework. This new type of composite membrane exhibit excellent permeability as well as selectivity, which successfully address problem of tradeoff between the permeability and selectivity during nanofiltrtaion. It thus demonstrates promise for nanofiltration based on its facile production

and easy optimization through the size distribution of MOF nanoparticles, which can be ex-situ prepared.

Chapter 3 presents an investigation of pore engineering of UiO-66 nanoparticles and applications for nanofiltration with the purpose of exploring the importance of nanoparticles' chemical environment. This was strategically achieved using engineered UiO-66 nanoparticle obtained from 2-amino/methyl-terephthalic acids linkers for the synthesis of modified UiO-66 nanoparticles, (UiO-66-CH_3 and UiO-66-NH_2).The composite membranes obtained from the engineered nanoparticles shows superiority of the membranes in terms of their permeability and selectivity, which was attributed to the chemical environment around the nanopores.

Chapter 4 highlights the remarkable performances of these membranes designed by deposition method. The filtration results obtained from experiments using these composite membranes demonstrated that deposition is a novel technique for preparation of membranes, which has potential for large-scale nanofiltration.

Keywords: Metal–Organic Framework; UiO-66; pore engineering, composite membrane; chemical environment.

Preface

This dissertation is the result of studies under the supervision of Associate Professor (Dr.) Toshiaki Taniike during 2016-2019 sessions. The purpose of this dissertation is to synthesize nano-sized Metal-Organic Frameworks and apply for nanofiltration membranes. Chapter 1 describes general introduction in accordance with the objective of the research work. Chapter 2 describes the design of semi-continuous selective layer based on deposition of UiO-66 nanoparticles for nanofiltration. Chapter 3 presents strategies in engineering pore of UiO-66 nanoparticles and its applications for design of nanofiltration composite membranes. Chapter 4 highlights the remarkable performances of the membranes designed by deposition method.

SHANGKUM, Yildun Goji

Taniike Laboratory

Graduate School of Advanced Science and Technology, Japan Advanced Institute of Science and Technology.

Referee

Referee-in Chief: Associate Professor (Dr.) Toshiaki Taniike

Japan Advanced Institute of Science and Technology

Referees: **Professor (Dr.) Masayuki Yamaguchi**

Japan Advanced Institute of Science and Technology

Associate Professor (Dr.) Yuki Nagao

Japan Advanced Institute of Science and Technology

Associate Professor (Dr.) Shun Nishimura

Japan Advanced Institute of Science and Technology

Associate Professor (Dr.) Kenji Hirai

Research Institute for Electronic Science Hokkaido

University, Japan

Acknowledgement

I wish to express my sincere appreciation to God Almighty for protection, provision of good health and resources before and during this research program leading to successful completion.

I am deeply grateful to my Supervisor-Associate Professor (Dr) Toshiaki Taniike for his supervision, support, advice, guide and help rendered to me during my studies as well as immense financial support throughout the period of this research, else the dream would been a mere mirage. To my Referees from JAIST: Professor (Dr.) Masayuki Yamaguchi, Associate Professor (Dr.) Yuki Nagao, Associate Professor (Dr.) Shun Nishimura and Associate Professor (Dr.) Kenji Hirai from Research Institute for Electronic Science Hokkaido University, Japan, efforts and time taken to review my dissertation is gratefully appreciated.

To D. Eng. (Mrs.) Patchanee Chammingkwan, I am sincerely grateful for diligent guide as well as useful suggestions during experimentation and discussion of the results. Professor Holden William's kind assistance and efforts in teaching and revising my manuscript is wholeheartedly appreciated. In addition, immense contributions of the following personalities: Dr. Toru Wada, Dr. Priyank Mohan and Dr. Ashutosh Thakur in the course of writing this dissertation are sincerely appreciated.

In addition, my deep appreciation goes to Professor Tatsuo Kaneko (Second Supervisor) and his wife Dr. (Mrs) Okajima Kaneko for kind financial/material support to me at Japan as well as family members at Nigeria during hard times along this study. To my Minor Research Supervisors: Professor Kazuaki Matsumura, Professor Takashi Morinaga, I am very grateful

for their support through provision of experimental facilities for the Minor Research work. Similarly, I am sincerely grateful to Pastor and Mrs. Makio Katoh and all members of Tatsunokuchi Church for prayers and financial assistance.

Financial support provided to me through TETfund scholarship as well as study leave by University of Jos, Plateau State, Nigeria, is sincerely appreciated. In addition, I am very grateful to these personalities: Professor D. A Dakul, Professor D. A Dashak, Late Professor J. N Egila, Dr. J. Gushit, Dr. J. J Gongden, Dr. Adeyanju Olusola, Elder (Dr) William Mangset and Elder Yohanna Duwerra for constantly supporting me through prayers during the process of TETfund application.

My sincere appreciation goes to Mr. A.T.G. Guse and Late sister- Mrs. Patricia James Edward for their endless love, encouragement and financial support that enable me to continue my academic pursuits to this level.

In addition, I am grateful to my dearest wife Mrs. Dogak Shangkum Yildun Goji and daughter Muyenen Yildun Goji for supporting me through prayers as well as exercising patience while I was away from home for the period of this research program at Japan. I am grateful to my parents-in-law for their kind support through prayers in tough times.

Finally, I sincerely appreciate members of Taniike, Kaneko and Terano Laboratories for the good times we shared together as well as assistance in different ways in the course of this research program.

SHANGKUM, Yildun Goji

Contents

List of Figures

List of Tables

List of Abbreviations

Abbreviation	Definition
DMF	Dimethylformamide
FT-IR	Fourier transform infrared spectroscopy
MOFs	Metal-organic frameworks
MB	Methyl Blue
NF	Nanofiltration
MF	Microfiltration
RO	Reverse osmosis
SEM	Scanning Electron microscopy
TEM	Transmission Electron microscopy
XRD	X-Ray Diffraction
HKUST	Hong Kong University of Science and Technology
LAG	Liquid-assisted grinding
SFG	Solvent-free grinding
MIL	Materials Institute Lavoisier
ILAG	Liquid assisted grinding
SD	Spray drying
UF	Ultrafiltration
UiO	University of Oslo
ZIF	Zeolite Imidazolate
PES	Polyethersulfone
PAN	Polyacrylonitrile
RC	Regenerated cellulose
$ZrCl_4$	Zirconium tetrachloride
MeOH	Methanol
DI	Deionize $_{water}$
UV/vis	Ultraviolet-visible spectroscopy
PVDF	Polyvinylidene difluoride
MWCNT	Multi-walled carbon nanotube

TGA	Thermogravimetric analysis
BET	Brunauer Emmett Teller
GCMC	Grand Canonical Monte Carlo
BDC	1,4-benzenedicarboxylate
MW	Molecular weight
CN	Coordination number

Chapter 1
General Introduction

1.1 Metal-Organic Frameworks

Metal Organic Frameworks (MOFs) are crystalline network of single metal ion or a metal cluster connected to multidentate organic linkers, linked by strong covalent bonds. Framework of MOFs can be produced by combination of metal nodes and organic ligands due to fixed coordination geometries and structures (Figure 1-1). They possess intrinsically tunable structures with high degree of designability, adjustability and structural flexibility with multifunctional groups, which can be extended to several analogous (isostructural) frameworks that are synthesized from different metallic components and identical linkers [1,2]. They constitute a new class of porous materials that have emerged as focus of fascination for both academy and industry due to their unprecedented properties, which imply a plethora of potential applications [3-5]. Owing to their properties such as crystalline structure with extremely high porosity [6], high surface area (> 1000 m^2/g) [7], diversity of building units for reticular synthesis [8], tunable chemical nature [9], pore size, shape, structure, robust and flexible structures [10], MOFs became popular materials in which many research studies have been done.

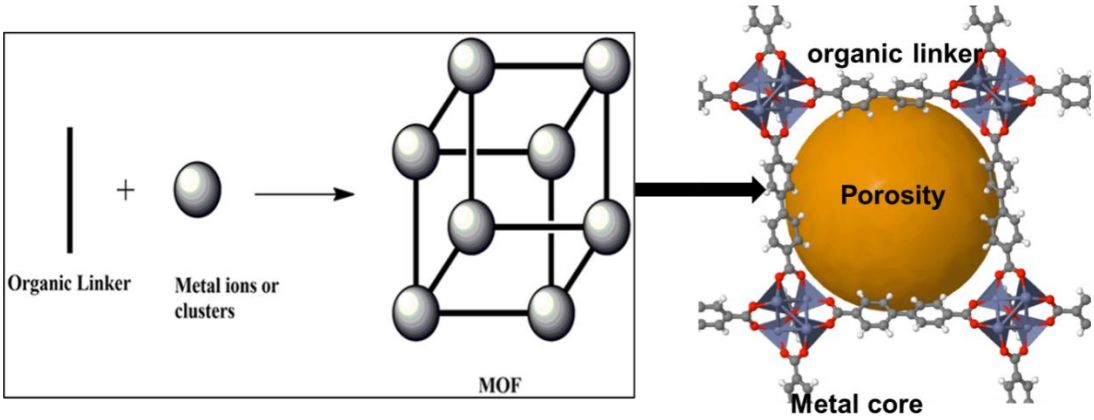

Figure1-1. Illustration of building blocks and structure of metal organic frameworks [3].

In an effort to fully understand chemistry and tailor structural features, large number of synthetic approaches have been pursued to achieve functional, surface-modified, and morphology-engineered crystals [11].

1.2 Synthesis Methods

Selection of methods and solvent is crucial for synthesis of MOFs with desired characteristics [12]. The most widely used method for MOFs synthesis is solvothermal method. This is due to process being simple and easily controlled. However, there are drawbacks such as time consuming and usually producing large particles size [12,13]. Other alternative synthesis routes used are discussed in detail as below. These include electrochemical synthesis, mechanochemical synthesis, microwave-assisted synthesis, spray-drying synthesis, and sonochemical synthesis. Therein, common parameters are temperature, concentration of metal, solubility of metal salts, ligands in solvents and pH of solution [12].

1.2.1 Electrochemical Synthesis

This technique involves continuous supply of metal ions through anodic dissolution in reaction containing reaction mixtures: organic linker and electrolyte. Advantages of electrochemical route for industrial process are possibility to run continuous process and to obtain solids at a high yield with respect to short reaction time and milder conditions. However, its potential disadvantages involve deposition of metal cations on cathode, resulting into the hydrogen formation in the process [14-16]. Several kinds of MOFs including HKUST, MIL-100 (Al), MIL-53 (Al) and NH_2-MIL-53 (Al) have been synthesized by anodic dissolution in an electrochemical cell where effects of solvents, electrolyte, temperature and voltage-current density on product yields were studied [17,18].

1.2.2 Mechanochemical Synthesis

Mechanochemical synthesis involves mechanical breakage of intramolecular bonds followed by chemical transformation. Key concept behind this synthesis method is to promote chemical reactions by milling or grinding solids without any or with minimal amount of solvents [19, 20]. Variations relevant to mechanochemical synthesis include: (i) solvent-free grinding (SFG), which is the simplest method by avoiding usage of solvent; (ii) liquid-assisted grinding (LAG), which is versatile and quick; and (iii) ion-and-liquid assisted grinding (ILAG), which employs catalytic liquid with trace amounts of salt additives to accelerate the MOF formation [11]. For instance, Friscic and co-worker reported synthesis of UiO-66 and UiO-66-NH_2 at gram scale by grinding solid reactants in presence of methanol and N,N-dimethylformamide (DMF) for 90 minutes [21]. Klimakow *et al.* synthesized HKUST-1 and its benzenetribenzoate-based analogue (MOF-14) via a LAG approach [22].

1.2.3 Microwave-Assisted Synthesis

Microwave-assisted synthesis is based on interaction of electromagnetic waves with a material containing mobile electric charges like polar molecules in a solvent or conducting ions in a solid. The irradiation interacts directly with reactants, resulting in more efficient and faster heating compared to classical conduction-based heating. The merits of this method are at high efficiency, shorter reaction time, phase selectivity, morphology control and particle size reduction [23,24]. McKinstry *et al.* synthesized HKUST-1 using ethanol as a solvent by microwave irradiation [25]. Schlesinger and his co-workers compared different synthetic methods such as solvothermal, microwave-assisted, mechanochemical and ultrasonic method for preparation of $[Cu_3 (btc)_2(H_2O)_3]$ [26].

1.2.4 Spray-Drying Synthesis

Spray drying (SD) is a well-established process in industry for decades. The SD strategy enables construction of multicomponent MOF superstructure and encapsulation of guest species with the superstructure. Basic principle behind this synthetic method is the production of dispersed powder from a liquid or slurry that is rapidly evaporated with a hot gas. Generally, this method is very useful to synthesize MOFs that are built up from mononuclear metal ions, smaller metal clusters or SBUs [3,27,28]. Camur*et al.* simultaneously synthesized and shaped Zr-MOFs and Zr-fumarate into spherical MOF microbeads in a mixture of water and acetic acid by continuous-flow spray-drying method [29].

1.2.5 Sonochemical Synthesis

Sonochemical synthesis involves and exposure of a reaction mixture to ultrasound energy, which causes molecules to undergo chemical changes into compounds with novel morphologies and unique properties. These ultrasonic radiations are produced at high temperatures and pressures in reaction medium [30]. Advantages of this method include rapid synthesis, economical, reproducible, and environment friendly. MOFs with small crystal size can be obtained via this method within short reaction time. Armstrong *et al.* synthesized HKUST-1 sonochemically and studied parameters such as reactor volume, reaction time, sonication tip size, sonication amplitude, and solvent and reactant concentrations [31]. Morsali *et al.* developed a three dimensional cadmium metal–organic framework by ultrasound irradiation, in which effects of irradiation time and concentrations of reagents were studied on formation of uniform nanoplates [32]. This synthesis method and conditions for synthesis are essential requirements and crystalline phases of MOFs, desired yields, morphology and possibilities of optimization to large-scale processes at nanosized level.

1.3 Synthesis of Nano-Sized MOFs

Synthesis of well-defined nanoparticles of MOFs with precision in size and morphology has been drawing attention. The challenge exists at the fact that a small variation in the reaction conditions could significantly affect the quality of the product and also the structure of MOFs [33,34]. Therefore, factors such as the coordination environment, coordination connection, central metal ions, organic ligand, molar ratio of metal to organic ligand, reagent concentrations, co-solvents, pH, temperature and time must be carefully selected for the precision synthesis [34,35]. The size and morphology of MOFs are more easily controlled in the presence of a modulator, a molecular additive that regulates the crystallization process to generate uniform crystals usually with reduced sizes. Effective control over these parameters as well as fundamental understanding of the crystallization process facilitates tuning of morphology, structure, and properties of MOFs, which contributes to the enhancement of performances for the desire applications [36].

1.3.1 Modulators

Purpose of using modulators in synthesis of MOFs is to control size, shapes of nanoparticles as well as to aid in crystallization process. Therefore, modulation synthesis refers to regulation of coordination equilibrium by a modulator, which either competitively coordinates with metals or suppresses deprotonation of linkers for crystallization to occur. In general, crystallization process is divided into (i) an induction period, where primary particles are formed, (ii) nucleation period where particles form crystal nuclei (primary nucleation), and (iii) a growth period, where molecules are arranged on surface of existing nuclei followed by subsequent growth into larger crystals [37-39]. These stages for crystallization of MOFs are illustrated in Figures 1-2.

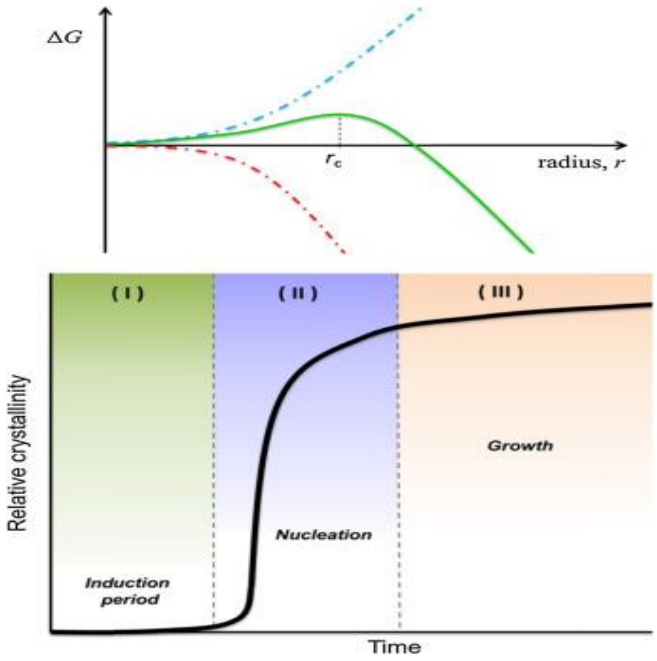

Figure 1-2. Crystallization process of MOFs [38].

This nucleation processes can be described as change in free energy (ΔG) of system and is governed by equation (1) given below

$$\Delta G_V = \Delta G_v \ {}_{+}\Delta G_S \qquad (1),$$

where ΔG_V accounts for free energy of coagulation into solid bulk whilst ΔG_s accounts for free energy gained by creating solid particles on the surface. For a given particle with radius r, ΔG_v is proportional to r^3, whereas ΔG_S is proportional to particle surface r^2. Once the critical radius of r_c is reached, the growth of the particle is highly favoured and eventually leads to bulk solid phase [40,41]. The internal structure, crystal size, morphology, and outer surface functionalities of some MOFs have been controlled with different kinds of modulators [42]. Modulators act as a regulator of crystallization kinetics and crystal morphology during the synthesis process and tune surface of particles for desired applications. As shown in Figure 1-

3, the synthesis in presence of a modulator gives MOF particles those are isolated and uniform in size as compared synthesis without a modulator.

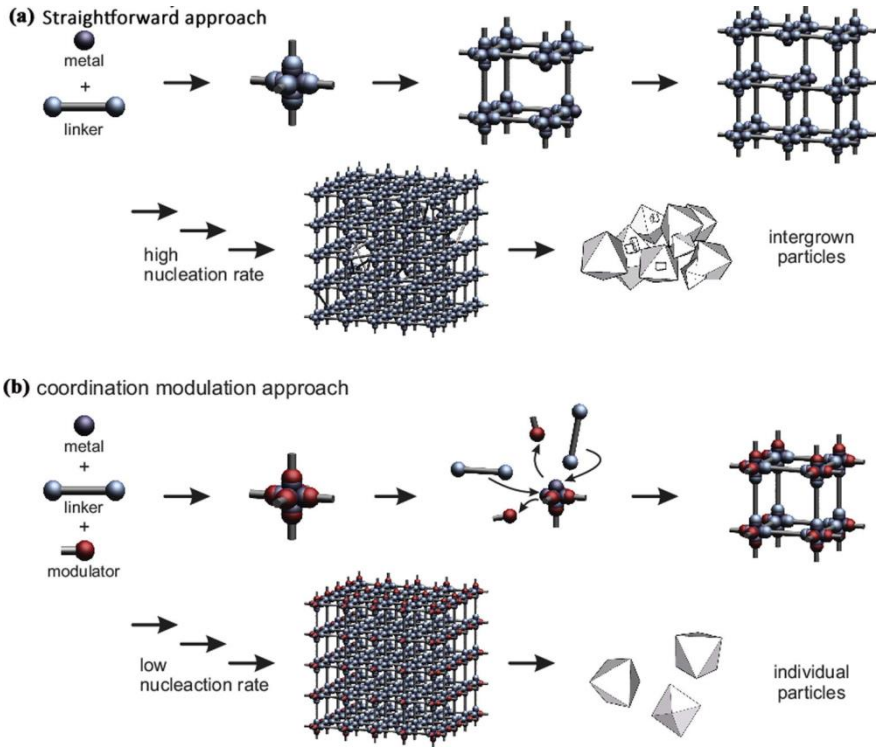

Figure1-3. Illustration of the mechanism for MOF formation in the absence or presence of a modulator [37].

1.3.2 Mechanistic Aspect of Modulated Synthesis

Modulated synthesis of MOFs is as an excellent mean for controlling the size and morphology of MOFs crystals [43]. Recently, the modulated synthesis has been widely used (i) for simply synthetic reproducibility, (ii) for facilitating the control of the material properties, and (iii) for improving the yield [44]. The mechanisms of the modulated synthesis are roughly classified into coordination and non-coordination modulation mechanisms [45]. Modulators are further categorized into the following types: (a) As a capping agent to slow down intergrowth of the nuclei, which is helpful to control shape and size of MOFs nanocrystals as well as to enable

the reproducible synthesis; (b) As a deprotonating agent to facilitate the deprotonation of targeting linking molecules; (c) As a reacting agent, which is common for acid-modulated reactions due to the fast formation of the soluble modulator-capped metal clusters; d) As a functionalization agent, which involves incorporation of functionalized modulators into MOF structures by compensating for missing cluster defects [46-49]. Likewise, use of modulator sometimes results into imperfections represented by missing linkers or missing clusters.

1.3.3 Defect Engineering

Defective MOFs have myriad applications such as adsorption heat pump (defects tune hydrophobic/hydrophilic properties), catalysis by creating Brønsted or Lewis acid sites, electrochemical applications, bio-applications, electronic applications by altering electronic band structure, and so on. Therefore, many approaches have been suggested to introduce defects in crystal lattice of MOFs. They include: (i) using acid modulator to synthesize MOFs with missing ligands, (ii) acid etching of MOFs, (iii) fast crystallization to synthesize MOFs with missing ligands, (iv) using mixed ligands to restrict proper coordination and (v) post modification [34,35,50]. Figure 1-4 illustrated missing cluster and missing linker defects, which were caused by acid modulation.

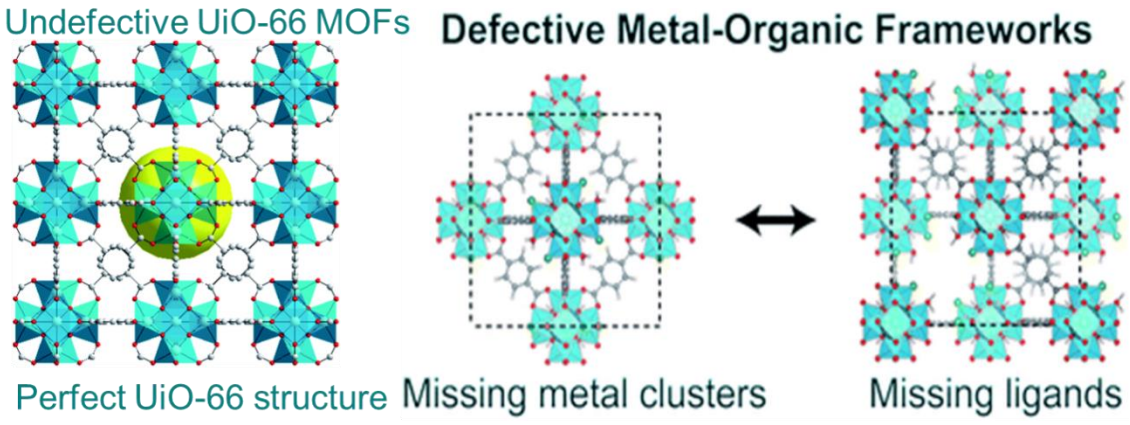

Figure 1-4. Illustration of defect formation [51].

1.3.4 Selected Examples of Modulated Synthesis

Modulators have been employed, depending on application or the design purpose. For instance, Schaate *et al* [35] systematically studied the effects of monocarboxylic acid on the crystal size formation of Zr-MOF. The crystal sizes were tuned by changing the amount of the acid. MOF-5 was prepared with tunable size using trimethylamine as a modulator and polyvinylprrolidone as a capping agent, where monodisperse MOF-5 crystals of cubic and octahedron shape with uniform size ranging from tens of nanometer to micrometre were obtained [47,48]. Acid/base co-modulation strategy was proposed to synthesize monodisperse UiO-66 crystals, where acetic acid controlled the crystal shape while trimethylamine as a base facilitated formation of missing linker defects. The obtained monodisperse MOF crystals had a octahedral shape with tunable sizes ranging from 500-2000 nm and high thermal stability [48,49]. Cliff *et al.* showed that shapes of UiO-66 crystals could be effectively modulated from intergrown morphologies to well-defined octahedrons by adding benzoic acid or acetic acid [52]. Though our group is fully convinced that the above-mentioned and other modulators were useful for the individual purposes, they have certain demerits such as high toxicity and volatility to handle, increased complexity and heterogeneity of the reaction mixture and resultant materials. For instance, the use of trifluoracetic acid readily catalyzes the hydrolysis of N,N-dimethylformamide during the synthesis and generating formic acid as un-desired by-product [53-57]. Therefore, in our former research, water was used as a clean and safe modulator to control the particle size and morphologies in UiO-66 framework [58]. Water played a vital role in controlling the nano-size and uniform shapes of crystals. The obtained UiO-66 nanoparticles were utilized in the design of a thin deposition layer of composite membranes feature with high flux and selectivity for nanofiltration.

1.4 Application of MOFs

1.4.1 Catalytic Applications

MOFs possess fascinating and tailorable properties such as high surface area, engineered porosity, multifunctional ligands, and so on. In addition, advent of "defect engineering" to yield MOFs with ccoordinately unsaturated metal centres have recently attracted attention for their unusual reactivity [33,59]. MOFs have been used as heterogeneous photocatalysts wastewater treatment, hydrogen production, artificial photosynthesis, and pollutants degradation [60]. Furthermore, MOFs are used as catalysts or catalyst supports for a diversity of organic transformations including Friedel–Crafts reactions, Knoevenagel condensation, aldol condensation, oxidation, coupling reactions, cyano silylation, and carbon dioxide fixation [61-64].

1.4.2 Sensing Applications

MOFs display possibility to respond a guest-induced change in optical absorption spectrum [65,66]. In combination with their structural flexibility, large surface area, and big pore volume, MOFs have been applied to sensor applications such as solvatochromism/vapochromism, photoluminescence, radioluminescence, interferometry formation, electromechanical sensor [67,68]. Response to external stimulation such as gravimetric, mechanical, optical or environmental changes are manifested in form of changes in structure and properties with a guest-dependent response [69].

1.4.3 Biomedical Applications

Nanosized MOFs have been found to possess excellent properties for drug delivery because of their (i) structural and compositional tunability for precise material design, (ii) high porosity permeation cargo payload, and (iii) relatively labile coordination bond connections, which

make MOFs intrinsically biodegradable in a biological environment [70-72]. These nanosized MOFs have been successfully applied for delivery of chemotherapeutic agents, imaging contrast agents, proteins and gene therapy drugs [73-76].

1.4.4 Sorption Applications

Due to hydrolytic stability of certain MOFs, they have emerged as excellent material attractive for water sorption application. High water capture capacity and good recyclability of MOFs make them highly desirable for water vapor sorption-based applications, including water harvesting from low-humidity air [77]. Generally, water sorption applications require a MOF sorbent to meet the following prerequisites: (i) high hydrolytic stability for recycling performance, (ii) large porosity and surface area for high water vapor uptake, (iii) relatively mild regeneration condition, (iv) isotherm with steep uptake (pore filling or condensation), and (v) high deliverable capacity [78,79].

1.4.5 Separation Applications

Recently, MOF composites and derivatives have been receiving a tremendous interest in separation applications including micro/ultra/nanofiltration, reverse osmosis, electro-osmosis, pervaporation, distillation, and gas separation [80-82]. The design principle of MOFs allows their pore properties (e.g. pore size, pore volume, and chemical functionality of pore walls) to be systematically tuned by judicious choice of metal, ligand constituent, and synthesis approach, which makes these microporous materials promising for molecular separation. Nanocomposite membranes that incorporates functional nanoparticles in a polymeric matrix is a promising approach to promote selectivity, chemical and thermal stability, and mechanical properties of the membranes. In similar fashion, combining MOFs with suitable materials endows it with opportunity to develop novel membrane materials. More excitingly, for first time, Chen *et al*, demonstrated the application of a microporous MOF, MOF-508, in the gas

chromatographic separation of alkanes based on size and shape-selective matching [83]. Owing to the sub-nanometer-sized pores, MOFs are often employed for nanofiltration, where nanoparticles of MOFs are dispersed in polymeric membranes as permeation-enhancing fillers.

1.5 Water Purification Technologies

One of the most pervasive problems afflicting people throughout the world is inadequate access to clean water [84,85]. Water purification technologies are broadly classified into thermally driven technology such as distillation and membrane-based technology [86,87] as shown in Figure 1-5. Among these, the membrane-based technology offers pure water with low energy requirement, ease of operation, simple to scale up, and minimal chemical additives [88], therefore making them popular among researchers and industrial use. Polymeric membranes were often used for their versatility, but due to some inherent limitations, nanochannel-based filtration has gained growing interests, where MOFs definitely play a crucial role for such developments.

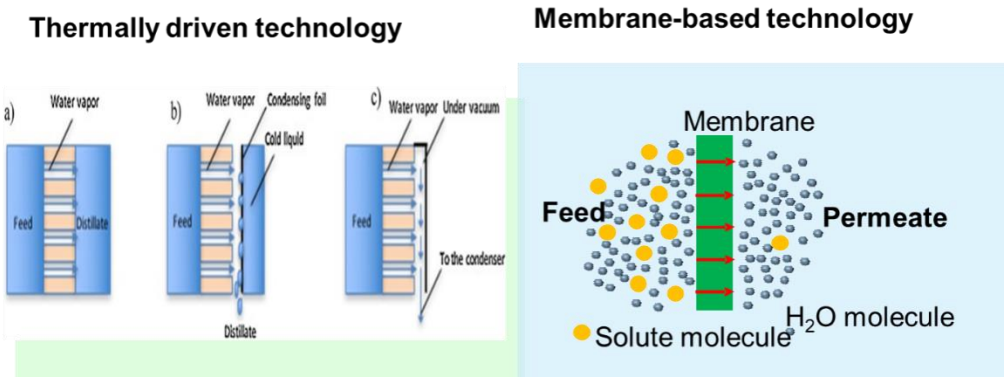

Figure. 1-5. Water purification technologies.

Broadly, membranes classified based on their morphology and rejection mechanisms. As shown in Figure 1-6, morphologically symmetric membranes are those made up of a single

material, while at asymmetric membranes possess two or more components. Thin film composite membranes represent the latter class, which comprises of a thin selective layer and a mechanical support layer. In terms of rejection mechanisms, membranes are classified into i) porous membranes which excludes solute based on its size, and ii) non-porous membranes reject solute based on solution diffusion [89-92].

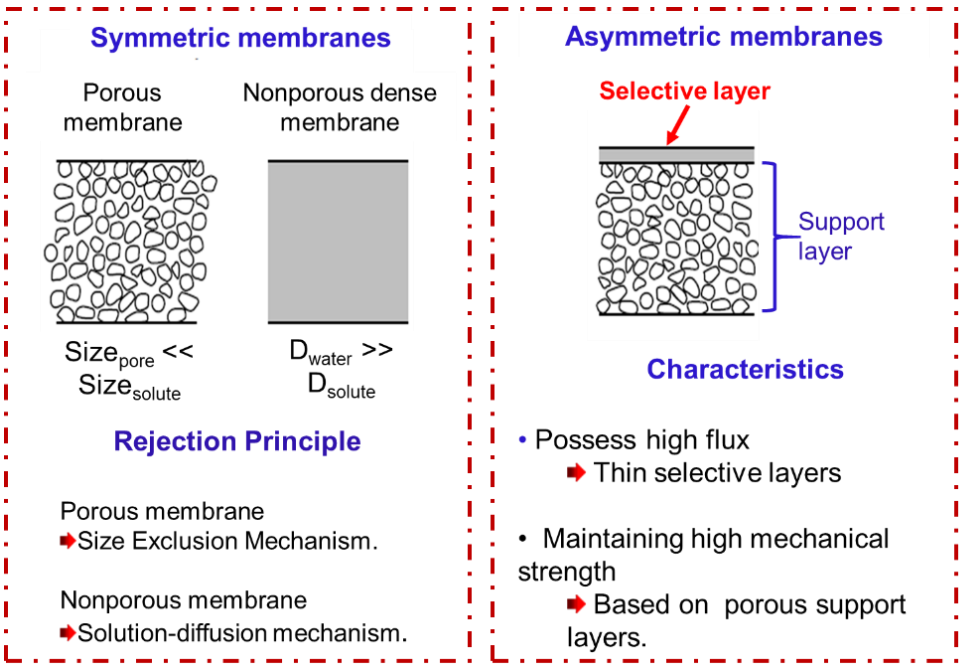

Figure 1-6. Membrane classifications based on the morphology and rejection mechanism.

1.5.1 Membrane Filtration Processes

Filtration processes are classified in terms of solutes' size to be rejected (Figure 1-7). Microfiltration (MF) membranes have pore sizes ranging from 0.1 to 10 µm. They are mainly used for the removal of large particulates, colloids, and bacteria from feed streams. This is popular technology especially in food & beverage industries for treating wastewater before discharging it to a municipal sewer [93]. Ultrafiltration (UF) is a process that is similar to microfiltration, but with a smaller size of solutes targeted from 0.01 to 0.1 µm. UF membranes

are used in rejecting solutes like viruses, polypeptides, and are widely used in protein concentration and wastewater treatment. Nanofiltration (NF) is particularly interesting as it can be used in combination with existing unit operations like evaporation, distillation and extraction, where recovery of solvent (mainly water) is important. NF is likely to be more viable than MF or UF in a sense that a resultant clean solvent is readily re-used. It offers several advantages such as low operating pressure, high flux, high retention of multivalent anion salts and organic matter, relatively low investment and low operation and maintenance costs [87, 88]. NF often offers valuable alternative to reverse osmosis (RO), which requires high operating pressure and energy cost. Thus, membranes with lower rejections of solutes but with higher water permeability could be of practical importance. In other words, research efforts on reverse osmosis membranes can also cause major impact on nanofiltration science and technology. Reverse osmosis membranes are dense membranes without predefined pores. Hence, permeation is slower and rejection is not because of sieving, but of solution-diffusion mechanism. The low permeability of reverse osmosis membranes requires high pressures, and consequently, relatively high-energy consumption. This effect is even more pronounced in the presence of an osmotic pressure due to high concentrations of solutes that counteract the applied pressure [94].

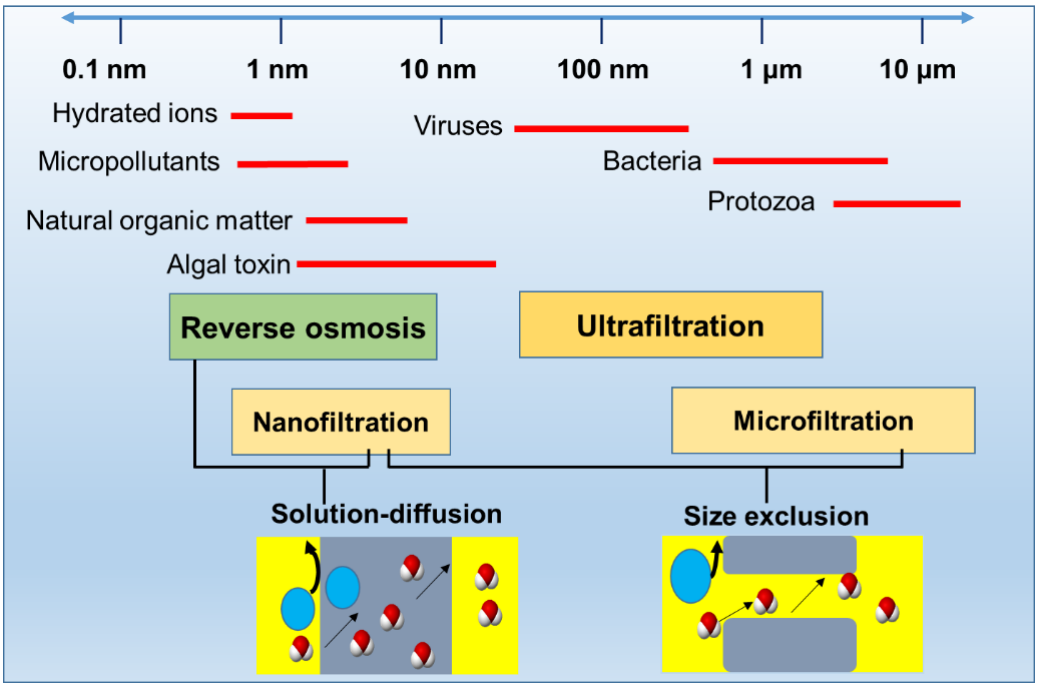

Figure 1-7. Classification of membrane filtration processes.

1.5.2 Problems of Utilizing Polymeric Membranes in Water Purifications

While membranes-based filtration have their own importance and are considered as a popular technology, there are certainly some challenges which constantly need scientific approach towards their solutions. One major problems of conventional polymeric membranes' applications in water treatment is a tradeoff between selectivity and permeability. As given in Figure 1-8, researchers have shown that improvement in selectivity tends to sacrifice permeability. This therefore has made researchers working on this issue and there is still a large scope to improve this tradeoff trend [95].

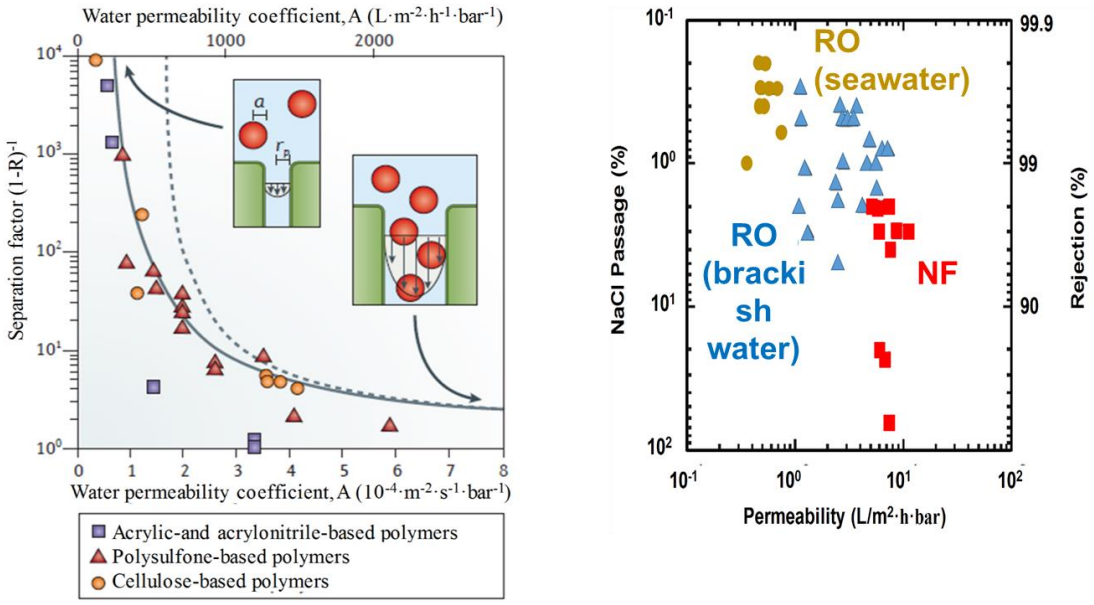

Figure 1-8. Tradeoff in polymeric membranes [95,96].

At present, membrane fouling is still a great challenge and major obstacle for wide spread implementation of membrane processes [97,98]. During water treatment processes, different fouling mechanisms can provide complex matrix. For instance, cake-like deposition on membrane surface as shown in Figure 1-9 will reduce permeate flux, increase feed pressure, reduce productivity, increase system downtime, increase membrane maintenance and operation costs due to membrane cleaning, and decrease life span of membrane modules. Different kinds of foulants such as (bio, organic, inorganic and colloidal foulants) [99-101] can be deposited on membrane surfaces as shown Figure 1-9. Therefore, better understanding of overall fouling picture is the prime objective to develop and design a novel membrane for better and acceptable effluent qualities.

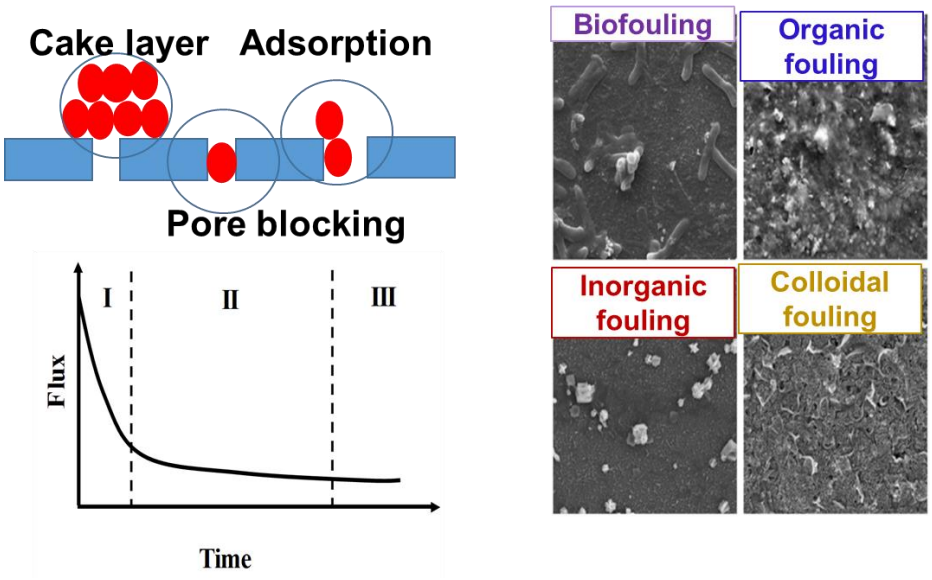

Figure 1-9. Schematic representation of fouling in polymeric membranes and different types of foulants [99-101].

1.5.3 New Classes of Materials for Membranes Design

Due to the aforementioned dilemma in the utilization of polymeric membrane for filtration, it is necessary to search for new classes of materials, such as nanochannel-based as the next generation for membrane preparation [91]. These materials have exhibited permeability from one to several orders of magnitudes and therefore can overcome the tradeoff in conventional membranes. Such materials include carbon nanotube, nanoporous graphene, and MOFs. Exploring the usage of MOF in the field of filtration would help to solve current scenario of water scarcity problem. MOFs materials like ZIF and UiO-66 nanoparticles have been used as selective layer by many researchers due to mild condition for crystallization on polymeric support resulting into flexible composite membrane and high stability in water /and other chemical environment$_s$ respectively. However, ZIF suffered from instability in chemical environment whilst utilization of UiO-66 required harsh synthesis condition for its *in-situ*

crystallization on polymeric support. Therefore, it has been difficult over years to obtain MOF-based membrane possessing both stability and flexibility. These unstable and inflexible MOF-based membranes affect their applications for conventional roll-to-roll processes.

Thus, it is important to design membranes without crystallizing it on polymeric support. This can be achieved by deposition of synthesized UiO-66 nanoparticles on polymeric support to offer both flexibility and stability. This UiO-66 is made of Zr cluster with 12 linkers' connectivity, which is highest linkers and coordination number in MOF that has so far known. These linkers cover metal node and thereby prevent them from attack of water and chemical and as such, UiO-66 is the most stable MOF. Thus, deposition of UiO-66 nanoparticle on a flexible support membrane to form a discontinuous or semi-continuous selective layer is promising novel technique. The irregularly stacked nanoparticles would offer two kinds of pathways: selective channel and non-selective void pathways. The void pathway is tortuous and tend to be dead-ended when the deposition layer becomes thicker. At such dead end, water needs to pass through nanochannel channels, where rejection of solute occurs as shown in Figure 1-10.

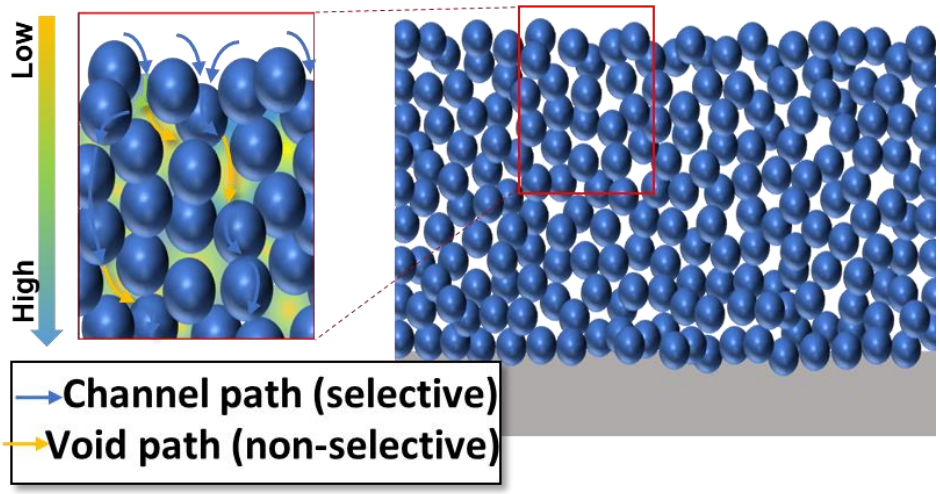

Figure 1-10. Schematic diagram for design of flexible and stable MOFs composite membrane on polymeric support by deposition method.

1.5.4 Our Previous Researches

In an effort to solve selectivity-permeability tradeoff and fouling problems in polymeric membranes, our previous researches successfully addressed these through: i) development of nanocomposite membranes filled with UiO-66 nanoparticles and its application to nanofiltration in which selective layer made from preformed UiO-66 nanoparticles offer the transport pathway for water molecules through pore aperture size (6 Å) as well as retaining its flexibility, stability of composite membranes ii) synthesis of poly(ethylene glycol) methacrylate-grafted UiO-66 nanoparticles composite membranes where grafted hydrophilic polymer from UiO-66 nanoparticles enhanced fouling resistance of the nanocomposite membranes. The goals were accomplished largely through composite membranes design.

1.6 Purpose of the Thesis

Nanofiltration is an extremely complex process in which it separation mechanisms are dependent on microhydrodynamic, interfacial properties /events at membrane surface and within membrane nanopores. Selectively-permeability tradeoff and fouling are the prevalent challenges that have hindered successful application polymeric membranes for nanofiltration. In order to mitigate these challenges in conventional membranes for pure water purification technology, utilization of already developed deposition technique as a way of incorporating nanoparticles into polymeric conventional membranes is of paramount importance. Deposition of nanosized UiO-66 MOFs polymeric support would offer an exceptionally high permeability and selectivity as well as possessing both stability and flexibility.

Therefore, objectives of this study is to address selectively-permeability tradeoff and fouling through systematic investigation on design principle for MOF-deposited composite membranes for nanofiltration achieved through:

(a) Synthetic control of nanoparticle size using water as modulator for evaluation of:

(i) Particle size effects on nanofiltration performance.

(ii) Development of bimodal membrane.

(b) Pore engineering of nanoparticles and investigation of their effects on filtration performances achievable through:

(i) Manipulation of pore surfaces by modified ligands.

(ii) Nanofiltration and chemical selectivity of the membranes.

1.7 References

[1] Furukawa, H.; Cordova, K. E.; O'Keeffe, M.; Yaghi, O. M. The Chemistry and Applications of Metal-Organic Frameworks. Sci. **2013**, 341, 1230444.

[2] Zhou, H. C.; Long, J. R.; Yaghi, O. M. Introduction to Metal Organic Frameworks. Chem. Rev. **2012**, 112, 673–674.

[3] Rubio-Martinez. M.; Avci-Camur, C.; Thornton, A. W. Imaz, I.; Maspoch, D.; Hill, M. R. New Synthetic Routes towards MOF Production at Scale. Chem. Soc. Rev. **2017**, 46, 3453–3480.

[4] Butova, V. V.; Soldatov, M. A.; Guda, A. A.; Lomachenko, K. A.; Lamberti, C. Metal-Organic Frameworks: Properties, Structure, Properties, Methods of Synthesis and Characterization. Rus. Chem. Rev. **2016**, 85, 280–307.

[5] Dhakshinamoorthy, A.; Garcia. H. Metal-Organic Frameworks as Solid Catalysts for the Synthesis of Nitrogen-Containing Heterocycles. Chem. Soc. Rev. **2014**, 43, 5750 –5765.

[6] Furukawa, H.; Ko, N.; Go, Y. B.; Aratani, N.; Choi, S. B.; Choi, E.; Yazaydin, A. O.; Snurr, R. Q.; O'Keeffe, M.; Kim, J.; Yaghi, O. M. Ultrahigh Porosity in Metal-Organic Frameworks. Sci. **2010**, 329, 424– 428.

[7] Grunker, R.; Bon,V.; Muller, P.; Stoeck, U.; Krause, S.; Mueller, U.; Senkovska, I.; Kaskel, S. A New Metal–Organic Framework with Ultra-High Surface Area. Chem. Commun. **2014**, 50, 3450–3452.

[8] Yaghi, O. M.; O'Keeffe, M.; Ockwig, N. W.; Eddaoudi, M.; Kim, J. Reticular Synthesis and the Design of New Materials. Nat. **2003**, 423, 705–714.

[9] Eddaoudi, M.; Kim, J.; Rosi, N.; Vodak, D.; Wachter, J.; O'Keeffe, M.; Yaghi, O.M. Systematic Design of Pore Size and Functionality in Isoreticular MOFs and their Application in Methane Storage. Sci. **2002**, 295, 469– 472.

[10] Eddaoudi, M.; Moler, D. B.; Li, H.; Chen, B.; Reineke, T. M.; O'Keeffe, M.; Yaghi, O. M. Modular chemistry: Secondary Building Units as a Basis for the Design of Highly Porous and Robust Metal-Organic Carboxylate Frameworks. Acc. Chem. Res. **2001**, 34, 319–330.

[11] Stock, N.; Biswas, S. Synthesis of Metal-Organic Frameworks (MOFs): Routes to Various MOFs Topologies, Morphologies, and Composites. Chem. Rev. **2012**, 112, 933–969.

[12] Remya, V. R.; Kurian, M. Synthesis and Catalytic Application of Metal-Organic Frameworks: A Review on Recent Literature. Inter. Nano. Lett. **2019**, 9, 17–29.

[13] Seetharaj, R.; Vandana, P. V.; Arya, P.; Mathew, S. Dependence of Solvents, pH, Molar Ratio and Temperature in Tuning Metal Organic Framework Architecture. Arab. J. Chem. **2019**, 12, 299–315.

[14] Czaja, A. U.; Trukhan, N.; Muller. Industrial Applications of Metal-Organic Frameworks. Chem. Soc. Rev. **2009**, 38, 1284–1293.

[15] Martinez Joarisi, A.; Juan-Alcaniz, J.; Serra-Crespo, P.; Kapteijn, F.; Gascon, J. Electrochemical Synthesis of Some Archetypical Zn^{2+}, Cu^{2+},and Al^{3+} Metal-Organic Frameworks. Cryst. Growth Des. **2012**, 12, 3489–3498.

[16] Al-Kutubi, H.; Gascon, J.; Sudhölter, E. J. R.; Rassaei, L. Electrosynthesis of Metal Organic Frameworks: Challenges and Opportunities. Chem. Electro. Chem. **2015**, 462–474.

[17] Li, M. Y.; Dinca, M. Reductive Electrosynthesis of Crystalline Metal-Organic Frameworks. J. Amer. Chem. Soc. **2011**, 12926–12929.

[18] Campagnol, N.; Van Assche, T.; Boudewijns, T.; Denayer, J.; Binnemans, K.; De Vos, D.; Fransaer, J. High pressure, High Temperature Electrochemical Synthesis of Metal–Organic Frameworks: Films of MIL-100 (Fe) and HKUST-1 in Different Morphologies. J. Mater. Chem. A. **2013**, 1, 5827–5830.

[19] Boldyrev, V. V. Mechanochemistry and Mechanical Activation of Solids. Sol. State Ionics. **1993**, 63, 537–543.

[20] Stolle, A. Szuppa, T. Leonhardt, S. E. S.; Ondruschka, B. Ball Milling in Organic Synthesis: Solutions and Challenges. Chem. Soc. Rev. **2011**, 40, 2317–2329.

[21] Uzarevic, K.; Wang, T. C.; Moon, S. Y.; Fidelli, A. M.; Hupp, J. T. ; Farha, O. K.; Friscic, T. Mechanochemical and Solvent-Free Assembly of Zirconium-Based Metal–Organic Frameworks. Chem. Commun. **2016**, 52, 2133–2136.

[22] Klimakow, M.; Klobes, P.; Thunemann, A. F.; Rademann K.; Emmerling, F. Mechanochemical Synthesis of Metal-Organic Frameworks: A Fast and Facile Approach Towards Quantitative Yields and High Specific Surface Area. Chem. Mater. **2010**, 22, 5216–5221.

[23] Khan, N. A.; Jhung, S. H. Synthesis of Metal-Organic Frameworks (MOFs) with Microwave or Ultrasound: Rapid Reaction, Phase-Selectivity, and Size Reduction. Coord. Chem. Rev. **2015**, 285, 11–23.

[24] Vakili, R.; Xu, S.; Al-Janabi, N.; Gorgojo, P.; Holmes, S. M.; Fan, X. Microwave-Assisted Synthesis of Zirconium-Based Metal-Organic Frameworks (MOFs): Optimization and Gas Adsorption. Micro. Meso. Mater. **2018**, 260, 45–53.

[25] McKinstry, C.; Cussen, E. J.; Fletcher, A. J.; Patwardhan, S. V.; Sefcik, J. Scalable Continuous Production of High Quality HKUST-1 via Conventional and Microwave Heating. Chem. Eng. J. **2017**, 326, 570–577.

[26] Schlesinger, M.; Schulze, S.; Hietschold, M.; Mehring, M. Evaluation of Synthetic Methods for Microporous Metal–Organic Frameworks Exemplified by the Competitive Formation of $[Cu_2(btc)_3(H_2O)_3]$ and $[Cu_2(btc)(OH)(H_2O)]$. Micro. Meso. Mater. **2010**, 132, 121–127.

[27] Marquez, A. G.; Horcajada, P.; Grosso. D; Ferey, G.; Serre, C.; Sanchez, C.; Boissiere, C. Green Scalable Aerosol Synthesis of Porous Metal–Organic Frameworks. Chem. Commun. **2013**, 49, 3848–3850.

[28] Garzón-Tovar, L.; Cano-Sarabia, M.; Carné-Sánchez, A.; Carbonell, C.; Imaz, I.; Maspoch, D. A Spray-Drying Continuous-Flow Method for Simultaneous Synthesis and Shaping of Micro Spherical High Nuclearity MOF Beads. React. Chem. Eng. **2016**, 1, 533–539.

[29] Camur, C. V.; Troyano, J.; Carvajal, J. P.; Legrand, A.; Farrusseng, Imaz, I.; Maspoch, D. Aqueous Production of Spherical Zr-MOF Beads via Continuous-Flow Spray-Drying. Green Chem. **2018**, 20, 873–878.

[30] Burgaz, E.; Erciyes, A.; Andac M.; Andac, O. Synthesis and Characterization of Nano-Sized Metal-Organic Fameworks-5 (MOF-5) by Using Consecutive Combination of Ultrasound and Microwave Irradiation Methods. Inorganic. Chimica. Acta. **2019**, 485, 118–124.

[31] Armstrong, M. R.; Senthilnathan, S.; Balzer, C. J.; Shan, B.; Chen, L.; Mu, B.; Particle Size Studies to Reveal Crystallization Mechanisms of the Metal-Organic Framework HKUST-1 During Sonochemical Synthesis. Ultrason. Sonochem. **2017**, 34, 365–370.

[32] Masoomi, M. Y.; Bagheri, M.; Morsali, A. Porosity and Dye Adsorption Enhancement by Ultrasonic Synthesized Cd (II) Based Metal-Organic Framework. Ultrason. Sonochem. **2017**, 37, 244–250.

[33] Bachman, J. E.; Smith, Z. P.; Li, T.; Xu, T.; Long, J. R. Enhanced Ethylene Separation and Plasticization Resistance in Polymer Membranes Incorporating Metal-Organic Framework Nanocrystals. Nat. Mater. **2016**, 15, 845–849.

[34] Li , Y. S.; Bux, H.; Feldhoff, A.; Li, G. L.; Yang, W. S.; Caro, J. Controllable Synthesis of Metal–Organic Frameworks: From MOF Nanorods to Oriented MOF Membranes. Adv. Mater. **2010**, 22, 3322–3326.

[35] Schaate, A.; Roy, P.; Godt, A.; Lippke, A.; Waltz, F.; Wiebcke, M.; Behrens, P. Modulated Synthesis of Zr-Based Metal–Organic Frameworks: From Nano to Single Crystals. Chem. Eur. J. **2011**, 17, 6643–6651.

[36] Wanga, S.; Lva, Y.; Yaoa, Y.; Yub, H.; Lua, G. Modulated Synthesis of Monodisperse MOF-5 Crystals with Tunable Sizes and Shapes. Inorg. Chem. Comm. **2018**, 93, 56–60.

[37] Lu, G.; Cui, C.; Zhang, W.; Liu, Y.; Huo, F. Synthesis and Self-Assembly of Monodispersed Metal-Organic Framework Microcrystals. Chem. Asian J. **2013**, 8, 69–72.

[38] Desraju, C. R.; Vittal, J. J.; Ramanan A. Crystal Engineering: A textbook World Scientific. 2011, 1–216.

[39] Seoane, B.; Castellanos, S.; Dikhtiarenko, A.; Kaptein, F.; Gascon, J. Multi-Scale Crystal Engineering of Metal-Organic Frameworks. Coord. Chem. Rev. **2016**, 307, 147–187.

[40] Zahn, G.; Zerner, P.; Lippke, J.; Kemp, F. L.; Lilienthal, S.; Schroder, C. A.; Schneider, A. M.; Behrens, P. Insight into the Mechanism of Modulated Syntheses: in Situ Synchrotron Diffraction Studies on the Formation of Zr-fumarate MOF. Cryst. Eng. Comm. **2014,** 16, 9198–9207.

[41] Guo, H. L.; Zhu, Y. Z.; Wang, S.; Su, S. Q.; Zhou, L.; Zhang, H. J. Combining Coordination Modulation with Acid–Base Adjustment for the Control Over Size of Metal–Organic Frameworks. Chem. Mater. **2012**, 24, 444–450.

[42] McGuire, C. V.; Forgan, R. S. The Surface Chemistry of Metal–Organic Frameworks. Chem. Commun. **2015**, 51, 5199.

[43] Marshall, R. J.; Hobday, C. L.; Murphie, C. F.; Griffin, S. L.; Morrison, C. A.; Moggach, S. A. Forgan, R. S. Amino Acids as Highly Efficient Modulators for Single Crystals of Zirconium and Hafnium Metal–Organic Frameworks. J. Mater. Chem. A. **2016**, 4, 6955–696.

[44] Bai, Y.; Dou, Y.; Xie, L-H.; Rutledge, W.; Li, J. R.; Zhou, H. C. Zr-Based Metal–Organic Frameworks: Design, Synthesis, Structure, and Applications. Chem. Soc. Rev. **2016**, 45, 2327–2367.

[45] Hu, Z.; Castano, I.; Wang, S.; Wang, Y.; Peng, Y.; Qian, Y.; Chi, C.; Wang, X.; Zhao, D. Modulator Effects on the Water-Based Synthesis of Zr/Hf Metal−Organic Frameworks: Quantitative Relationship Studies between Modulator, Synthetic Condition, and Performance. Cryst. Growth Des. **2016**, 16, 2295−2301.

[46] Guillerm, V.; Gross, S.; Serre, C.; Devic, T.; Bauer, M.; Férey, G. Azirconium Methacrylate Oxo cluster as Precursor for the Low-Temperature Synthesis of Porous Zirconium (IV) Dicarboxylates. Chem. Commun. **2010**, 46, 767–769.

[47] Shearer, C.; Vitillo, J. G.; Bordiga, S.; Svelle, S.; Olsbye, U.; Lillerud. K. P. Functionalizing the Defects: Postsynthetic Ligand Exchange in the Metal Organic Framework UiO-66. Chem. Mater. **2016**, 28, 7190–7193.

[48] Wang, S.; Lv, Y.; Yaoa, Y.; Yub, H.; Lua, G. Modulated Synthesis of Monodisperse MOF-5 Crystals with Tunable Sizes and Shapes. Inorg. Chem. Comm. **2018**, 93, 56–60.

[49] Vermoortele, F.; Bueken, B.; Bars, G. L.; Ben Van deVoorde, B. V.; Vandichel, M.; Houthoof, K.; Vimont, A.; Daturi, M.; Waroquier, M.; Speybroeck, V. V.; Christine Kirschhock, C.; DeVos, D. E. Synthesis Modulation as a Tool to Increase the Catalytic Activity of Metal−Organic Frameworks: The Unique Case of UiO-66 (Zr) . J. Am. Chem. Soc. **2013**, 135, 11465−11468.

[50] Ren, J.; Ledwabaa, M.; Musyoka, N. M.; Langmia, H. W.; Mathe, M.; Liaod S.; Pang, W. Review Structural Defects in Metal–Organic Frameworks (MOFs): Formation, Detection and Control Towards Practices of Interests Review Structural Defects in Metal–Organic Frameworks (MOFs): Formation, Detection and Control Towards Practices of Interests. Coord. Chem. Rev. **2017**, 349, 169–197.

[51] Svane, K. L.; Bristow, J. K.; Galeb, J. D.; Walsh, A. Vacancy Defect Configurations in the Metal– Organic Framework UiO-66: Energetics and Electronic Structure. J. Mater. Chem. A, **2018**, 6, 8507–8513.

[52] Cliffe, M. J.; Hill, J. A.; Murray, C. A.; Coudert, F. X.; Goodwin, A. L. Defect-Dependent Colossal Negative Thermal Expansion in UiO-66 (Hf) Metal-Organic Framework. Phys. Chem. Phys. **2015**, 17, 11586−11592.

[53] Zhao, Y.; Zhang, Q.; Li, Y.; Zhang, R.; Lu, G. Large-Scale Synthesis of Monodisperse UiO-66 Crystals with Tunable Sizes and Missing Linker Defects via Acid-Base Modulation. ACS Appl. Mater. Interfaces. **2017**, 9, 15079–15085.

[54] Atzori, C.; Shearer, G. C.; Maschio, L.; Civalleri, B.; Bonino, F.; Lamberti, C.; Stian Svelle, S.; Lillerud, K. P.; Bordiga, S. Effect of Benzoic Acid as a Modulator in the Structure of UiO-66: An Experimental and Computational Study. J. Phys. Chem. C. **2017**, 121, 9312−9324.

[55] Cai, G.; Jiang, H.-L. A Modulator-Induced Defect-Formation Strategy to Hierarchically Porous Metal-Organic Frameworks with High Stability. Angew. Chem. **2017**, 129, 578−582.

[56] Gutov, O. V.; Hevia, M. G.; Escudero-Adán, E. C.; Shafir, A. Metal-Organic Framework (MOF) Defects Under Control: Insights into the Missing Linker Sites and Their Implication in the Reactivity of Zirconium-Based Frameworks. Inorg. Chem. **2015**, 54, 8396−8400.

[57] Wang, K.; Li, C.; Liang, Y.; Han, T.; Huang, H.; Yang, Q.; Liu, D.; Zhong, C. Rational Construction of Defects in a Metal-Organic Framework for Highly Efficient Adsorption and Separation of Dyes. Chem. Eng. J. **2016**, 289, 486−493.

[58] Trinh, D. X.; Tran, T. P. N.; Taniike, T. Fabrication of New Composite Membrane Filled with UiO-66 Nanoparticles and Its Application to Nanofiltration. Sep. Purif. Technol. **2017**, 177, 249–256.

[59] Gascon, J.; Aktay, U.; Hernandez-Alonso, M. D.; van Klink, G. P. M.; Kapteijn, F.: Amino-Based Metal-Organic Frameworks as Stable, Highly Active Basic Catalysts. J. Catal. **2009**, 261, 75–87.

[60] Babu, R.; Roshan, R.; Gim, Y.; Jang, Y. H.; Kurisingal, J. F.; Kim, D. W.; Park, D. Inverse Relationship of Dimensionality and Catalytic Activity in CO_2 Transformation: a Systematic

Investigation by Comparing Multidimensional Metal–Organic Frameworks. J. Mater. Chem. A. **2017**, 5, 15961–15969.

[61] Huang, Y. B.; Liang, J.; Wang, X. S.; Cao, R. Multifunctional Metal–Organic Framework Catalysts: Synergistic Catalysis and Tandem Reactions. Chem. Soc. Rev. **2017**, 46, 126–157.

[62] Yang, D.; Gates, B. C. Catalysis by Metal Organic Frameworks: Perspective and Suggestions for Future Research. ACS Catal. **2019**, 9, 1779−1798

[63] Zhu, C.; Mao, Q.; Li, D.; Li, C.; Zhou, Y.; Wu, X.; Luo, Y.; Li, Y. A Readily Available Urea Based MOF that Act as a Highly Active Heterogeneous Catalyst for Friedel–Crafts Reaction of Indoles and Nitrostryenes. Catal. Commun. **2018,** 104, 123–127.

[64] Allendorf, M. D.; Foster, M. E.; Léonard, F.; Stavila, V.; Feng, P. L.; Doty, F. P.; Leong, K.; Ma, E. Y.; Johnston, S. R.; Talin, A. A. Guest-Induced Emergent Properties in Metal−Organic Frameworks. J. Phys. Chem. Lett. **2015**, 6, 1182−1195.

[65] Drache, F.; Bon,V.; Senkovska, I.; Adam, M.; Alexander Eychmüller, A.; Kaskel, S. Vapochromic, Luminescence of a Zirconium-Based Metal–Organic Framework for Sensing Applications. Eur. J. Inorg. Chem. **2016**, 4483–4489.

[66] Stylianou, K. C, Heck, R.; Chong, S. Y.; Bacsa, J.; Jones, J. T. A.; Khimyak, Y. Z.; Bradshaw, D.; Rosseinsky, M. J.A Guest-Responsive Fluorescent 3D Microporous Metal-Organic Framework Derived from a Long-Lifetime Pyrene Core. J. Am. Chem. Soc. **2010**, 132, 4119– 4130.

[67] Chang, Z.; Yang, D. H.; Xu, J.; Hu, T. L.; Bu, X. H. Flexible Metal–Organic Frameworks: Recent Advances and Potential Applications. Adv. Mater. **2015**, 27, 5432–5441.

[68] Assen, A. H.; Yassine, O.; Shekhah, O.; Eddaoudi, M.; Salama, K. N. MOFs for the Sensitive Detection of Ammonia: Deployment of MOF Thin Films as Effective Chemical Capacitive Sensors. ACS Sens. **2017**, 2, 1294−1301.

[69] Kumar, P.; Deep, A.; Ki-Hyun, K. Metal-Organic Frameworks for Sensing Applications. Trends in Analyt. Chem. **2015**, 73, 39–53.

[70] Keskin, S.; Kızılel, S. Biomedical Applications of Metal Organic Frameworks. |Ind. Eng. Chem. Res. **2011**, 50, 1799–1812.

[71] Beg, S.; Rahman, M.; Jain, A.; Sain, S.; Midoux, P.; Pichon, C.; Ahmad, F. J.; Akhter, S. Nanoporous Metal- Organic Frameworks as Hybrid Polymer–Metal Composites for Drug Delivery and Biomedical Applications. Review, Drug Discovery Today **2017**, 22, 625–636

[72] Chowdhury, M. A. Metal-Organic-Frameworks for Biomedical Applications in Drug Delivery, and as MRI Contrast Agents. J. Biomed. Mat. Res. A. **2017**, 105A, 1184–1194.

[73] Lu, K. Metal-Organic Frameworks for Biomedical Applications. PhD Dissertation, Submitted to Faculty of the Division of the Physical Sciences Department of Chemistry. 2016, 1–224.

[74] Liang, K.; Ricco, R.; Doherty, C. M.; Styles, M. J.; Bell, S.; Kirby, N.; *et al*. Biomimetic Mineralization of Metal-Organic Frameworks as Protective Coatings for Biomacromolecules. Nat. Commun. **2015**, 6, 1–8.

[75] Sun, C. Y.; Qin, C.; Wang, C. G.; Su, Z. M.; Wang, S.; Wang, X. L.; *et al*. Chiral Nanoporous Metal-Organic Frameworks with High Porosity as Materials for Drug Delivery. Adv. Mater. **2011**, 23, 5629–5632.

[76] Taylor-Pashow, K. M. L.; Rocca, J. D.; Huxford, R. C.; Lin, W. Hybrid Nanomaterials for Biomedical Applications. Chem. Commun. **2010**, 46, 5832–5849.

[77] Horcajada, P.; Chalati, T.; Serre, C.; Gillet, B.; Sebrie, C.; Baati, T.; Eubank, J. F. D.; Clayette, H. P.; Kreuz, C.; Chang, J-S.; Hwang, Y. K.; Phuong, N. B. M.; Cynober, L.; Gil, S.; Férey, G.; Couvreur, P.; Gref, R. Porous Metal–Organic-Framework Nanoscale Carriers as a Potential Platform for Drug Delivery and Imaging. Nat. **2010**, 9, 172–177.

[78] Fathieh, F.; Kalmutzki, M. J.; Kapustin, E. A.; Waller. P. J.; Yang, J.; Yaghi, O. M. Practical Water Production from Desert Air. Sci. Adv. **2018**, 4, 3198 –3207.

[79] Kapustin, E. A. A Crystal with Nearly 200% of Its Body Weight in Water. Chem. **2018**, 4, 16–26.

[80] Li, W. Metal–Organic Framework Membranes: Production, Modification, and Applications. Prog. Mater. Sci. **2019**, 100, 21–63.

[81] Fujiwara M.; Imura, T. Photo Induced Membrane Separation for Water Purification and Desalination Using Azobenzene Modified Anodized Alumina Membranes. ACS. Nano. **2015**, 9, 5705–5712.

[82] Liu, Y.; Ban, Y.; Yang, W. Microstructural Engineering and Architectural Design of Metal–Organic Framework Membranes. Adv. Mater. **2017**, 29, 1606949–1606965.

[83] Chen, B. L.; Liang, C. D.; Yang, J.; Contreras, D. S.; Clancy, Y. L.; Lobkovsky, E. B.; Yaghi, O. M.; Dai, S. Microporous Metal–Organic Framework for Gas Chromatographic Separation of Alkanes. Angew. Chem. Int. Ed. **2006**, 45, 1390–1393.

[84] Hilal, N.; Wright, C. J. Exploring the Current State of Play for Cost-Effective Water Treatment by Membranes. Nat. Part. J. Clean Water **2018**, 8, 1–3.

[85] WWAP (United Nations World Water Assessment Programme). The United Nations World Water Development Report 2015: Water for a Sustainable World (UNESCO, Paris, 2015).

[86] Camacho, L. M.; Dumée, L.; Zhang, J.; Jun-de, L.; Duke, M.; Gomez, J.; Gray, S. Advances in Membrane Distillation for Water Desalination and Purification Applications. Water **2013**, 5, 94–196.

[87] Greenlee, L. F.; Lawler, D. F.; Freeman, B. D.; Marrot, B.; Moulin, P. Reverse Osmosis Desalination: Water Sources, Technology, and Today's Challenges. Water Res. **2009**, 43, 2317–2348.

[88] Zhang, R.; Liu, Y.; He, M.; Su, Y.; Zhao, X.; Elimelech, M.; Jiang, Z. Antifouling Membranes for Sustainable Water Purification: Strategies and Mechanisms. Chem. Soc. Rev. **2016**, 45, 5888−5924.

[89] Baker, R W. Membrane Technology and Application. John Wiley & Sons, Ltd; 2004. ISBN: 0-470-85445-6.

[90] Strathmann, H.; Koc, K.; Amar, P.; Baker, R. The Formation Mechanism of Asymmetric Membranes. Desal. **1975**, 16 179–203.

[91] Baransi-Karkaby, K.; Bass, M.; Freger, V. In Situ Modification of Reverse Osmosis Membrane Elements for Enhanced Removal of Multiple Micropollutants. Membr. **2019**, 9, 1–14.

[92] Wen L, Xiao K, Sainath A. V. S, Komura M., Kong X. Y, Xie G, *et al*. Engineered Asymmetric Composite Membranes with Rectifying Properties. Adv. Mater. **2016**, 28, 757–763.

[93] Goh, P. S.; Ismail, A. F. A Review on Inorganic Membranes for Desalination and Wastewater Treatment. Desal. **2018**, 434, 60–80.

[94] Geise, G. M.; Lee, H. S.; Miller, D. J.; Freeman, B. D.; Macgrath, J. E.; Paul, D. R. Water Purification by Membranes: The Role of Polymer Science, J. Polym. Sci. Part B. **2010**, 481685–481718.

[95] Werber, J. R.; Osuji, C. O.; Elimelech, M. Materials for Next-Generation Desalination and Water Purification Membranes. Nat. Rev. Mater. **2016**, 1, 1–16.

[96] Geise, G. M.; Park, H. B.; Sagle, A. C.; Freeman, B. D.; MacGrath, J. E. Water Permeability and Water/Salt Selectivity Tradeoff in Polymers for Desalination. J. Membr. Sci. **2011**, 369, 130–138.

[97] Wang, L.; Song, L. Flux Decline in Crossflow Microfiltration and Ultrafiltration: Experimental Verification of Fouling Dynamics, J. Memb. Sci. **1999**, 160, 41–50.

[98] Zhu, A. Z.; Christofides, P. D.; Cohen, Y. Effect of Thermodynamic Restriction on Energy Cost Optimization of RO Membrane Water Desalination. Ind. Eng. Chem. Res. **2009**, 48, 6010–6021.

[99] Jianga, S.; Lib, Y.; Ladewig, B. P. Review A Review of Reverse Osmosis Membrane Fouling and Control Strategies. Sci. of the Total Environ. **2017**, 595, 567–583.

[100] Guo, W.; Ngo, H.; Li, J. Bioresource Technology A Mini-Review on Membrane Fouling. Bioresour. Technol. **2012**, 122, 27–34.

[101] Song, L. Flux Decline in Crossflow Microfiltration and Ultrafiltration and Modeling of Membrane Fouling. J. Membr. Sci. **1998**, 139, 183-200.

Chapter 2

Design of Semi-Continuous Selective Layer Based on Deposition of UiO-66 Nanoparticles for Nanofiltration

2.1 Introduction

Clean water scarcity is one of the forefront global challenges as a consequence of population growth, climate change and industrialization. Among water purification technologies, membrane-based filtration plays vital role in accessing superior water quality with an integrated sustainability in terms of no chemical additive, low energy consumption, minimal land usage and ease of operation [1]. Filtration is generally classified into microfiltration, ultrafiltration, nanofiltration and reverse/forward osmosis [2], according to size of solute to be rejected, in which use of polymeric membranes is predominant due to certain advantages: For example, the mechanical flexibility of polymeric membranes is suitable for large-scale roll-to-roll processing and integration in advanced filtration modules, a range of pore forming techniques enables fabrication of desired pore networks at a relatively low cost compared to an inorganic equivalent, and so on [3,4]. On negative side, polymeric membranes tend to suffer from insufficient resistance to fouling, mechanical instability in process stream, and a tradeoff between the permeability and selectivity [5-7]. One of approaches to tackle these problems is hybridization of polymeric membranes with other materials, especially nanomaterials [4,8-10].

Recently, nanochannel materials have attracted increasing attention in the field of membrane-based filtration. The attraction comes from a surface-dominated behavior of a fluid in nanochannels, which is different from that of bulk fluid [11]. For instance, a high surface atomic density and a low corrugation explain a nearly friction-less flow in nanochannels of multiwall nanotubes and graphitic materials [11-13]. Stacked graphene oxide offers ideal capillaries for facile transport of monolayered water molecules as horizontally spanned interlayer spaces of ~7 Å [14], while a disorder stacking offers vertical pathway for permeation [15]. Fast transportation with molecular-level selectivity through well-defined channels makes

nanochannel materials a promising candidate to address permeability-selectivity tradeoff problem in conventional membranes.

Among various nanochannel materials, metal-organic frameworks (MOFs) deserve special attention as they equip exceptionally high porosity, tunable pore size and structural diversity [16-18]. Contrary to rigid crystallographic structures for other porous materials, MOFs possess a flexible framework that can be tuned by selection of organic ligands and metal ions /clusters, thus making them particularly attractive for separation and purification purposes [19]. Among attempts to integrate MOFs into flexible polymeric membranes for water purification, a major challenge can be identified at how to form a MOF-based selective layer on a heterogeneous support in a defectless fashion [20-24]. Li et al [23] fabricated a continuous thin layer of a ZIF-8 on a polyethersulfone (PES) support by impregnating PES with an aqueous solution of metal precursor and subsequently interacting it with the organic ligand. As reagents reacted at an interface of the aqueous and organic phases, ZIF-8 nuclei that were initially formed within pores grew, filled pores, and eventually formed a thin selective layer on the membrane surface. Zhang et al [24] employed a coordination-driven in-situ self-assembly method to fabricate ZIF-8/poly (sodium 4-styrenesulfonate) (PPS) selective layer on polyacrylonitrile (PAN) support. It started from the coordination of Zn^{2+} metal precursor with carboxylate groups of the hydrolyzed PAN substrate, and dipping the Zn^{2+}-coordinated substrate in a mixed solution of the organic ligand and PPS to form a composite overlayer that consisted of in-situ generated ZIF-8 nanoparticles uniformly dispersed in the PPS matrix. The resultant membrane showed an excellent permeability corresponding to the flux of 265 L/m^2 h MPa at efficient rejection of methylene blue (MB). A key issue is that nucleation and growth of MOFs usually require hours under thermal treatment and/or in the presence of a harsh solvent, [25] and this severely limits combination between a MOF and a polymeric support that can form a uniform selective layer before damaging polymeric support. Moreover, as nucleation of MOF crystals likely occurs in

a solution rather than on a substrate surface, it is not easy to control thickness of selective layer in in-situ processes unless a cyclic layer-by-layer technique is employed [24,26]. In a practical sense, a facile and scalable process that can control formation of a selective layer without deteriorating the substrate is required to fully exploit advantageous of MOFs for water purification.

In our recent publication, a novel strategy was proposed to form a MOF-based composite membrane for nanofiltration [27], in which a suspension of UiO-66 nanoparticles as one of most stable framework in water [28-30] was deposited onto a regenerated cellulose (RC) support via suction filtration. The nanoparticles were filled in pore network or loaded on the external surface of the support membrane to form a selective layer. This new type of the composite membrane exhibited excellent permeability of 785.8 L/m^2 h and almost 100% rejection in the filtration of a MB aqueous solution, as a consequence of dominant permeation through the selective nanochannels of UiO-66 with respect to the non-selective leakage through interparticle voids. Even though the selective layer was comprised by discontinuous agglomeration of the nanoparticles, it was indeed regarded as semi-continuous in the filtration.

On basis of the developed strategy, this chapter focuses on investigation of the following issues of the new type of composite membrane:

(i) The effect of size and loading of UiO-66 nanoparticles on the performance of the resultant composite membranes for the filtration of a MB aqueous solution. It was found that smaller nanoparticles yielded a selective layer superior in terms of the permeability and selectivity, while a selective layer made by larger nanoparticles was more tolerant for the fouling.

(ii) Design of bimodal composite membranes with the selective layer composed by a mixture of smaller and larger nanoparticles. By filling interparticle voids among the

larger nanoparticles with the smaller nanoparticles, permeability, selectivity, and tolerance for the fouling could be simultaneously improved.

2.2 Experimental

2.2.1 Materials and methods

Zirconium tetrachloride ($ZrCl_4$, 99%) and terephthalic acid (99%) were purchased from Sigma-Aldrich and were used as received. N,N-dimethylformamide (DMF) and methanol (MeOH) as solvents were purchased from Wako Chemical Industries Ltd. A regenerated cellulose (RC) membrane (RC58, diameter 47 mm, pore size 0.2 μm, Whatmann G.E. Healthcare) was used as a support membrane. Methylthioninium chloride (methylene blue (MB), 98.5%) was purchased from Kanto Chemical Co., Inc. and was used as a solute for filtration experiments. Deionized (DI) water was used throughout the experiments.

2.2.2 UiO-66 preparation

Under nitrogen atmosphere, a solution of $ZrCl_4$ (1.63 mmol in 30 mL of DMF) was added to a solution of terephthalic acid (2.28 mmol in 30 mL of DMF). Thereafter, a specified amount of DI water (0.2-2.0 mL) was added at once. The mixture was heated at 100 °C for 12 h under constant stirring and nitrogen atmosphere to yield a white dispersion of UiO-66 nanoparticles. The nanoparticles were collected by centrifugation and repetitively washed with 50 mL of DMF for three times. Thereafter, the solid product was extensively washed by MeOH to completely remove DMF and finally dried at 90 °C for 24 h. Thus obtained samples are named as UiO1-UiO5, which correspond to the addition of DI water of 2.0, 1.6, 0.8, 0.4, and 0.2 mL, respectively.

2.2.3 UiO-66 characterization

The crystalline structure of UiO-66 nanoparticles was analyzed by X-ray diffraction (XRD, Rigaku SmartLab) using Cu Kα radiation in the range of 2θ = 5-35° at the step of 0.1° per 150 s. The crystallite size (D) of UiO-66 was estimated using Scherrer's equation:

$$D = \frac{0.94\,\lambda}{\beta \cos\theta} \quad (1),$$

where λ = 1.54 Å for Cu Kα, β = full-width at half-maximum, and θ = Bragg's angle. Fourier transform infrared spectra (FTIR) were acquired on a Jasco FT/IR-6100 spectrometer in the range of 400-2400 cm^{-1} with a resolution of 4 cm^{-1}. A dried sample was diluted with potassium bromide powder, and then pressed into a pellet for the measurement in the transmission mode. The morphology of UiO-66 nanoparticles was observed on a transmission electron microscope (TEM, Hitachi H7100) at an accelerated voltage of 100 kV. A dried sample was dispersed in MeOH, deposited onto a copper grid by drop casting, and then dried under air to evaporate the solvent. The particle size was acquired based on the TEM image analysis using ImageJ software. N_2 adsorption and desorption isotherms of the nanoparticles were acquired at 77 K using a BELSORP mini-HS II instrument (BEL JAPAN, Inc.). The grand canonical Monte Carlo method software was used to calculate pore size distribution. About 30 mg of a sample was charged into a sample cell and sealed with a brass filler and a rubber cap. The sample was out gassed at 180 ºC for 24 h in vacuo prior to the measurement.

2.2.4 Membrane preparation and characterization

A composite membrane was prepared by suction filtration of a dispersion of UiO-66 nanoparticles in water. A RC membrane was placed on a filter glass holder and wet with DI water. 4.0 mg of UiO-66 nanoparticles (unless stated) was dispersed in 30 mL of DI water by sonication for 1 h, and then deposited on the RC membrane by suction filtration at a constant

differential pressure of 50 mbar. After 30 min of filtration, differential pressure was increased to 100 mbar and kept for 15 min to partially dry the membrane.

The morphology of prepared composite membranes was observed by scanning electron microscope (SEM, Hitachi S-4100) operated at an accelerated voltage of 20 kV. A sample piece was attached on carbon tape and subjected to Pd/Pt sputtering for 100 s prior to the measurement. The cross-sectional morphology was also observed, where a membrane sample was fractured using liquid nitrogen.

2.2.5 Filtration performance

The filtration performance of the composite membranes was evaluated based on the MB rejection from its aqueous solution (1.0 μM) at the constant differential pressure of 100 mbar. The concentrations in the feed (C_0) and permeate (C_p) solution were measured by UV/vis spectroscopy (Jasco V670) based on absorption intensity at 665 nm. Permeate solution was collected at interval time of 1 or 2 min and rejection (R) was calculated using Eq. (2):

$$R\ (\%) = \left(\frac{C_0 - C_p}{C_0}\right) \times 100 \qquad (2).$$

The flux was determined from the cumulative permeate volume at the specified filtration time as shown in Eq. (3):

$$J = \left(\frac{V}{A \times t}\right) \qquad (3)$$

where J represents flux (L/m^2 h), V is cumulative permeate volume, A is effective membrane area (calculated as 9.61 cm^2), and t is filtration time. The results were obtained as an average from at least two filtration experiments using independently prepared membranes.

2.3 Results and discussion

2.3.1 UiO-66 Synthesis characterization

A series of UiO-66 samples were prepared by varying the addition amount of water during synthesis at fixed molar ratio between zirconium tetrachloride ($ZrCl_4$) and terephthalic acid. X-ray diffraction (XRD) patterns were recorded to confirm formation of UiO-66. As illustrated in Figure 2-1a, all samples exhibited intense diffraction peaks at 2θ = 7.4° and 8.5°, corresponding to (111) and (002) planes of the UiO-66 crystal [31-34]. Other minor diffraction peaks (as assigned in Figure 1a) also agreed well with the face-centered cubic lattice of the UiO-66 crystal [34]. By increasing the water amount, the diffraction peaks became broader, which is an indication of the crystallite size reduction. The crystallite sizes that were derived from Scherrer's equation (Table 2-1**)** monotonously increased from 25 to 83 nm by decreasing the water amount. Minor and broad diffractions at 2θ = 5.9°, 9.6° and 10.6° were additionally observed for UiO3, UiO4, and UiO5. These diffractions were attributed to secondary crystalline phase, called the **reo**-type, which originated from defective nanodomains with missing clusters [35]. The functional groups present in the prepared UiO-66 samples were examined by Fourier transform infrared spectroscopy (FTIR). As illustrated in Figure 1b, all of samples exhibited vibrational characteristics typical for UiO-66. Two strong bands at 1396 and 1579 cm^{-1} are assigned to symmetric and asymmetric strechings of O-C-O in the carboxylate groups of the terephthalic acid ligand, respectively [33,36]. The band at 1509 cm^{-1} represents the C=C vibration from the aromatic ring [37]. The characteristic peak at 745 cm^{-1} is ascribed to a mixture of the OH and C-H vibrational bendings [33] and the bands at 666, 551 and 474 cm^{-1} are assigned to μ_3-O streching, Zr(O-C) streching and μ_3-OH streching, respectively [33].

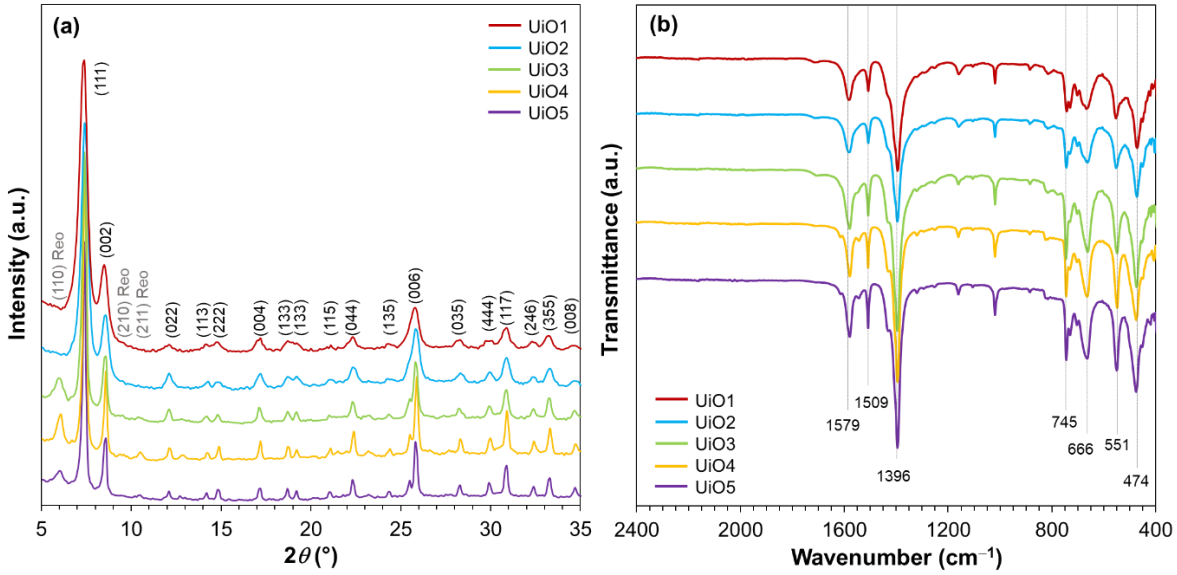

Figure 2-1**.** a) XRD patterns, and b) FTIR spectra of UiO-66 nanoparticles.

Table 2-1. Characteristics of UiO-66 Nanoparticles.

Sample	Water amount[a] (molar ratio)	Crystallite size from XRD[b] (nm)	Particle size from TEM[c] (nm)
UiO1	68 (2.0 mL)	25 (18)	14
UiO2	55 (1.6 mL)	37 (21)	20
UiO3	27 (0.8 mL)	46 (37)	75
UiO4	14 (0.4 mL)	66 (51)	88
UiO5	6.8 (0.2 mL)	83 (52)	108

[a]Molar ratio of added water with respect to $ZrCl_4$; [b]Determined using Scherrer's equation based on the (002) plane. The values in the parenthesis were determined based on the (111) plane; [c]The median particle size acquired from TEM images using ImageJ software.

The morphology of UiO-66 nanoparticles was observed by a transmission electron microscope (TEM) and the particle sizes acquired from TEM images are listed in Table 2-1. As can be seen in Figure 2-2, all of the samples exhibited similar morphology, i.e. intergrown particles of a polygonal shape. The particle size monotonously increased along the decrease in the water amount, in agreement to the XRD results. A slight deviation of the particle size obtained from the two analyses might originate from the polygonal shape and/or multiple crystal domains of nanoparticles. The dependence of the particle size on the water amount clearly indicated the role of water to accelerate the formation of crystal nuclei. Ragon et al,[38] reported that the crystallization of UiO-66 became significantly faster in the presence of water, which was ascribed to the ease of the Zr_6-cluster formation. Indeed, the reaction mixture became turbid more rapidly when a larger amount of water was added.

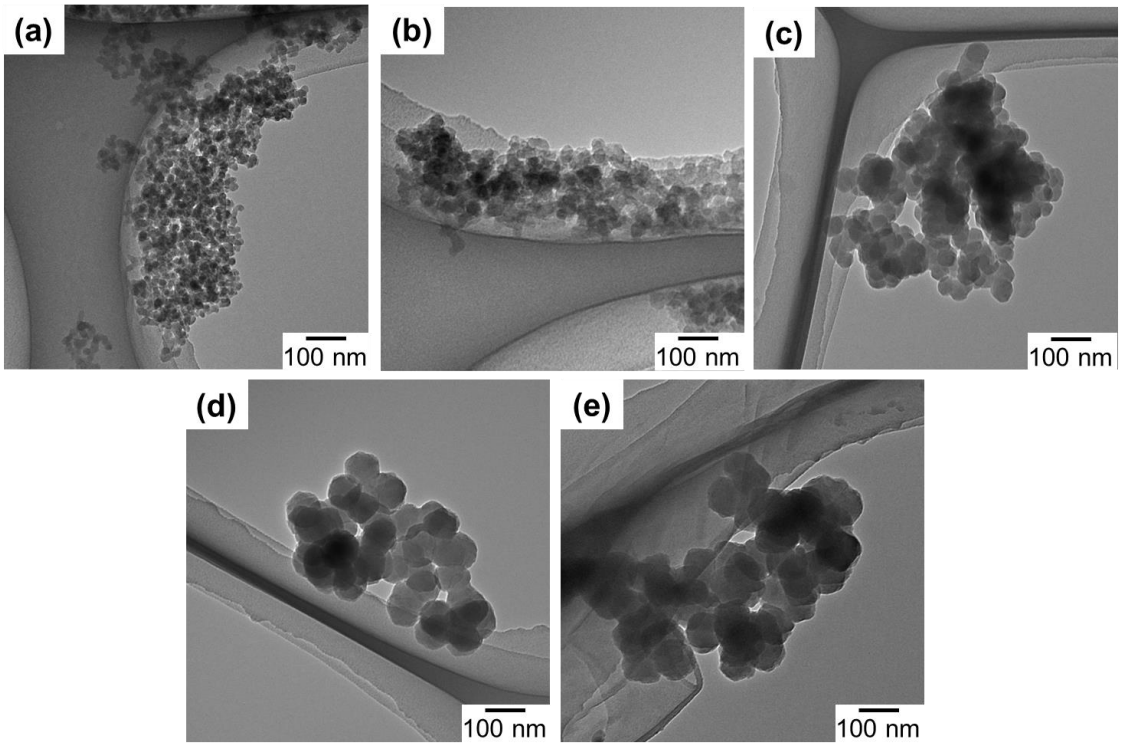

Figure 2-2**.** TEM images of UiO-66 nanoparticles: a) UiO1, b) UiO2, c) UiO3, d) UiO4, and e) UiO5.

From N_2 adsorption/desorption isotherms at 77 K (Figure 2-3), UiO1-5 nanoparticles were found to be predominantly microporous. Their mode pore sizes of 0.63-0.65 nm were similar among each other and consistent with the literature for tetrahedral pore structure of UiO-66.

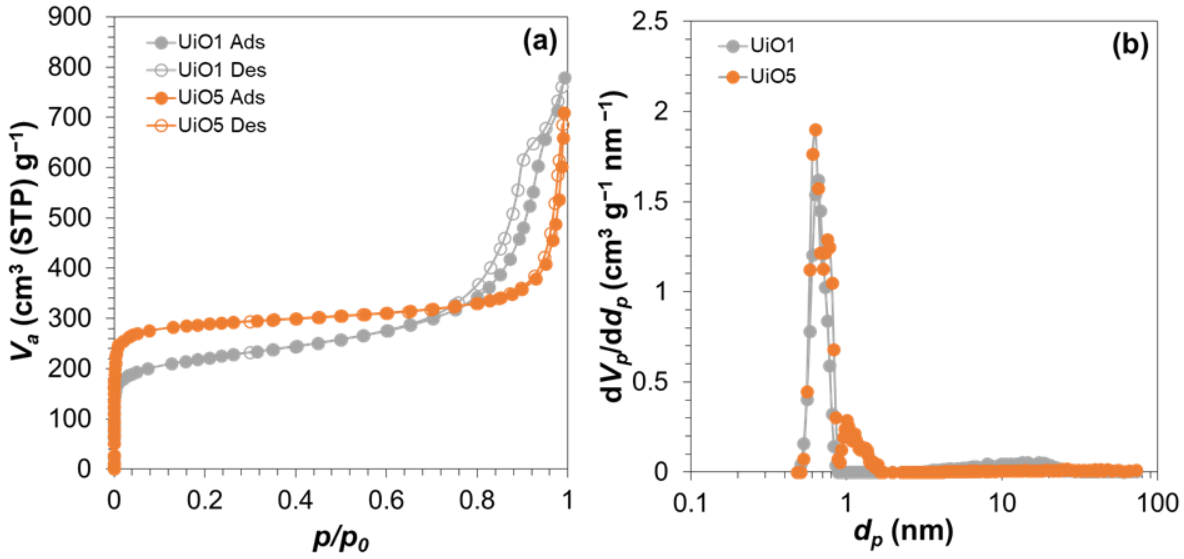

Figure 2-3**.** N_2 adsorption/desorption results for UiO1 and UiO5 nanoparticles: a) Isotherms and b) Micropore size distribution.

2.4 Membrane preparation and filtration performance

A series of UiO-66-deposited composite membranes were prepared by depositing 4.0 mg of preformed UiO1-UiO5 nanoparticles. Water was selected as a dispersing medium, which never damages the morphology of the support membrane. A top-view image of the RC membrane exhibited a highly porous morphology (Figure 2-4a), which became invisible after the nanoparticle deposition (Figure 2-4b). Scanning electron microscope (SEM) images of the UiO5 membrane (Figure 2-4b,c) revealed that thin layer was made of the nanoparticles that were disorderly deposited without the formation of cracks and pinholes. A similar morphology was observed for the deposition of the other smaller nanoparticles, except the fact that the

surface corrugation became more microscopic as the particle size became smaller (Figure 2-4d-g).

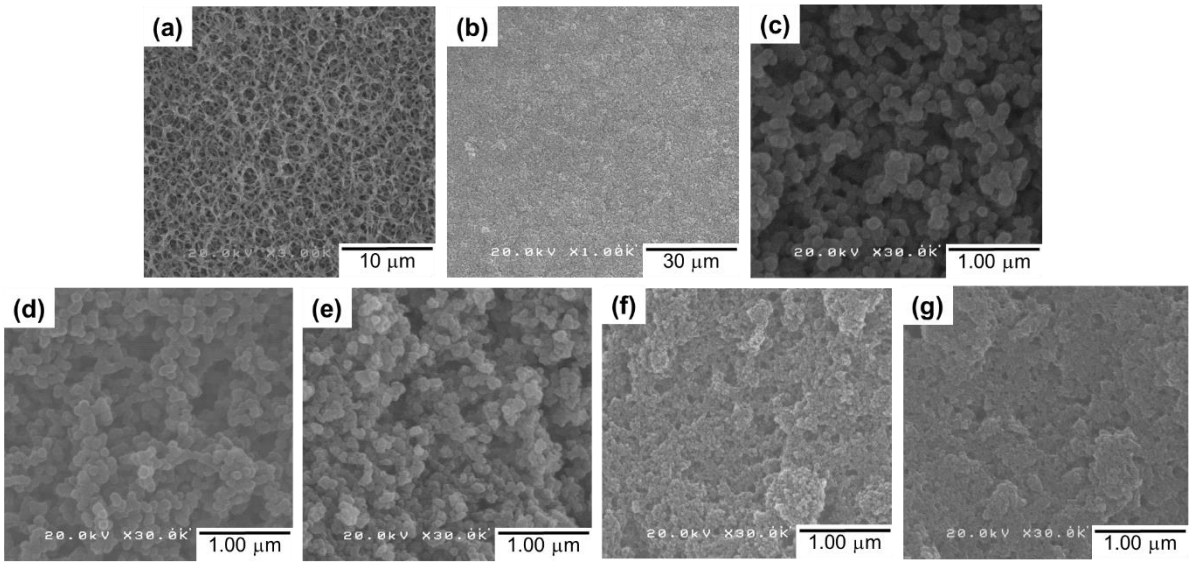

Figure 2-4**.** Top-view SEM images of the composite membranes: a) RC substrate, b) and c) UiO5 at different magnifications, d) UiO4, e) UiO3, f) UiO2, and g) UiO1.

The cross-sectional SEM images of the UiO5, UiO4 and UiO2 membranes (Figure 2-5a-c, respectively) showed formation of a thin layer of nanoparticles (approx. 6 μm) on top of the porous support. The intrusion of the nanoparticles into the porous network of the support membrane was hardly observed, and it was similar for the other two samples. This is plausibly because of the intergrown morphology of the nanoparticles: The interconnected nanoparticles were not separable as isolated particles, and therefore, plugged the porosity of the membrane during the deposition to form a semi-continuous deposition layer. Magnification of the cross-section of the thin layer (Figure 2-5d-f) illustrated that disordered packing of the nanoparticles generated interparticle voids, whose dimension was enlarged along the particle size. The

thickness of the deposition layer was hardly affected by the particle size, suggesting that packing density, i.e. the void fraction, was similar among the samples.

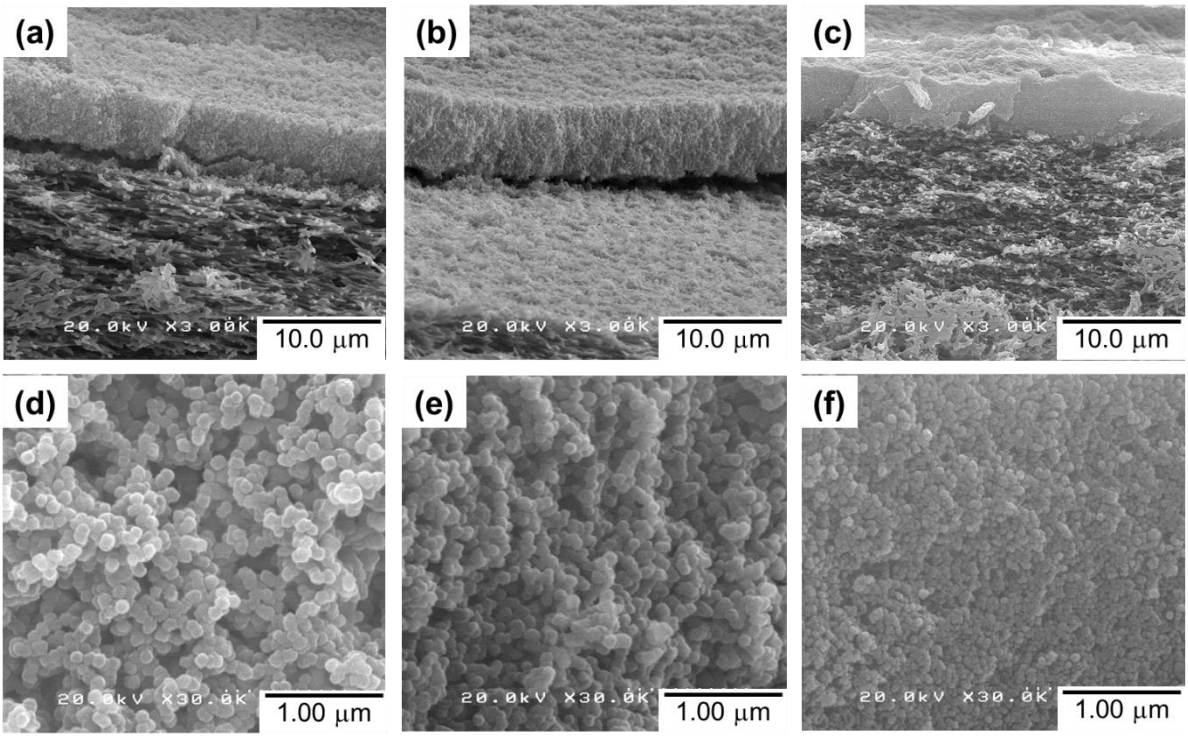

Figure 2-5**.** Cross-sectional SEM images of the composite membranes: a,d) UiO5, b,e) UiO4, and c,f) UiO2 at different magnifications.

The filtration performance of composite membranes was evaluated based on the rejection of methylene blue (MB) from its aqueous solution. Figure 2-6a shows results of the filtration in 5 min, where the RC membrane was used as a reference. The RC membrane exhibited fastest permeation, but the rejection quickly dropped to 70% within 5 min owing to its pore size (0.2 μm) far larger than the molecular size of MB [39]. Relatively high rejection at 1 min (i.e. the first 50 mL of the permeate volume) was explained by the adsorption of MB to cellulose [27]. After consuming the adsorption capacity, the rejection quickly dropped. The deposition of UiO-66 nanoparticles greatly improved the filtration performance: The perfect rejection was

maintained in 5 min for all the samples, irrespective of nanoparticle size. This fact supported absence of the pinholes in the deposition layer as well as the effectiveness of an idea to form a selective layer by packing UiO-66 nanoparticles. The permeate volume increased linearly by time, indicating that the fouling by the rejected MB molecules did not happen in 5 min. The permeation flux was found to be dependent on the size of UiO-66 nanoparticles (Figure 2-6b). The flux tended to increase for smaller nanoparticles, even though dimension of interparticle voids became smaller.

The interconnected morphology led to formation of interparticle voids, whose dimension was comparable to corresponding primary particle size: UiO1 formed the interparticle voids in the mesoporous dimension (confirmed by the presence of a hysteresis loop), the voids for UiO5 were in the range of macropores (no hysteresis loop), and so on. These results also suggested that the microscopic corrugation of the surfaces of the deposition layer (rather than the pore features) led to an enlargement of the effective membrane area, as is the case for cross-linked polyamide composite membranes having the crumpled textures [40,41,42]. The saturation of flux below 75 nm (i.e. UiO3 to UiO1) might be explained by presence of a counter factor such as concave hydrophobicity interfaces [43], tortuosity of the flow path, etc. The flux for UiO1 was calculated as 7734 ± 44 L/m^2 h bar, which was close to our previous value [27] and it was 20-500 times greater than those of commercial membranes for ultra/nanofiltration such as PVDF (100-300 L/m^2 h bar) [44] and UTC-20 (15 L/m^2 h bar) [45]. The flux values reported were 246 L/m^2 h bar for a graphene oxide composite membrane [46], and 80-100 L/m^2 h bar for cross-linked graphene oxide membranes [47].

There have been many literatures reported on utilization of MOFs for the water purification, in most of which MOF nanoparticles were embedded in a polymeric selective layer as a permeability enhancing fillers. A few literatures employed MOFs as the main constituent of the selective layer. In one literature [48], a polycrystalline UiO-66 selective layer was produced

based on in-situ seeding followed by secondary growth on an Al_2O_3 hollow fiber. The resultant membrane showed permeability of 0.2-2.2 L/m^2 h bar. In other two literatures [49,50], UiO-66 nanoparticles or Zn-TCP nanosheets were deposited onto a support membrane by suction filtration from their dispersion. The resultant membranes showed permeability of 2000-4000 L/m^2 h bar, similar to ours in the order. The origin of the significantly different permeability values among the first literature and the others (including ours) is at present unclear, while the external surface area may explain a part of difference. In the first literature [48], size of the in-situ grown building blocks was around 2 μm, while in the other two [49,50] and our cases, nano-sized building blocks were used. Remembering that the deposition of 4.0 mg of UiO5 (size = 108 nm) led to the permeability of 380 L/m^2 h and same gram of UiO1 (size = 14 nm) led to 770 L/m^2 h, then external surface area obviously plays an important role for the permeability of the membranes.

In our previous work, it was revealed that the selectivity of UiO-66-deposited composite membranes originates from the molecular sieving ability of the intraparticle channels of UiO-66 [27]. Briefly, it was found that adsorption capacity of the membrane was too small to explain the observed rejection, the deposition of poreless TiO_2 nanoparticles instead of UiO-66 never improved the rejection, and the observed cutoff between 1.22 and 2.28 nm was largely inconsistent with the dimension of the interparticle voids, and so on. Hence, deposited UiO-66 nanoparticles form a sort of semi-continuous selective layer, in which the passage of the filtrate occurs mainly through the intraparticle channels and that through non-selective interparticle voids is negligible. In actual, the leakage of MB molecules through the interparticle voids and the membrane fouling were hardly observed at the filtration volume and time of Figure 2- 6.

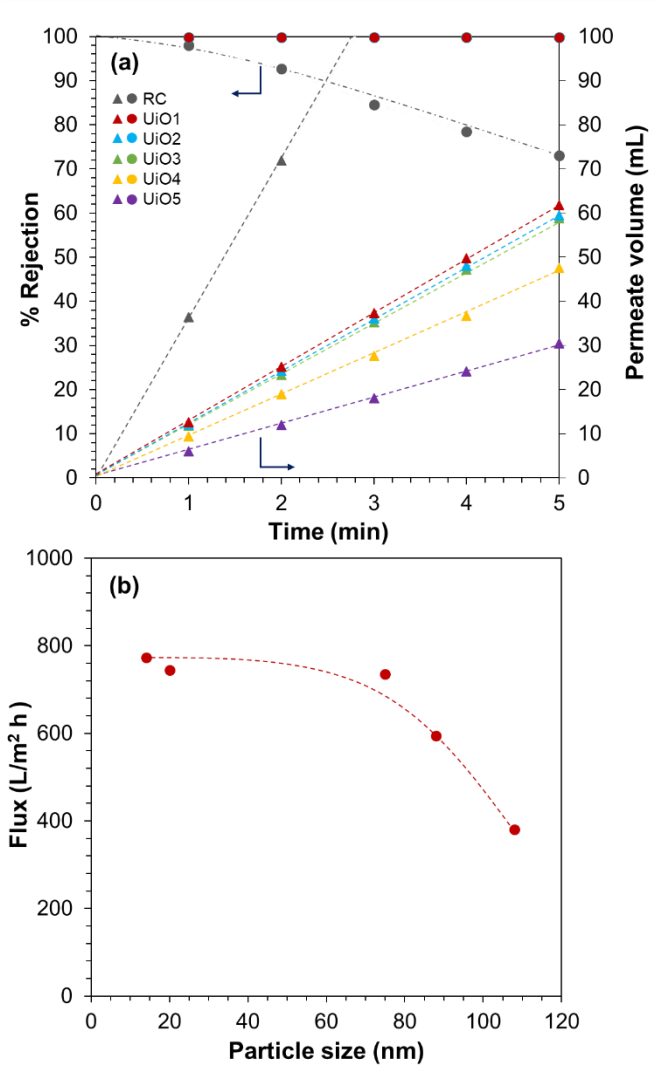

Figure 2-6**.** Filtration performance of UiO-66 composite membranes: a) MB rejection and permeate volume, and b) flux as a function of the UiO-66 particle size.

The performance of the composite membranes was investigated for a longer time of period, where an aqueous solution of MB of an appropriate concentration was continuously filled during the filtration in order to maintain the MB concentration of the feed solution at 1.0 μM. The result of filtration is as shown in Figure 2-7. It was found that nearly 100% rejection was maintained up to 2500 mL of permeate at duration of over 400 min. On the other hand, it was interesting to investigate the tolerance of the composite membranes for the leakage and fouling in extended filtration experiments. For this purpose, the filtration experiment was continued

until 350 mL of the feed solution was completely filtered. In the dead-end filtration setup, the progress of separation monotonously increases the MB concentration in the remaining feed, so that this experiment aimed to identify potential defects of composite membranes by exposing them to an increasing concentration of MB. The continuity of the performance at a constant MB concentration was also confirmed in separate experiments.

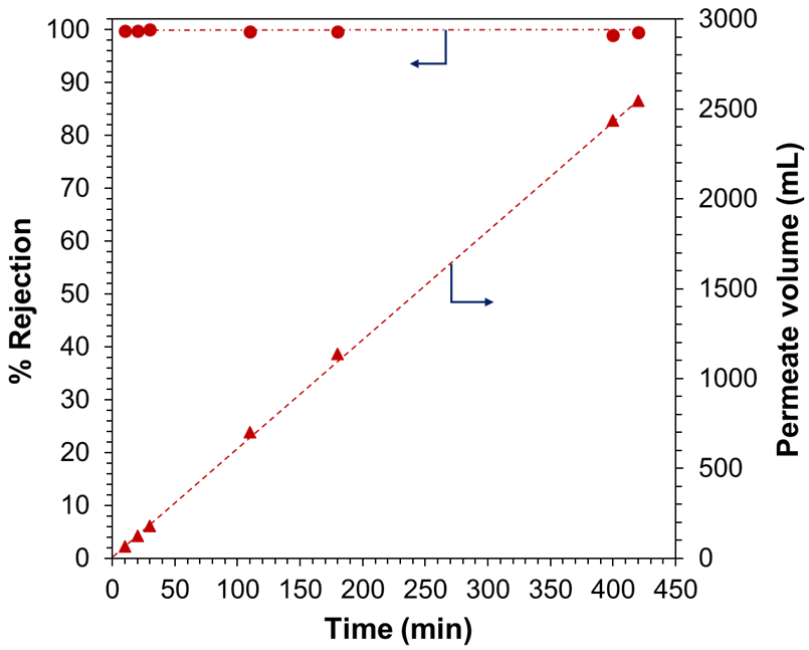

Figure 2-7. Performance of the UiO1 composite membrane in an elongated filtration.

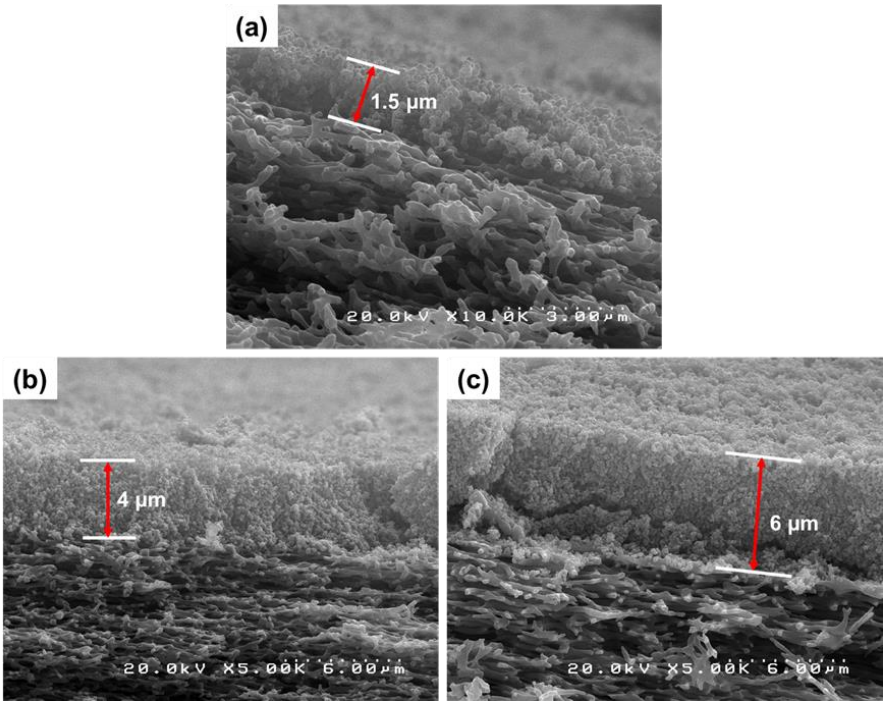

Figure 2-8. Cross-sectional SEM images of the UiO5 composite membranes at different loadings: a) 1.0 mg, b) 3.0 mg, and c) 4.0 mg.

Figure 2-9a,b describe filtration results for a series of composite membranes that were prepared by depositing 1-4 mg of UiO1 or UiO5 (see Figure 2-8 for thickness variation along the loading). Up to 5 min, the permeate volume increased linearly with time irrespective of amount and size of the deposited UiO-66 nanoparticles. The flux values at 5 min are compared in Figure 2-9c,d. When the deposition amount was decreased from 4 mg, the flux value increased monotonously for both UiO1 and UiO5, while UiO1 always retained the permeability greater than that of UiO5 at the individual loadings. Extended filtration over 5 min tended to deteriorate the permeability of the composite membranes due to the membrane fouling (Figure 2-9a,b). The extent of deterioration was quite sensitive to the formulation of the membranes (Figure 2-9c,d). The flux values at the 99% rejection were almost unchanged from those of the first 5 min for UiO5, whilst the flux at the 99% rejection was at maximum halved from that of the first 5 min for UiO1. It was considered that microscopic concavity created by the deposition

of UiO1 nanoparticles was more susceptive to the particle pore blocking from the accumulating solute. The extension of the filtration also caused the MB leakage through interparticle voids (Figure 2-9a,b). The leakage behavior was found to be opposite between the two kinds of the nanoparticles. The leakage tolerance improved monotonously to the deposition amount of UiO1, while the amount hardly suppressed the leakage for UiO5 (Figure 2-9e). The superiority of the UiO1-based membranes in terms of the permeability and selectivity appeared to be contradictive with a general tradeoff between these two parameters, but the following considerations would explain the obtained results: i) smaller nanoparticles created a deposition layer with more microscopic corrugation and thus enhanced external surface area (contact area between the filtrate and the membrane) improved the permeability; ii) the deposition of the smaller nanoparticles narrowed the interparticle voids, i.e. the pathway along which the leakage occurs, and in addition, the larger interfacial area inside the membranes suppressed a chance for the permeate to pass through the deposition layer without entering the nanochannels of UiO-66.

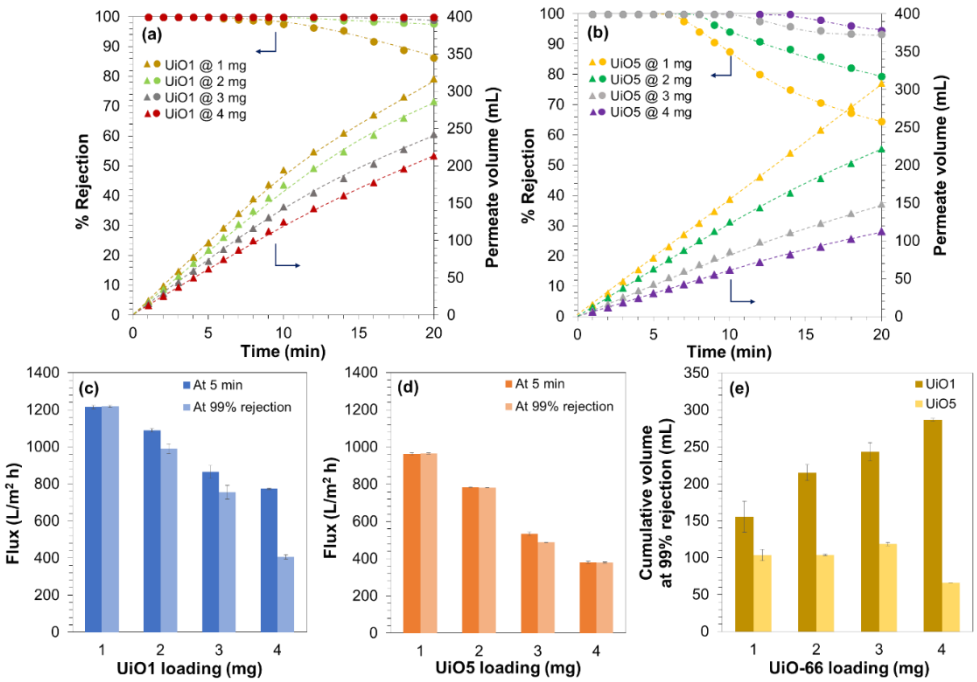

Figure 2-9**.** Filtration performance of the composite membranes with different amounts of UiO1 and UiO5: a,b) Time dependence of the filtration results for the first 20 min, c,d) the permeability compared by the flux values at the first 5 min and at the timing of the 99% rejection, and e) the tolerance for the MB leakage estimated by the cumulative volume of the filtrate until which the rejection was kept over 99%.

In order to assure origin of the MB rejection, an additional consideration was made based on the filtration results of 350 mL of MB aqueous solution. The total amount of MB that was rejected by the filtration of the complete 350 mL was derived from the cumulative rejection (Figure 2-9a), and then, this amount was normalized by loading of UiO-66 nanoparticles (Figure 2-10b). In our previous report, the MB adsorption capacity of UiO-66 nanoparticles having the particle size of 10 nm was determined as 2.8 μg/mg, where the nanoparticles were soaked in a MB solution for 42 h at room temperature and the adsorption capacity was derived from the reduced concentration of MB by the equilibrium adsorption [27]. The UiO-66 nanoparticles employed in this study were larger, so that 2.8 μg/mg could be regarded as the upper limit of the adsorption capacity of the UiO-66 nanoparticles. In Figure 2-10b, it is clear that the total rejection amount of MB was 10-30 times greater than the upper limit of the adsorption capacity, i.e. the MB rejection by the composite membranes was predominantly based on the molecular sieving mechanism [27]. A lower rejection efficiency at a greater loading suggested that not all of the UiO-66 nanoparticles were involved in the rejection, but an elevated loading was advantageous to fill in the interparticle voids.

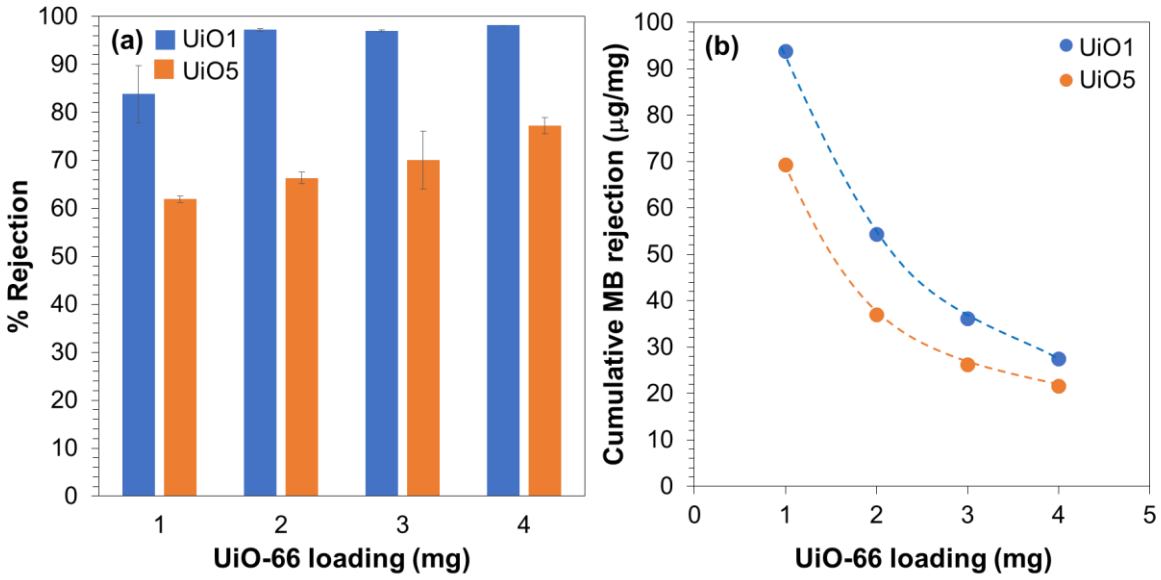

Figure 2-10**.** a) Cumulative rejection for the filtration of 350 mL of the MB aqueous solution, and b) cumulative amount of MB rejected per loading.

As described above, the size of UiO-66 nanoparticles exerted great impacts on the performance of the composite membranes: The smaller UiO1 nanoparticles yielded better permeability and tolerance for the MB leakage, while the larger UiO5 nanoparticles were resistant to the membrane fouling. At the end, we attempted to combine these advantages of the smaller and larger nanoparticles by depositing 4.0 mg of a mixture of UiO1 and UiO5 nanoparticles onto the support membrane (termed bimodal membranes). In a microscopic view, it was expected that a small weight fraction (but a much larger number) of the UiO1 nanoparticles would attach onto surfaces of the UiO5 nanoparticles, and this would result in an enlarged external surface area of selective layer and filled (or narrowed) interparticle voids. Figure 2-11a illustrates the cumulative MB rejection per loading for the complete filtration of 350 mL of the MB aqueous solution. It was found that the inclusion of a small weight fraction of the UiO1 nanoparticles notably improved the capacity of the membrane to reject MB. The extents of the improvement were much greater than those estimated from the weight average

(except 40:60). Most plausibly, the interparticle voids among the UiO5 nanoparticles were filled by the UiO1 nanoparticles, and as a result, the interparticle voids became as narrow as those of the UiO1-based membrane (corresponding to 100:0). The exceptional result for 40:60 would be explained by the fact that the packing density of bimodally distributed particles reaches its peak at 70% of the large particle fraction irrespective of the particle size ratio.[51] Figure 2-11b describes the permeability of the bimodal membranes measured at the first 5 min and at the timing of 99% rejection. As was expected, the inclusion of a small fraction of the UiO1 nanoparticles monotonously enhanced permeability of the membranes, and the flux value became almost comparable at the weight ratio of 30:70. Furthermore, the usage of UiO5 nanoparticles as the main component of the selective layer successfully endowed the fouling resistance of the UiO5-based membrane (corresponding to 0:100) to the bimodal membranes in a way not to sacrifice the permeability and the selectivity of the UiO1-based membrane.

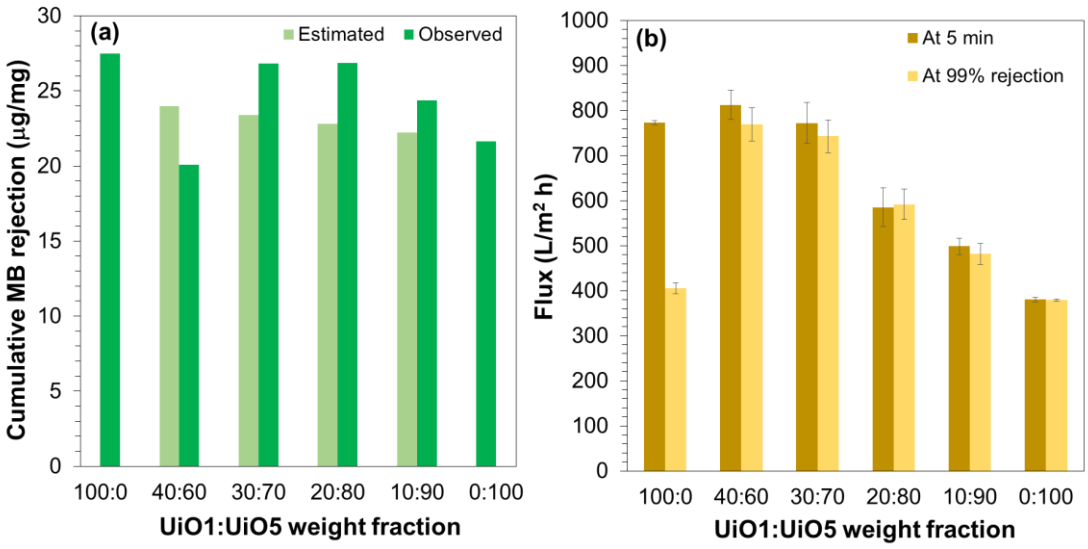

Figure 2-11**.** Filtration performance of bimodal composite membranes: a) Cumulative rejection for the filtration of 350 mL of the MB aqueous solution, and b) permeability compared by the flux values at the first 5 min and at the timing of the 99% rejection. The bimodal composite

membranes were prepared by depositing 4.0 mg of a mixture of UiO1 and UiO5 nanoparticles at different weight ratios.

2.4 Conclusions

The deposition of preformed nanoparticles onto a porous polymer support is a facile strategy to access a performant and flexible composite membrane having a semi-continuous selective layer of a metal-organic framework. In this chapter, a series of composite membranes were prepared by depositing UiO-66 nanoparticles onto a regenerated cellulose support, and the impacts of the size and its distribution of the nanoparticles were examined on the membrane performance for nanofiltration. Excellent permeability of 400-1200 L/m^2 h and rejection of 22-94 mg of methylene blue per gram of UiO-66 were obtained, where the origin of the selective permeation was attributed to the nanochannels of UiO-66. At a fixed loading of UiO-66 nanoparticles, smaller nanoparticles tended to form a selective layer having better permeability and selectivity. The former was explained by a larger external surface area of the microscopically corrugated selective layer, and the latter was mostly due to the creation of narrower interparticle voids. The utilization of larger nanoparticles was inferior to smaller ones in terms of the flux and rejection, but it greatly suppressed the membrane fouling. When the UiO-66 nanoparticles having two different sizes were co-deposited at an appropriate weight ratio, the resultant selective layer was found to equip the best level of the permeability, selectivity and fouling resistance. In conclusion, the present chapter successfully demonstrates promising aspects of the new type of MOF-based composite membranes for nanofiltration: Excellent performance is realized based on facile production and easy optimization through the size distribution of MOF nanoparticles, that can be ex-situ prepared.

2.5 References

[1] Zhang, R.; Liu, Y.; He, M.; Su, Y.; Zhao, X.; Elimelech, M.; Jiang, Z. Antifouling Membranes for Sustainable Water Purification: Strategies and Mechanisms. Chem. Soc. Rev. **2016**, 45, 5888−5924.

[2] Shon, H. K.; Phuntsho, S.; Chaudhary, D. S.; Vigneswaran, S.; Cho. J. Nanofiltration for Water and Wastewater Treatment **-** A Mini Review. Drink**.** Water Eng. Sci. **2013**, 6, 47–53**.**

[3] Ulbricht, M**.** Advanced Functional Polymer Membranes. Polymer **2006**, 47, 2217–2262**.**

[4] Ng, L.Y.; Mohammad, A .W.; Leo, C. P.; Hilal, N. Polymeric Membranes Incorporated with Metal/Metal Oxide Nanoparticles**:** A Comprehensive Review. Desal. **2013**, 308, 15–33.

[5] Nguyen, T.; Roddick, F. A.; Fan, L. Biofouling of Water Treatment Membranes**:** A Review of the Underlying Causes, Monitoring Techniques and Control Measures. Membr. **2012**, 2, 804**-**840.

[6] Anim**-**Mensah, A.; Govind, R. Prediction of Polymeric Membrane Separation and Purification Performances*:* A Combined Mechanical, Chemical and Thermodynamic Model for Organic Systems; Springer**:** 2015, pp. 5–15**.**

[7] Geise, G. M.; Park, H. B.; Sagle, A. C.; Freeman, B. D.; McGrath, J.E. Water Permeability and Water/Salt Selectivity Tradeoff in Polymers for Desalination. J. Membr. Sci. **2011**, 369, 130–138.

[8] Lee, A.; Elam, J. W.; Darling, S. B. Membrane Materials for Water Purification**:** Design, Development, and Application**.** Environ**.** Sci. Water Res. Technol. **2016**, 2, 17–42.

[9] Mohmood, I.; Lopes, C. B.; Lopes, I.; Ahmad, I.; Duarte, A. C.; Pereira, E. Nanoscale Materials and Their Use in Water Contaminants Removal - A Rev. Environ. Sci. Pollut. Res. **2013**, 20, 1239–1260.

[10] Kumar, S.; Ahlawat, W.; Bhanjana, G.; Heydarifard, S.; Nazhad, M. M.; Dilbaghi, N. Nanotechnology-Based Water Treatment Strategies. J. Nanosci. Nanotechnol. **2014**. 14, 1838–1858.

[11] Whitby, M.; Quirke, N. Fluid Flow in Carbon Nanotubes and Nanopipes. Nat. Nanotech**.** **2007**, 2, 87–94.

[12] Joshi, R. K.; Carbone, P.; Wang, F. C.; Kravets, V. G.; Su, Y.; Grigorieva, I. V.; Wu, H. A. Geim, A. K.; Nair, R. R. Precise and Ultrafast Molecular Sieving Through Graphene Oxide Membranes**.** Sci. **2014**, 343, 752–754**.**

[13] Han, Y.; Jiang, Y.; Gao, C. High-Flux Graphene Oxide Nanofiltration Membrane Intercalated by Carbon Nanotubes**.** ACS. Appl. Mater. Interfaces **2015**, 7, 8147−8155.

[14] Nair, R. R.; Wu, H. A.; Jayaram, P. N.; Grigorieva, I. V.; Geim, A. K. Unimpeded Permeation of Water Through Helium-Leak-Tight Graphene-Based Membranes. Sci. **2012**, 335, 442–444.

[15] Le, L. H.; Trinh, D. X.; Trung, N. B.; Tran, T. P. N.; Taniike, T. Fabrication of Assembled Membrane from Malonate-Functionalized Graphene and Evaluation of Its Permeation Performance. Carbon **2017**, 114, 519–525.

[16] Schneemann, A.; Bon, V.; Schwedler, I.; Senkovska, I.; Kaskel, S.; Fischer, R. A. Flexible Metal-Organic Frameworks. Chem. Soc. Rev. **2014**, 43, 6062–6096.

[17] Cheng, X.; Jiang, X.; Zhang, Y.; Lau, C. H.; Xie, Z.; Ng, D.; Smith, S. J. D.; Hill, M. R.; Shao, L. Building Additional Passageways in Polyamide Membranes with Hydrostable Metal Organic Frameworks to Recycle and Remove Organic Solutes from Various Solvents. ACS Appl. Mater. Interfaces **2017**, 44, 38877–38886.

[18] Lee, J-Y.; She, Q.; Huo, F.; Tang, C. Y. Metal-Organic Framework-Based Porous Matrix Membranes for Improving Mass Transfer in Forward Osmosis Membranes. J. Membr Sci**.** **2015**, 492, 392−399.

[19] Lu, W.; Wei, Z.; Gu, Z. -Y.; Liu, T. -F.; Park, J.; Park, J.; Tian, J.; Zhang, M.; Zhang, Q.; Gentle III, T.; Bosch, M.; Zhou, H.-C. Tuning the Structure and Function of Metal-Organic Frameworks via Linker Design**.** Chem. Soc. Rev. **2014**, 43, 5561–5593.

[20] Ma, J.; Guo, X.; Ying, Y.; Liu, D.; Zhong, C. Composite Ultrafiltration Membrane Tailored by MOF@GO with Highly Improved Water Purification Performance. Chem. Eng. J. **2017**, 313, 890−898.

[21] Li, W.; Zhang, Y.; Li, Q.; Zhang, G. Metal-Organic Framework Composite Membranes**:** Synthesis and Separation Applications. Chem. Eng. Sci. **2015**, 135, 232−257.

[22] Sun, H.; Tang, B.; Wu, P. Development of Hybrid Ultrafiltration Membranes with Improved Water Separation Properties Using Modified Superhydrophilic Metal-Organic Framework Nanoparticles**.** ACS Appl. Mater**.** Interfaces **2017**, 9, 21473−21484.

[23] Li, Y.; Wee, L. H.; Volodin, A.; Martens, J. A.; Vankelecom, I. F. J. Polymer Supported ZIF-8 Membranes Prepared via an Interfacial Synthesis Method**.** Chem**.** Commun. **2015**, 51, 918–920.

[24] Zhang, R.; Ji, S.; Wang, N.; Wang, L.; Zhang, G.; Li, J-R. Coordination-Driven In-Situ Self-Assembly Strategy for the Preparation of Metal-Organic Framework Hybrid Membranes. Angew. Chem. Int. Ed. **2014**, 53, 9775–9779.

[25] Shan, B.; James, J. B.; Armstrong, M. R.; Close, E. C.; Letham, P. A.; Nikkhah, K.; Lin, Y. S.; Mu, B. Influences of Deprotonation and Modulation on Nucleation and Growth of UiO-66**:** Intergrowth and Orientation. J. Phys. Chem. C. **2018**, 122, 2200–2206.

[26] Fuoco, A.; Khdhayyer, M. R.; Attfield, M. P.; Esposito, E.; Jansen, J. C.; Budd, P. M. Synthesis and Transport Properties of Novel MOF/PIM-1/MOF Sandwich Membranes for Gas Separation. Membr. **2017**, 7, 7.

[27] Trinh, D. X.; Tran, T. P. N.; Taniike, T. Fabrication of New Composite Membrane Filled with UiO-66 Nanoparticles and Its Application to Nanofiltration. Sep. Purif. Technol. **2017**, 177, 249–256.

[28] Wang, C.; Liu, X.; Demir, N. K.; Chen, J. P.; Li, K. Applications of Water Stable Metal-Organic Frameworks. Chem. Soc. Rev. **2016**, 45, 5107–5134.

[29] Furukawa, H.; Ko, N.; Go, Y. B.; Aratani, N.; Choi, S. B.; Choi, E.; Yazaydin, A. Ö.; Snurr, R. Q.; O'Keeffe, M.; Kim, J.; Yaghi, O. M. Ultrahigh Porosity in Metal-Organic Frameworks. Sci. **2010**, 329, 424–428.

[30] Wu, F.; Lin, L.; Liu, H.; Wang, H.; Qiu, J.; Zhang, X. Synthesis of Stable UiO-66 Membranes for Pervaporation Separation of Methanol/Methyl Tert-Butyl Ether Mixtures by Secondary Growth. J. Membr. Sci. **2017**, 544, 342–350.

[31] Liu, X.; Demir, N. K.; Wu, Z.; Li, K. Highly Water-Stable Zirconium Metal-Organic Framework UiO-66 Membranes Supported on Alumina Hollow Fibers for Desalination, J. Am. Chem. Soc. **2015**, 137, 6999–7002.

[32] Cavka, J. H.; Jakobsen, S.; Olsbye, U.; Guillou, N.; Lamberti, C.; Bordiga, S.; Lillerud, K. P. A New Zirconium Inorganic Building Brick Forming Metal Organic Frameworks with Exceptional Stability. J. Am. Chem. Soc. **2008**, 130, 13850–13851.

[33] Valenzano, L.; Civalleri, B.; Chavan, S.; Bordiga, S.; Nilsen, M. H.; Jakobsen, S.; Lillerud, K. P.; Lamberti, C. Disclosing the Complex Structure of UiO-66 Metal Organic Framework: A Synergic Combination of Experiment and Theory. Chem. Mater. **2011**, 23, 1700–1718.

[34] Kandiah, M.; Usseglio, S.; Svelle, S.; Olsbye, U.; Lillerud, K.P.; Tilset, M. Post-Synthetic Modification of the Metal-Organic Framework Compound UiO-66. J. Mater. Chem. **2010**, 20, 9848−9851.

[35] Cliffe, M. J; Wan, W.; Zou, X.; Chater, P. A.; Kleppe, A. K.; Tucker, M. G.; Wilhelm, H.; Funnell, N. P; Coudert, F. -X.; Goodwin, A. L. Correlated Defect Nanoregions in a Metal-Organic Frameworks. Nat. Commun. **2014**, 5, 4176–4178.

[36] DeCoste, J. B.; Peterson, G. W.; Schindler, B. J.; Killops, K. L.; Browe, M.A.; Mahle, J. J. The effect of Water Adsorption on the Structure of the Carboxylate Containing Metal-Organic Frameworks Cu-BTC, Mg-MOF-74, and UiO-66. J. Mater. Chem. A **2013**, 1, 11922−11932.

[37] DeCoste, J. B.; Peterson, G. W.; Jasuja, H.; Glover, T. G.; Huang, Y.; Walton, K. S. Stability and Degradation Mechanisms of Metal-Organic Frameworks Containing the $Zr_6O_4(OH)_4$ Secondary Building Unit. J. Mater. Chem. A. **2013**, 1, 5642–5650.

[38] Ragon, F.; Horcajada, P.; Chevreau, H.; Hwang, Y. K.; Lee, U.-H.; Miller, S. R.; Devic, T.; Chang, J.-S.; Serre, C. In-Situ Energy-Dispersive X-ray Diffraction for the Synthesis Optimization and Scale-Up of the Porous Zirconium Terephthalate UiO-66. Inorg. Chem. **2014**, 53, 2491–2500.

[39] de Souza Macedo, J.; da Costa Júnior, N. B.; Almeida, L. E.; da Silva Vieira, E. F.; Cestari, A. R.; de Fátima Gimenez, I.; Carreño, N. L.V.; Barreto, L. S. Kinetic and Calorimetric Study of the Adsorption of Dyes on Mesoporous Activated Carbon Prepared from Coconut Coir Dust. J. Colloid. Interface Sci. **2006**, 298, 515–522.

[40] Lennox, M. J.; Düren, T. Understanding the Kinetic and Thermodynamic Origins of Xylene Separation in UiO-66(Zr) via Molecular Simulation. J. Phys. Chem. C **2016**, 120, 18651−18658.

[41] Karan, S.; Jiang, Z.; Livingston, A. G. Sub-10 nm Polyamide Nanofilms with Ultrafast Solvent Transport for Molecular Separation. Sci. **2015**, 348, 1347–1351.

[42] Cui, Y.; Liu, X.-Y.; Chung, T-S. Ultrathin Polyamide Membranes Fabricated from Freestanding Interfacial Polymerization: Synthesis, Modifications, and Post-Treatment. Ind. Eng. Chem. Res. **2017**, 56, 513−523.

[43] Zhu, J.; Qin, L.; Uliana, A.; Hou, J.; Wang, J.; Zhang, Y.; Li, X.; Yuan, S.; Li, J.; Tian, M.; Lin, J.; Van der Bruggen, B. Elevated Performance of Thin Film Nanocomposite Membranes Enabled by Modified Hydrophilic MOFs for Nanofiltration. ACS. Appl. Mater. Interfaces **2017**, 9, 1975−1986.

[44] de Souza Araki, M.; deMorais Coutinho, C.; Gonçalves, L. A. G.; Viotto, L. A. Solvent Permeability in Commercial Ultrafiltration Polymeric Membranes and Evaluation of the Structural and Chemical Stability Towards Hexane. Sep. Purif. Technol. **2010**, 71, 13–21.

[45] Van der Bruggen, B.; Vandecasteele, C. Flux Decline during Nanofiltration of Organic Components in Aqueous Solution. Environ. Sci. Technol. **2001**, 35, 3535–3540.

[46] Jiang, Y.; Wang, W.N.; Liu, D.; Nie, Y.; Li, W.; Wu, J.; Zhang, F.; Biswas, P.; Fortner, J. D. Engineered Crumpled Graphene Oxide Nanocomposite Membrane Assemblies for Advanced Water Treatment Processes. Environ. Sci. Technol. **2015**, 49, 6846−6854.

[47] Zhang, P.; Gong, J. -L.; Zeng, G. -M.; Deng, C. -H.; Yang, H-C.; Liu, H-Y.; Huan, S.Y. Cross-linking to Prepare Composite Graphene Oxide-Framework Membranes with High-Flux for Dyes and Heavy Metal ions Removal. Chem. Eng. J. **2017**, 322, 657– 666.

[48] Wang, X.; Zhai, L.; Wang, Y.; Li, R.; Gu, X.; Yuan, Y. D.; Qian, Y.; Hu, Z.; Zhao, D. Improving Water-Treatment Performance of Zirconium Metal-Organic Framework Membranes by Postsynthetic Defect Healing. ACS Appl. Mater. Interfaces **2017**,9, 37848−37855.

[49] Cao, J.; Su, Y.; Liu, Y.; Guan, J.; He, M.; Zhang, R.; Jiang, Z. Self-Assembled MOF Membranes with Underwater Superoleophobicity for Oil/Water Separation. J. Membr. Sci. **2018**, 566, 268−277.

[50] Ang, H.; Hong, L. Polycationic Polymer-Regulated Assembling of 2D MOF Nanosheets for High-Performance Nanofiltration. ACS. Appl. Mater. Interfaces **2017**, 9, 28079−28088.

[51] Meng, L.; Lu, P.; Li, S. Packing Properties of Binary Mixtures in Disordered Sphere Systems. Particuology **2014**, 16, 155–166.

Chapter 3

Pore Engineering of UiO-66 Nanoparticles and Applications to Nanofiltration

3.1 Introduction

Most membranes designed for nanofiltration utilize pressure driven processes, which remove sub-micron or sub-nanometer scale solute from feed stream (e.g. cell debris from a biomolecule solution, hydrated salts from water) based on solution-diffusion mechanism. [1-4]. Recent research interests in this area have been directed towards designing new class of membranes, which utilize engineered nanoparticles with well-defined and/or oriented pores/channels for higher permeability and rejection [5,6].

Therefore, designing composite membranes based on deposition of chemically stable UiO-66-metal-organic frameworks (MOF) on a porous polymer substrate has recently been discovered as a promising approach which resulted in highly permeable, size-selective, stable, and flexible composite membranes [7-10]. The remarkable performance of these composite membranes in nanofiltration processes are due to ability of the deposited nanoparticles to offer pore network in form of nanochannels [11-13]. These deposited nanoparticles have been found to enhance the hydrophilicity and antifouling characteristics of polymeric substrate and most importantly, they offer a predominant permeation network for filtrates with excellent rejection ability for solutes at low operating pressure through nanochannels [14,15]. For instance, Dai *et al* [16] strategically developed a novel method to form MOF-based composite membrane for nanofiltration, in which a suspension of UiO-66 nanoparticles as one of most stable frameworks was deposited onto a regenerated cellulose (RC) support membrane via suction filtration. The nanoparticles were found to fill into pore network and exhibited an excellent permeability of 7860±374 L/m^2 h and almost 100% rejection for filtration of methylene blue (MB) aqueous solution. This excellent performance was attributed to dominant permeation through the selective nanochannels of deposited UiO-66 in contrast to non-selective leakage through interparticle voids among the nanoparticles. In chapter 2, [17] a semi-continuous selective layer

of composite membranes using a series of UiO-66 nanoparticles with different average particle size was designed. These were synthesized using water as a modulator in nucleation and growth of the nanoparticles. It was found that size and packing of UiO-66 nanoparticles had great influences on performance of the composite membranes for filtration of MB solution. Smaller nanoparticles with a greater external surface area provided a selective layer, which was superior in terms of flux and rejection, whilst deposition of larger nanoparticles afforded a selective layer having more tolerance for fouling. Due to this excellent performance realized from facile production and easy of optimization by size distribution of UiO-66 MOF nanoparticles achieved through *ex-situ* preparation, processing and design of water filtration membrane for large-scale filtration, separations, purification technologies would in nearest future achieved through this method.

Given vast possibilities that other MOFs materials could offer in terms of design and together with their intrinsic hybrid nature, recent researches have revealed the use of other nanochannel materials like carbon nanotubes [18-20], graphene [21,22] for water filtration/desalination membranes. These monodisperse nanoparticles of different size variation have gained much attention, due to their novel and high-performance dependence on the properties like nanoparticles dimension, surface area, and stability. Their unique properties result in a great possibility for number of applications. For instance, Zhang *et al,* [23] synthesized a functionalized multi-walled carbon nanotube (MWCNTs)-incorporated polyamide-based selective layer in a RO membrane, which exhibited a significantly increased water flux, from 26 L m^{-2} h^{-1} with the original membrane to 71 L m^{-2} h^{-1} with the MWCNTs-blended membrane.

Nevertheless, in most of these experimentally designed membranes for filtration purposes, the investigations has been geared towards understanding process of size sieving mechanism

mainly. In addition, most of these studies focuses on physical aspect of MOFs' filtration performance such as surface area, pore size, and pore volume. Apart from a high surface area and specialized pore volume, their chemical environment can be fine-tuned by selecting appropriate building unit in MOFs synthesis. Thus, the influence of chemical environment of pore on permeation and selectivity in filtration needs to be systematically investigated. However, this has rarely been attempted for MOF based composite membranes, though many membrane materials are believed to exhibit at least some electrostatic contributions to their separation [24,25]. Paradoxically, few studies to date have reported influence of hydrophilicity of functional groups on pore surface or trace in-pore chemistries within UiO-66-MOFs and other nanochannel materials on their filtration performance. Although investigation of influence of MOF pore environments on solute molecular dynamics is difficult, it is essentially important for understanding of intrinsic selectivity properties for improving MOF design practices and grasping the nature of interactions [26-30].

In general, primary factors that affect performance of membranes include physical and chemical nature of membrane materials, interaction between selective layer and support membrane, concentration polarization at membrane surface, and fouling of membrane [20,31-33]. Pore size alone however, does not fully control rejection of solute constituents and hence the need to study chemical environment around nanopore is vital. Therefore, the objective of this chapter is systematic investigation on design principle for MOF-deposited composite membranes for nanofiltration. This is achieved through:

(i) Tuning of pore environment of nanoparticles via manipulation of pore surfaces using modified ligands 2-amino/methyl-terephthalic acids linkers for the synthesis.

(ii) Investigation of their effects for nanofiltration and chemical selectivity.

3.2 Experimental

3.2.1 Materials and methods

Zirconium tetrachloride ($ZrCl_4$, 99%) and 2-amino terephthalic acid (99%) were purchased from Sigma-Aldrich. 2-Methylterephthalic acid (97.2%) was obtained from J &H Chemicals Co. Ltd. N,N-dimethylformamide (DMF) and methanol (MeOH) as solvents were purchased from Wako Chemical Industries Ltd. Methylene blue (MB, 98.5%) was purchased from Kanto Chemical Co Inc. Regenerated cellulose membrane (RC 58, diameter 47 mm and pore size 0.2 µm) was obtained from Whatmann G.E Healthcare; Germany and used as a support membrane. Deionized (DI) water was used throughout the experiments.

3.2.2 Preparation of UiO-66-X nanoparticles

Under controlled N_2 atmosphere, a solution of $ZrCl_4$ (1.63 mmol) in 30 mL of DMF was added to a solution of 2-aminoterephthalic acid (2.28 mmol) or 2-methylterephthalic acid (1.5 mmol) in 30 mL of DMF. The chemicals were mixed with aid of ultrasonnication. Thereafter, a specified amount of DI water 0.1-1.2 mL was added. The mixture was heated at 100 °C for 12 h at constant stirring under N_2 atmosphere to yield yellowish and milky dispersion of UiO-66-X (X= NH_2/CH_3) as for UiO-66-NH_2 and UiO-66-CH_3, respectively. The resulting solid products were isolated by centrifugation and extensively washed with MeOH to remove the residual DMF. Then, the solvent was exchanged with 50 mL fresh MeOH each day for three consecutive days. The purified samples was dried under vacuum at 90 °C for 24 h. The obtained samples were named as UiO1-NH_2–UiO6-NH_2 and UiO1-CH_3–UiO6-CH_3 correspond to the addition of 0.9, 0.7, 0.6, 0.5, 0.3, 0.1 mL, and 1.2, 0.9, 0.7, 0.6, 0.5, 0.3 mL of water respectively.

3.2.3 Characterization of UiO-66-X nanoparticles

Crystalline structure of UiO-66-X nanoparticles was analysed by X-ray diffraction (XRD, Rigaku SmartLab) using Cu Kα radiation in the range of 2θ = 5-35° at step increment of 0.1° per 150 s. The crystallite size (D) of the nanoparticles were estimated using Scherrer's equation:

$$D = \frac{0.94\,\lambda}{\beta \cos\theta} \quad (1),$$

where λ = 1.54 Å for Cu Kα, β = full-width at half-maximum, and θ = Bragg's angle. Fourier transform infrared spectra (FTIR) were acquired on a Jasco FT/IR-6100 spectrometer in the range of 400−2400 cm^{-1} with a resolution of 4 cm^{-1}. The dried sample was diluted with potassium bromide powder, and then pressed into a pellet for the measurement in the transmission mode. The morphology of UiO-66-X nanoparticle was observed on a transmission electron microscope (TEM, Hitachi H6750) at an accelerated voltage of 100 kV. A dried sample was dispersed in MeOH, deposited onto a copper grid by drop casting, and then dried under air to evaporate solvent. The particle size was acquired based on the TEM image analysis using ImageJ software. N_2 adsorption and desorption isotherms of engineered nanoparticles were acquired at 77 K using BELSORP mini-HS II instrument (BEL JAPAN, Inc.). About 30 mg of sample was charged into a sample cell and sealed with brass filler and rubber cap. The sample was outgassed at 180 ºC for 24 h in vacuo prior to measurement. Surface area was calculated by fitting the isotherm data in the P/P_o range of 0-1 using Langmuir model that was built-in in the BELMaster7™ software. Thermogravimetric analysis (TGA) was performed on ThermoPlus EVO II (Rigaku) thermal analysis. The sample was loaded on an alumina pan and the TGA measurements were run up to 800 °C at a temperature ramping rate of (10 °C/min) under a flow of dry air at rate of 100 mL/min. These conditions ensured that complete

combustion of organics and conversion of zirconium (IV) to it oxide occurred. The weight at 800 °C was normalized to 100% in order to quantify defects (missing clusters).

3.2.4 Preparation and characterization of composite membranes

Composite membranes of UiO-66-X (X= NH_2/CH_3) were prepared by suction filtration. A RC substrate membrane was placed on a filter glass holder and wet with DI water. A specified amount of the nanoparticles was dispersed in 30 mL of DI water by sonication for 1 h, and then deposited on the pre-wetted RC support substrate by suction filtration at a constant differential pressure of 50 mbar. After 30 min of filtration, the differential pressure was increased to 100 mbar and kept for 15 min to partially dry the membrane. The morphology of the prepared composite membranes were observed by scanning electron microscope (SEM, Hitachi S-4100) operated at an accelerated voltage of 20 kV.

3.2.5 Filtration performance

The RC membrane was placed in a filtration cell of 100 mL in volume. An aqueous solution of MB (1.0 µM) was suction filtered at a differential pressure of 100 mbar. A fixed volume of the filtrate was sampled every 1 or 2 min and the concentrations in the feed and permeate solution were determined by UV-Vis spectroscopy (Jasco V670) measurements based on the absorption intensity at 665 nm wavelength. The rejection (R) was calculated using Eq.

$$R\ (\%) = \left(\frac{C_0 - C_p}{C_0}\right) \times 100 \qquad (2),$$

The flux was determined from the cumulative permeate volume at the specified filtration time as shown in Eq. (3):

$$J = \left(\frac{V}{A \times t}\right) \qquad (3)$$

where J represents the flux (L/m^2 h), V is the cumulative permeate volume, A is the effective membrane area (calculated as 9.61 cm^2), and t is the filtration time. The results were obtained as an average from at least two filtration experiments using independently prepared membranes.

3.3 Results and discussion

3.3.1 Synthesis and Characterization of UiO-66-X nanoparticles

A series of UiO-66-X (X= NH_2/CH_3) nanoparticle samples were prepared by varying the addition amount of water at the fixed molar ratio of $ZrCl_4$ and 2-amino/methyl-terephthalic acid during the synthesis. The crystallinity and phase purity of as-synthesized samples were examined by XRD. The peaks at 2θ of 7.4, 8.8, 12.2° correspond to (111), (200), (222) planes, respectively as shown in Figure 3-1a. These peaks demonstrated good agreement with UiO-66 parent crystal, thus confirming the formation of the pure crystal phase [17-20,34]. As can be seen, most of the patterns of the sample contain a minor peak at 2θ = 6°. This peak is originated from **reo** nanoregions (secondary crystalline phase) as observed by Goodwin and co-workers [35]. The intensity of the **reo** peak (relative to that of UiO-66) is correlated with the concentration of missing cluster defects in the sample. This secondary crystalline phase originated from either missing clusters/linkers became more prominent in the absence of a sufficient amount of water as a modulator. Whilst in the case of UiO-66-CH_3, the peaks are observed at 2θ = 7.4, 8.7, 12.1° corresponding to the (111), (200), (311) planes respectively. The **reo** nanoregions (secondary crystalline phase) was also observed at 2θ = 5.9°, which showed an increasing intensity as water amount decreases as seen in Figure 3-1b. However, at the highest water amount, the peak intensity of the **reo** nanoregions significantly reduced and therefore it was observed that the use of water as modulator significantly enhance crystallinity in both UiO-66-CH_3 and UiO-66-NH_2 [19,34]. Therefore, it shows that water accelerates nucleation rate of Zr_6O_4 $(OH)_4$ cluster by sol-gel reaction leading to growth of crystals.

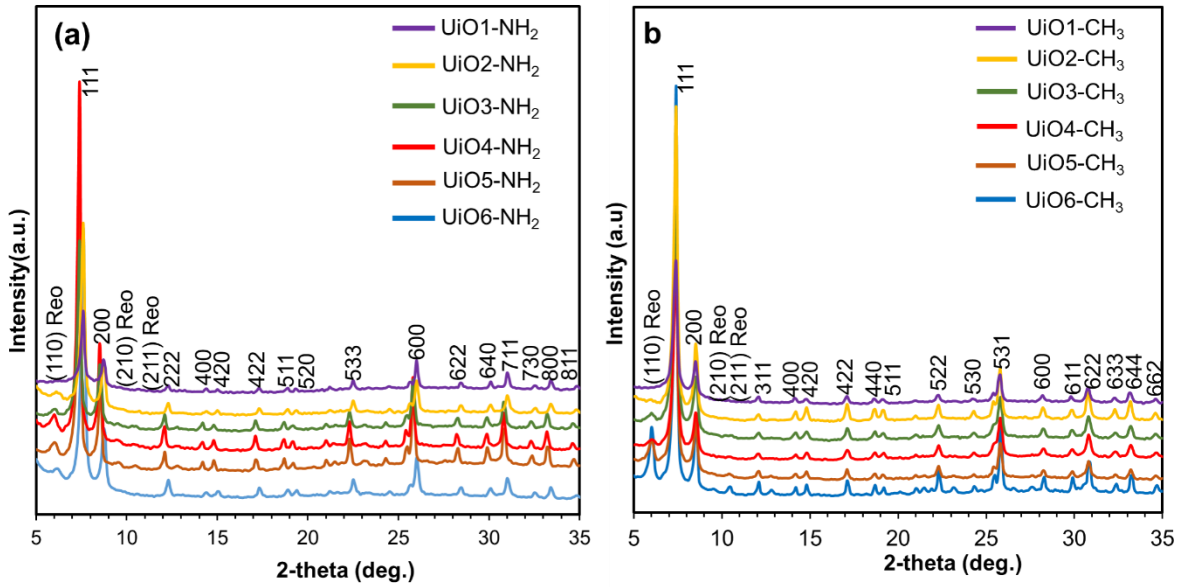

Figure 3-1. XRD patterns of modified UiO-66 samples.

The functional groups present in prepared UiO-66-NH_2 samples are as assigned in Figure 3-2a. From the figure, it is possible to distinguish two characteristic bands of amino group: medium intensity of NH_2 bending vibration observed at 1338 cm^{-1}, 1428 and strong C-N stretching vibration distinctive of aromatic amines observed at 1258 cm^{-1}. This assignment has been confirmed by the FTIR spectrum of the parent UiO-66 sample. The bands at 1567 cm^{-1} and 1385 cm^{-1} correspond to symmetric and asymmetric stretchings of O-C-O in carboxylate groups coordinated with zirconium metal centre. The band at 1498 cm^{-1} is ascribed to C=C vibration of the aromatic ring [13,19,35,36]. The characteristic band at 765 cm^{-1} is ascribed to a mixture of OH and C-H vibrational bendings [19], whilst those at 664, 655, 473 cm^{-1} are assigned to Zr(O-C) streching and μ_3-OH streching, which indicates successful synthesis of UiO-66-NH_2. Similarly, parent UiO-66 sample was compared with with that of UiO-66-CH_3 as shown in Figure 3-2b. FTIR spectrum of UiO-66-CH_3 which showed strong out-of-phase carboxylic -CO- peak at 1496 cm^{-1}, and O-C-O stretchings at 1581 cm^{-1} indicating strong reaction coordination of terephthalic acid ligand with the zirconium metal. Whilst the strong

doublet peaks at 1378 cm^{-1} and 1407 cm^{-1} represent the C-C vibration of CH_3 from aromatic ring. The characteristic peak at 762 cm^{-1} is ascribed to a mixture of the OH and C-H vibrational bendings [19] and bands at 664 cm^{-1}, 567 cm^{-1}, 467 cm^{-1} are assigned to Zr(O-C) streching and μ_3-OH streching, which indicates successful synthesis of UiO-66-CH_3 [12,13,19,37].

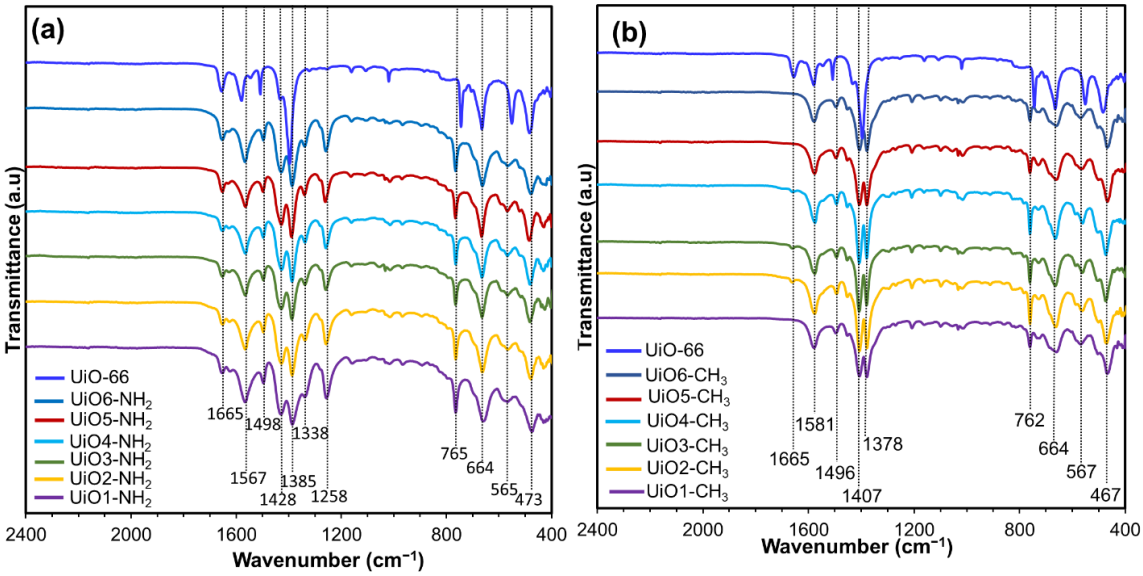

Figure 3-2. IR spectra of modified UiO-66 samples.

Table 3-1. Characteristic of UiO-66-X nanoparticles.

Sample	Water amount[a] (mL)	Crystallite size from XRD[b] (nm)	Particle size from TEM[c] (nm)	Sample	Water amount[a] (mL)	Crystallite size from XRD[b] (nm)	Particle size from TEM[c] (nm)
UiO1-NH_2	0.90	40	61±14	UiO1-CH_3	1.2	43	89±11
UiO2-NH_2	0.70	41	78±08	UiO2-CH_3	0.9	34	107±08
UiO3-NH_2	0.60	51	98±11	UiO3-CH_3	0.7	35	109±12
UiO4-NH_2	0.50	59	113±09	UiO4-CH_3	0.6	40	115±14
UiO5-NH_2	0.30	88	124±16	UiO5-CH_3	0.5	41	138±21
UiO6-NH_2	0.10	51	142±07	UiO6-CH_3	0.3	47	151±19

[a]Water amount added; [b]Determined using Scherrer's equation based on the (002) plane.
[c]Median particle size acquired from TEM images using ImageJ software.

The morphology of UiO-66-X nanoparticles (X= NH_2/CH_3) were observed by TEM and particle sizes were acquired from the TEM images using ImageJ software as listed in Table 1. The average size of the particles were distributed in the range between 150-60 nm as presented in the Table 1. Though not perfect, the particle sizes were found to increase along the decrease in the quantity of added water which demonstrated by the XRD crystallite size measured from XRD data. As can be seen in Figure 3-3a, the TEM images exhibited morphology of symmetrical triangular base pyramid crystals shapes. The crystal morphology in this work was found to be similar to those reported in the literature [14,38]. The dependence of the particle size on water amount clearly demonstrated the role of water to accelerate formation of crystal nuclei as reported by [35,39,40]. Ragon et al [41] reported that crystallization of UiO-66 became significantly faster in presence of water, which was ascribed to ease of Zr_6-cluster formation. This was also evident by the formation of a more turbid solution when a large amount of water was added during the synthesis.

In the same vein, particle size of UiO-66-CH_3 sample was found to be dependent on water amount addition, leading to an octahedral (quasi-spherical morphology) of the particles [38,42-44] as shown in Figure 3-3b. Depending on the water amount, the average size of the particle

varied in the range of 160-90 nm as in Table 1. Therefore, it has been determined that by using analogous synthetic conditions and simply changing the amount of water one can realize size-controlled nanoparticle formation.

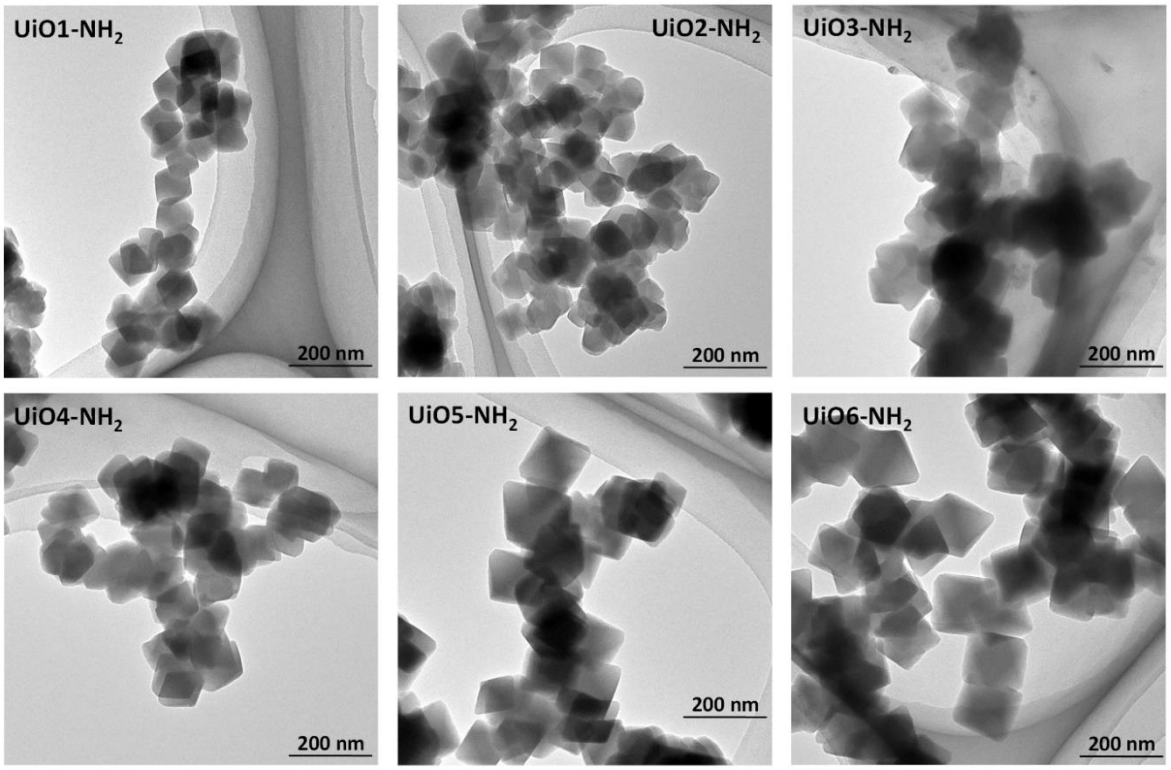

Figure 3-3a. TEM images of UiO-66-NH_2 nanoparticles.

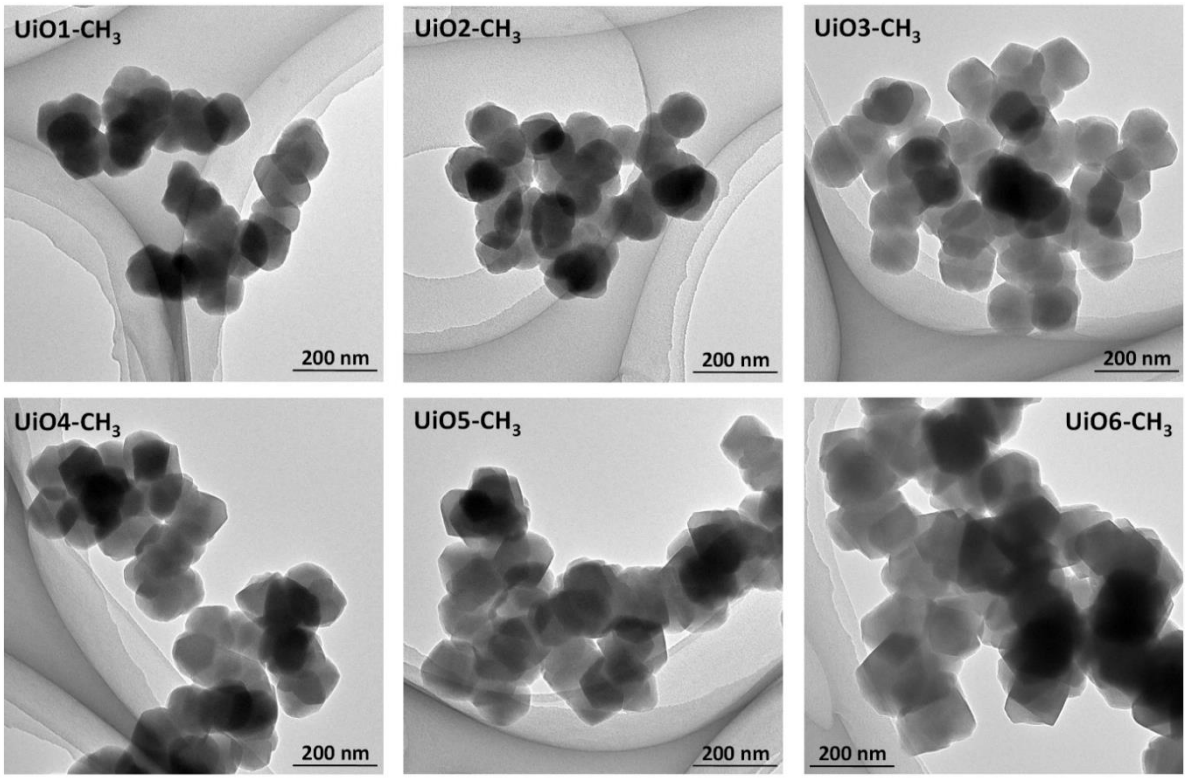

Figure 3-3b. TEM images UiO-66-CH_3 nanoparticles.

N_2 adsorption/desorption isotherms for the three kind of MOFs frameworks are presented in Figure 3-4. The adsorption showed a steep increment at a very low relative pressure (below P/P_o=0.05) irrespective of framework type and water amount. This corresponded to the filling of intraparticle channels. After this filling, the N_2 adsorption occurred only through the multilayer adsorption on external surfaces of the nanoparticles, and therefore, the increment became significantly marginal against the pressure. The slight increase in N_2 uptake could be attributed to the presence defects in the MOF [21,38]. The BET surface area and the pore volume were respectively estimated in the range of 800-1000 m^2/g and 0.37-0.44 m^3/g without clear tendency on the framework type and the water amount (Table 3-2). This suggested that

N_2 adsorption/desorption behaviors of UiO-66 nanoparticles were mostly originated from those for the perfect crystal.

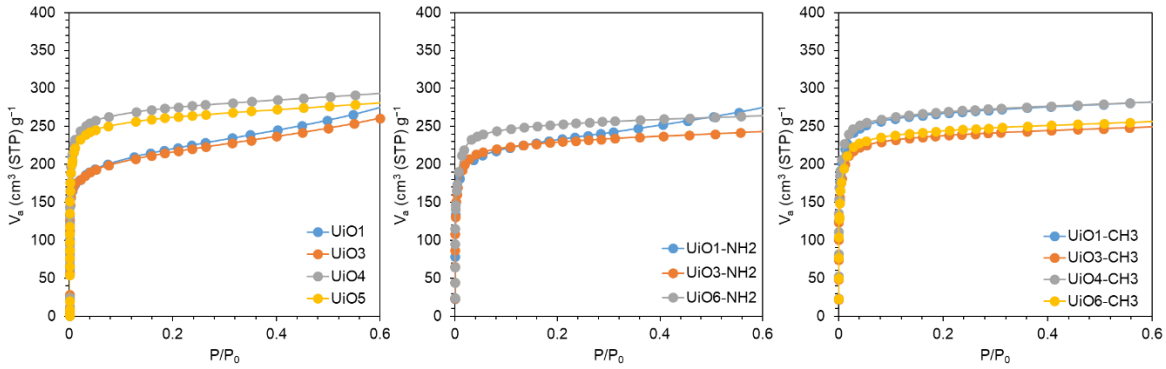

Figure 3-4. N_2 adsorption/desorption isotherms of some selected nanoparticles.

Table 3-2. Surface area and pore volume of selected UiO-66, UiO-66-NH_2 and UiO-66-CH_3 nanoparticles

Sample	BET surface area (m^2/g)	Pore volume at P/P0 = 0.4 (cm^3/g)
UiO1	803	0.380
UiO3	799	0.367
UiO4	1060	0.442
UiO5	1010	0.422
UiO1-NH2	861	0.390
UiO3-NH2	867	0.367
UiO6-NH2	958	0.402
UiO1-CH3	1010	0.427
UiO3-CH3	915	0.379
UiO4-CH3	1035	0.428
UiO6-CH3	925	0.389

The grand canonical Monte Carlo method software was employed to calculate pore size distribution of selected samples of different frameworks as shown in Figure 3-5. This method has been widely used for MOFs as it covers from micro to mesoporous range based on a unified theory. Consistent to N_2 adsorption/desorption isotherms; the pore size distribution was however not depended on water amount addition. It was observed that irrespective of

frameworks or ligand functionalization, the pore size distribution was sharply concentrated in the range of 0.7-0.8 nm, in good agreement with the theoretical pore size.

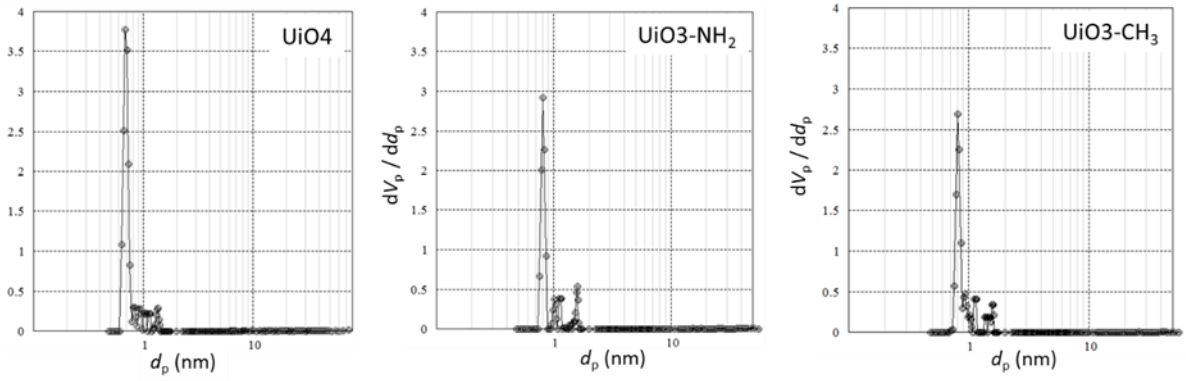

Figure 3-5. Pore size distribution for selected samples nanoparticles.

TGA has been widely used for estimating amount of structural defects contained in MOFs caused by missing clusters/linkers. A typical representation of TGA thermogram for UiO-66 family with general formula $Zr_6O_4(OH)_4BDC_6$, (where BDC is 1, 4-benzenedicarboxylate linker) is as shown in Figure 3-6. The heating of UiO-66 nanoparticles under O_2 causes three-step mass losses, which are i) solvent evaporation, ii) dehydroxylation, and iii) ligand decomposition from low to high temperature. The dehydroxylation is typically completed upto 200-300 °C, and this can change the chemical composition of UiO-66 into $Zr_6O_6BDC_6$. The ligand decomposition usually proceeds together with the oxidation of ZrO (Zr_6O_6) into ZrO_2 as final product. In both missing linkers and missing clusters, there is reduction of coordination number of a Zr_6O_4 $(OH)_4$ cluster against BDC [45-50]. From the profile, mass of the remaining ZrO_2 was set to X=1, and the mass gain by the oxidation was calculated as:

$$Z = 15.999/123.218 \quad (1)$$

The mass loss by the ligand decomposition is then derived from

$$Y \text{ (observed mass loss)} + 0.130 \quad (2)$$

The average coordination number (CN_{avg}) is expressed by

$$CN_{avg} = 12\ (Y+0.130) \times (\text{MW of } ZrO_2)/(\text{MW of BDC}) \quad (3)$$

However, for defect-free UiO-66, mass before the ligand decomposition (X+Y) is theoretically calculated as

$$1 + 12/12 \times (\text{MW of BDC})/(\text{MW of } ZrO_2) - 0.130 \quad (4)\ ,$$

where MW is molecular weight of BDC and ZrO_2 respectively.

This therefore leads to 2.20, 2.45, and 2.53 for normal UiO-66, UiO-66-NH_2, and UiO-66-NH_3, respectively. For a missing linker per cluster (i.e. CN=11) reduces the value of (X+Y) to 2.09, 2.31, and 2.39, respectively. This leads to 2.20, 2.45, and 2.53 for normal UiO-66, UiO-66-NH_2, and UiO-66-NH_3, respectively.

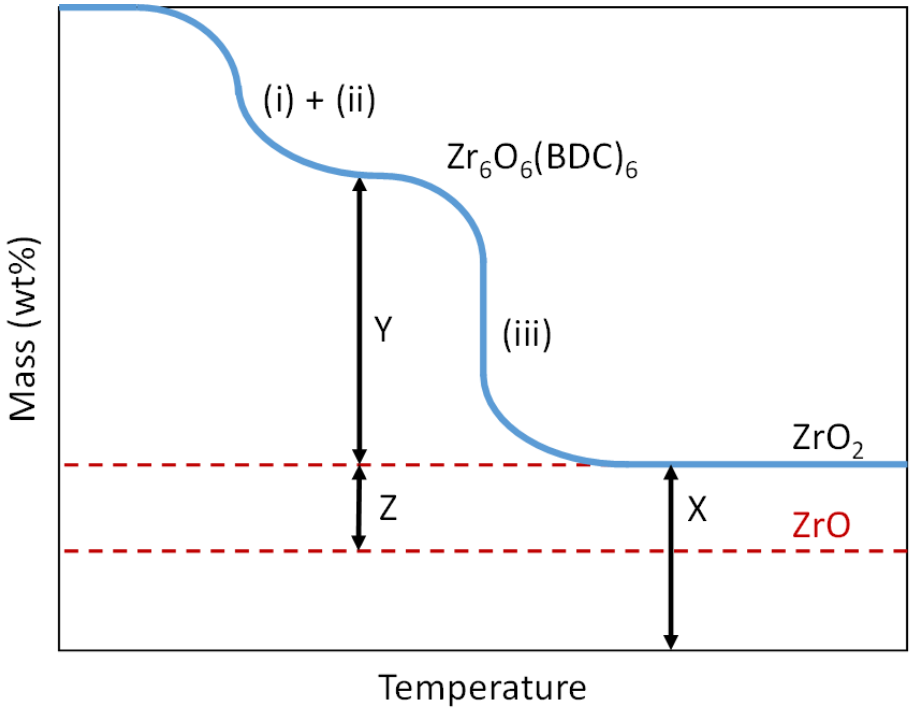

Figure 3-6. Typical mass loss curve of UiO-66.

Figure 3-7 therefore summarizes TGA results for three kinds of UiO-66 frameworks, where the mass change relative to the residual ZrO_2 was normalized to the remaining contents as represented. The ligand decomposition stability of the framework was found to have improved in the order of UiO-66-NH_2<< UiO-66-CH_3 < UiO-66. Comparing the decomposition temperatures among frameworks, it can be seen that basic UiO-66 frameworks decomposition starts around 350-550 °C while UiO-66-CH_3, UiO-66-NH_2 at 400°C, 300°C respectively. The lowest stability of UiO-66-NH_2 was attributed to inductive effect as results of functional groups presence on the benzene ring that tend, which withdraw electron. For example, the nitrogen atoms tends to withdraw electrons inductively and thereby weakens the neighboring carbon–carbon bonds, causing thermal breakdown of ZrMOFs at lower temperatures in the case of ZrMOF–NH_2 frameworks [11,51,52]. The black line (Figure 3-7) represented the theoretical organic decomposition amount for perfect crystals. The decrease in decomposition shows that the framework is more defective. Therefore, from Figure 3-7 it was observed that within the same type of frameworks, ligand decomposition temperature was found to be independent of added water amount (or particle size). However, the weight loss due to the ligand decomposition was found to have changed by addition of water amount. This was because when water amount was not sufficient, thus weight loss tended to be reduced, corresponding to formation of more missing linkers and/or clusters [50]. It was also found that an insufficient amount of water might have slowed down cluster formation, thereby resulting into bridging of incomplete clusters by ligand to form defective structures [50,52]. However, at sufficient water amount, addition, the weight before ligand decomposition became closer to that of perfect crystal for un-functionalized UiO-66. For instance, UiO-66-CH_3 weight before the ligand decomposition was around 2.3, which corresponded to coordination number of 10-11. Similarly, the coordination number was estimated around 11 in the case of UiO-66-NH_2. In

anyway, the presence of side functional groups enhances the defect formation probably because of increased bulkiness [19,49,50].

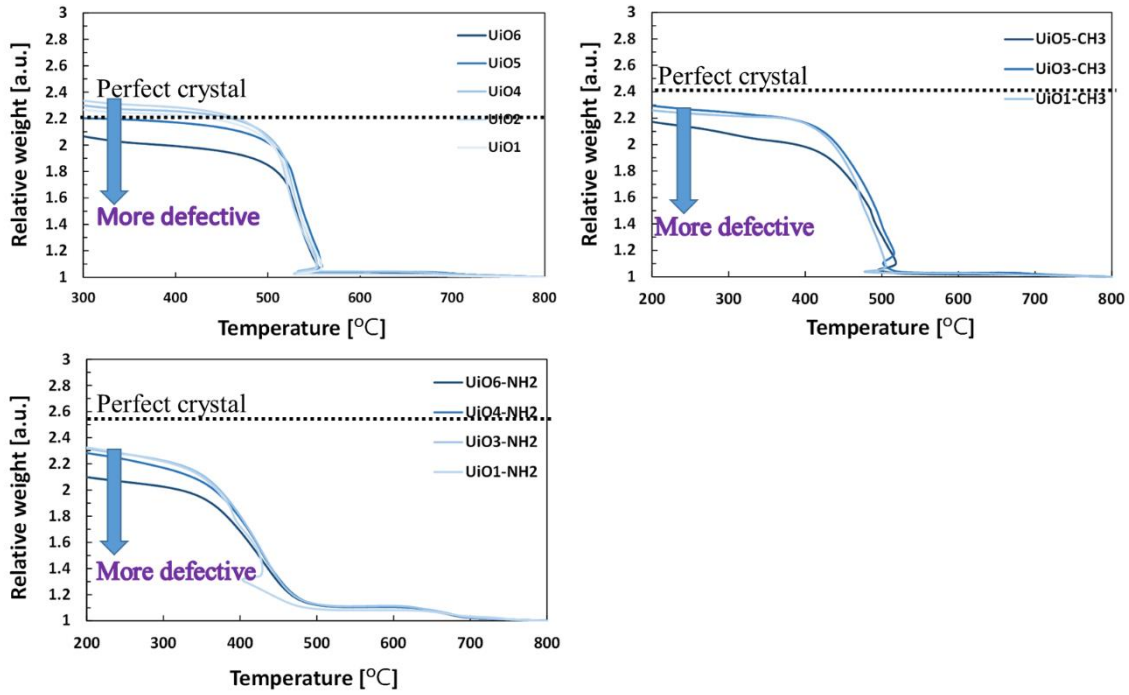

Figure 3-7. Organic content with respect to residual ZrO_2 of some selected nanoparticles.

Top-view images SEM images of composite membrane prepared using UiO1-NH_2–UiO6-NH_2 are shown in Figure 3-8. It shows strange and interesting crystals for some of UiO-66-NH_2 that existed as individual with distinct edges and exhibited a similar homogeneous crystalline morphology that are connected with neighbouring particles. The interconnection among the crystals were found to vary according to the water amount used in the synthesis of the nanoparticles. This revealed small increase in size of interparticle voids as the nanoparticles were homogeneously packed on the substrate membrane. Therefore, the smaller particles packing of UiO1-NH_2, UiO2-NH_2 on the surface of the substrate created no voids as compared to larger particles of UiO3-NH_2–UiO6-NH_2, thus may lead to an efficient nanofiltration performance.

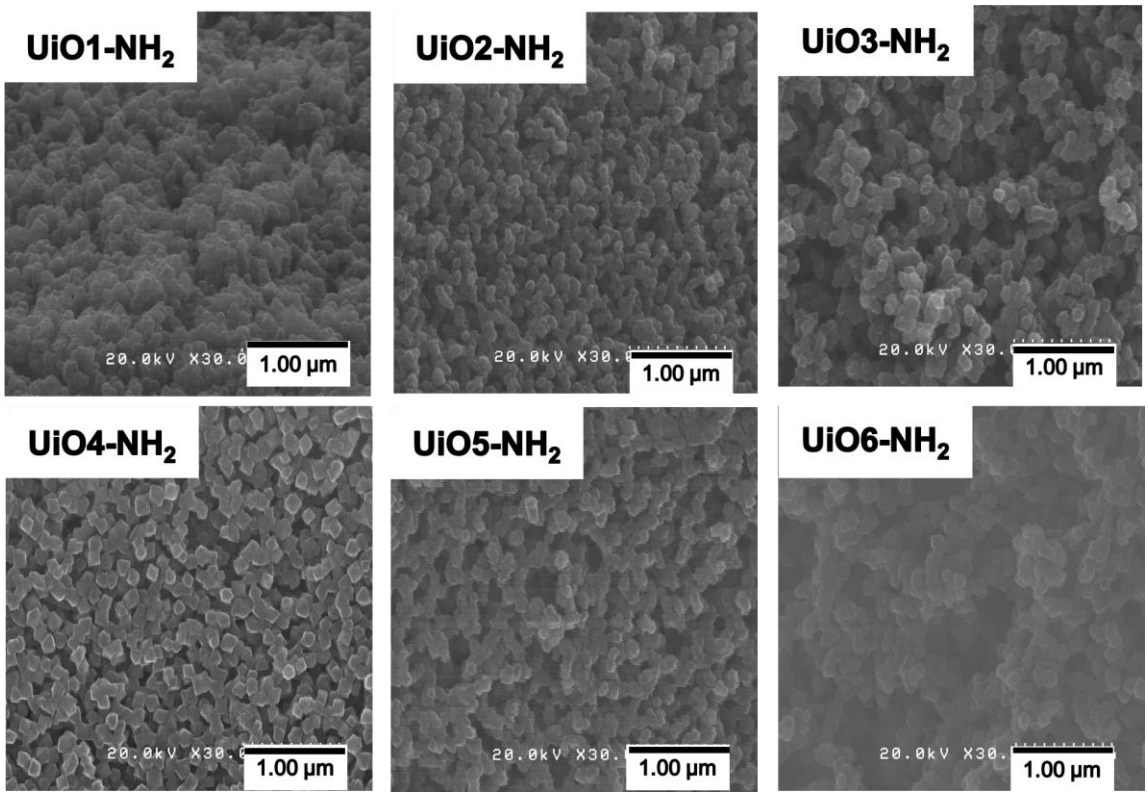

Figure 3-8**.** Top-view SEM images of the composite membranes: UiO1-NH_2 –UiO6-NH_2.

In order to confirm the effects of functional group modification on the crystallinity of the prepared MOF nanoparticles, the XRD crystallite size was compared with TEM particle size at different water amount for all the MOF samples (Figure 3-9). The particle size through TEM and crystallite size through XRD nanoparticles obtained for the pure UiO-66 nanoparticles (without any modification) are found to be same and therefore, the nanoparticles are believed to be monocrystalline. However, in the case of chemically modified systems, the nanoparticles seem to show polycrystalline behavior, which indicated that it might have been possible due to ligand effect where the nucleation rate becomes slower due to the bulkiness of modified ligands as compare unmodified ligands.

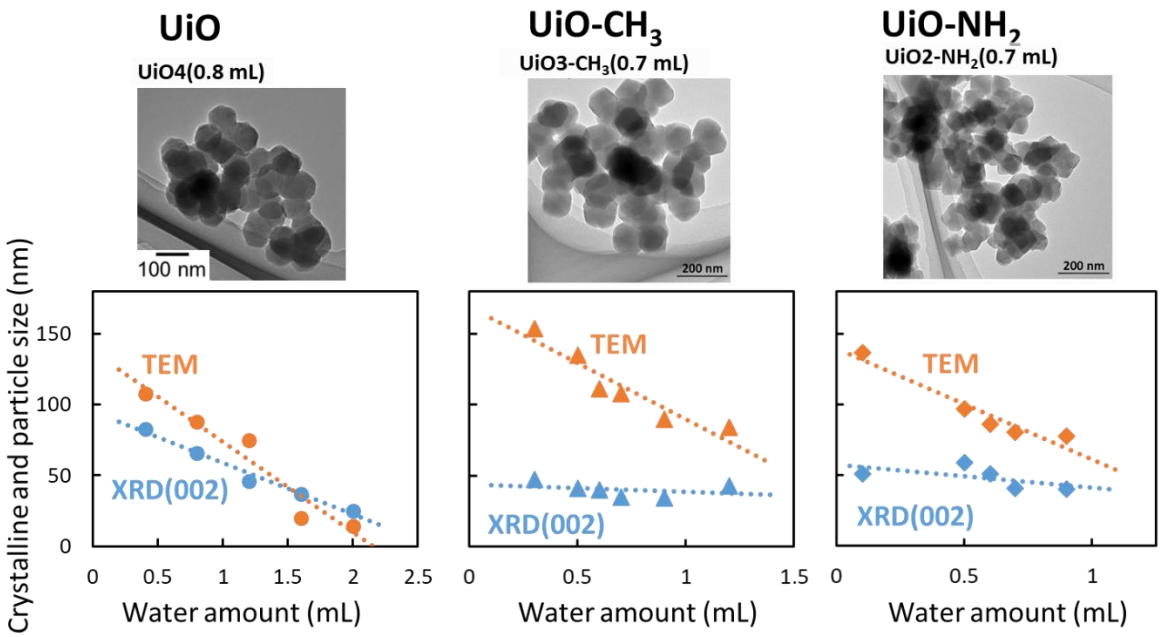

Figure 3-9. Effect of water amount on crystallite (calculated from XRD and particles size (TEM image analysis) of the synthesized nanoparticles.

3.4 Filtration performance

Filtration performance of composite membranes of some selected UiO-66-NH_2 evaluated based on the rejection of MB is as displayed in Figure 3-10. As reported earlier that the selectivity of UiO-66 deposited composite membranes originated from the molecular sieving ability of the intraparticle/selective channels of UiO-66. As shown in the Figure 3-10, it can be seen that a linear permeation curve along with the perfect MB rejection for the first 5 minutes of filtration was observed. In addition, the permeability changes with respect to the particle size where smaller particles resulted into higher permeability with respect to the particle size in systematically increasing pattern. Therefore comparing the results with those of non-

functionalized MOF, it shows that the filtration tendency are similar in all the cases regardless of the chemical nature of resultant MOF nanoparticles [16,17].

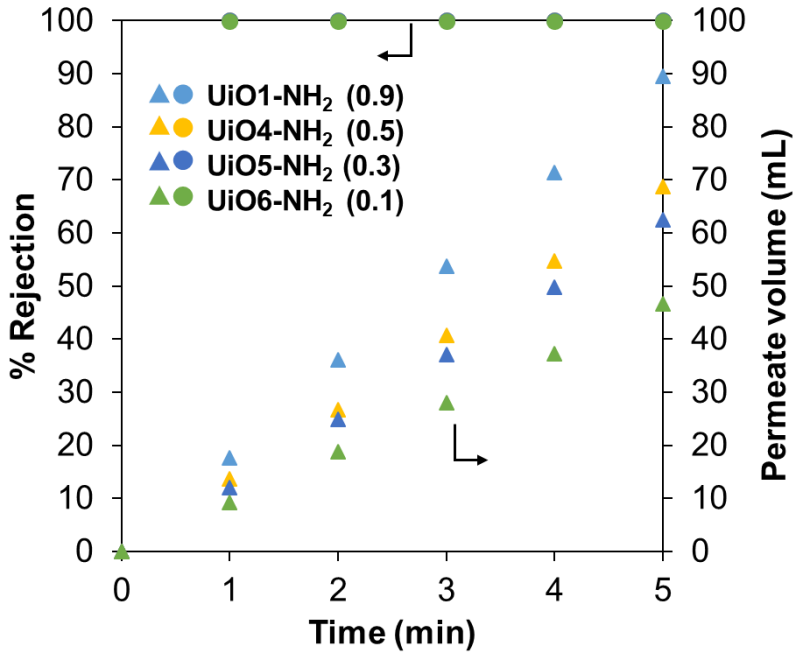

Figure 3-10**.** Filtration performance of some selected UiO-66-NH_2 composite membranes: MB rejection and permeate volume.

Particle size is a very important parameter that may affect the interactions between particles of the selective layer, membrane morphology, surface roughness, and separation performance and sholud be taken into account when designing a specific membrane [53]. Therefore, to further evaluate effect of particles size on flux of unmodified and modified MOFs, the dependence of the flux on the particle size estimated from TEM images was investigated and the plot is shown in Figure 3-11. It was observed that quantitatively, the flux dependence significantly differed and the modified UiO gave larger flux at a given size possibly because of defective structures, which created large aperture of nanochannel. However, qualitatively, the flux for all series of

nanoparticles was found to decrease with increase in particle size. Therefore, this indicated that the trend was similar to that for unfunctionalized UiO-66 nanoparticles.

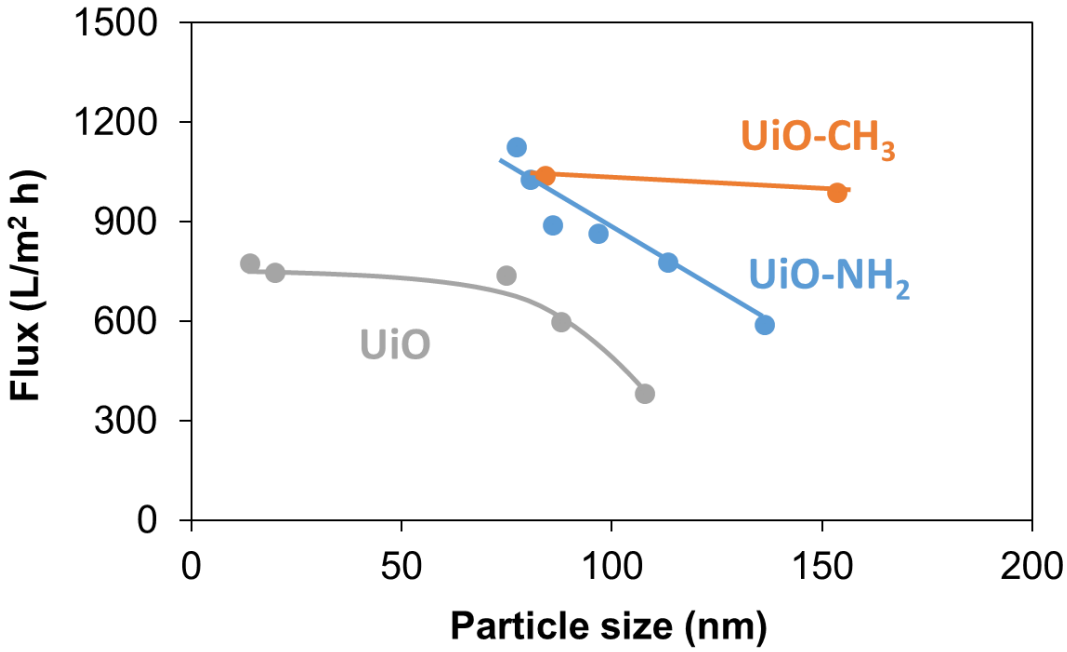

Figure 3-11. Filtration performance: Effect of different particle size on flux.

It is expected that nanoparticle size can enhance the filtration greatly. However, from the aforementioned, the particle size might have not represented the flux well; therefore, the plot was changed to crystallite size obtained through XRD analysis. As can be seen in Figure 3-12, the trend obtained was found to be better than for TEM particle size. In fact, the crystallite size was found to have affected the flux. The relationship demonstrated that MOF nanoparticles with the smaller and defective crystals (possibly possess larger aperture of the pore or channels in the crystallites) were found to be superior in terms of flux because of larger surface area. This was because the modification introduces a larger fraction of defects, which resulted in overall higher flux at given crystallite size or as MOF nanoparticles itself. This result suggests

that single crystal can be considered as a kind of building unit in the nanoparticles deposition membranes for water filtration, hence the importance of designing MOF nanoparticles.

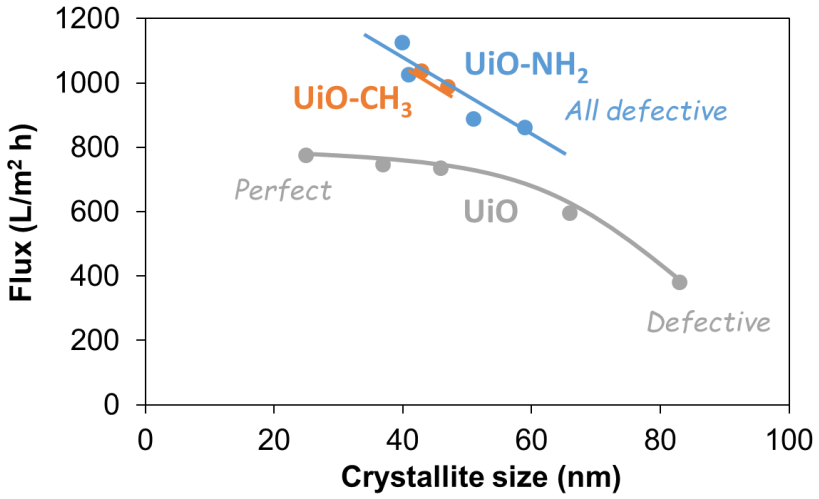

Figure 3-12. Effect performance: Effect of crystallite size versus flux.

In furtherance to achieve the set goals, the filtration performance of these newly synthesized MOF nanoparticles-based membranes were evaluated. As shown in Figure 3-13, it can be observed that there was linear permeation curve along with perfect MB rejection for the first 5 minutes of filtration. This remarkable improvement in terms of leakage/fouling could be due to modification through functionalization of UiO-66, which have the tendency of suppressing leakage/fouling. Furthermore, it can also be seen that permeability of the membranes changes with respect to the particle size, in which the smaller particles gave higher permeability in systematically increasing pattern. Nevertheless, comparing with the earlier results of the non-functionalized MOF membranes, the filtration tendency were found to be similar in trend regardless of the chemical nature of resultant MOF as earlier reported in case of UiO-66 with smallest diameter [16,17].

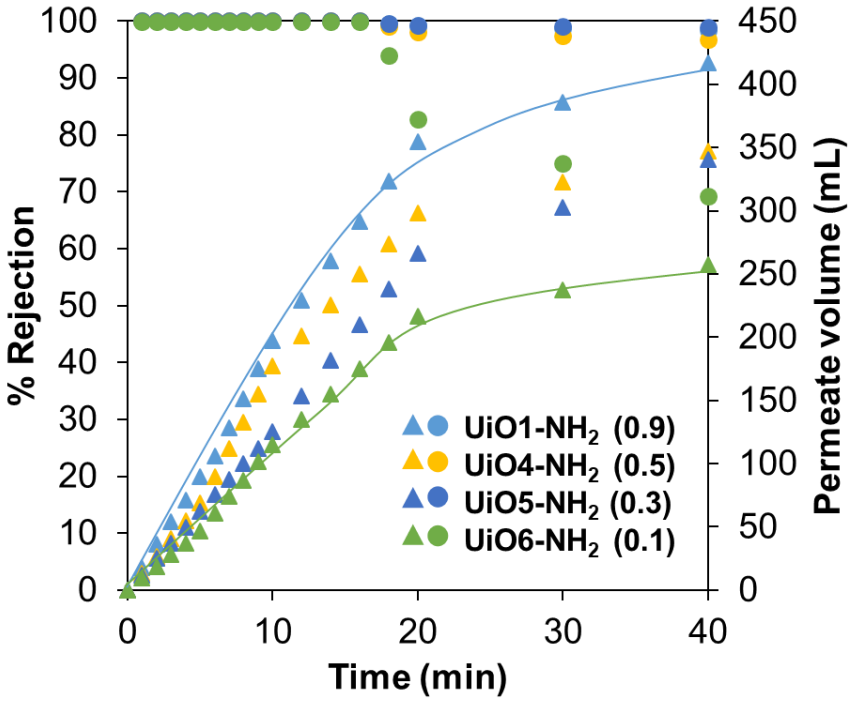

Figures 3-13. Filtration performance of some selected UiO-66-NH_2 composite membranes: Leakage and fouling.

In order to determine the tolerance ability for leakage of these modified nanoparticles, the cumulative volume of the filtrate over 99% rejection was kept and the tolerance for the MB leakage was estimated (Figure 3-14). As can be seen, the results indicated that irrespective of UiO type, tolerance to leakage was greater for smaller particles/crystallites, however modified UiO was found to be superior for leakage tolerance. It was believed that variation in particle morphology by ligand modification might have caused higher tolerance value through dense packing of selective layer in membrane as compared to the non-modified MOF based membranes. All of these results suggested that chemical environment and pore engineering have significant effect on filtration process.

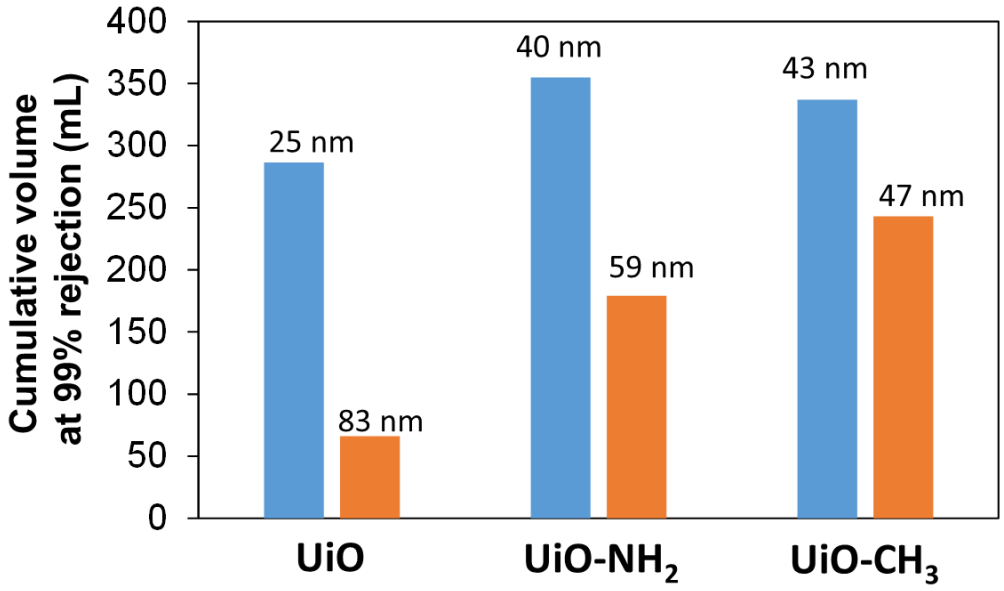

Figure 3-14. Cumulative rejection of composite membrane: Ligand effect on leakage tolerance.

It has been recognized that the transport of water and other solvents through nanochannel materials like MOFs is a complex process and often affected by many factors such as temperatures, pressures, and electric fields not only because of the structures, but also because of the diffusion properties. The water flow rate have been found to be dependent on the diameter of nanochannel materials.

Therefore, MOFs with proper pore apertures can be used to elevate the selectivity and permeability of composite membranes [32,54]. These composite membranes in an aqueous environment often have an attractive or repulsive response to water and other solvents. The material composition of the membrane and its corresponding surface chemistry would always determine its interaction with water. For instance, a hydrophilic membrane exhibits an affinity for water due to its high surface tension value as well it ability to form "hydrogen-bonds" with water molecules while hydrophobic membrane display opposite behaviour [55]. Furthermore,

though permeability of solvents such as methanol, ethanol, water, and acetone through composite membranes should depend on membrane, swelling as dominant factors in addition to solvent physical properties. However, superiority of the membranes in terms of the permeability and selectivity could also be attributed to the chemical environment around the nanopores. Therefore, in order to verify the role of chemical environments of these unmodified and modified nanoparticles, permeation test for methanol, water and acetone was carried.

The responses of these ligand-modified nanoparticles to different chemical environments was investigated using solvents of different viscosities viz: 0.56, 0.89, and 0.316 centipoise for methanol, water, and acetone respectively. The permeability of these solvents through unmodified and modified UiO (small particles sizes) is as displayed in Figure 3.15. Although particle size of UiO1-NH_2 and UiO1-CH_3 were much bigger than that of UiO1, their fluxes were found to be comparable or greater. For instance, flux for acetone was found to be higher because of its lowest viscosity. However, viscosity of methanol is lower, yet its flux was comparable to that of water. This was attributed to specific interaction as results of hydrogen bonding which enhances high water flux in spite its high viscosity [56-58]. Furthermore, water was found to display more sensitive response to membrane channel environment compared to other solvents. This could be as a result that NH_2 accelerates the permeation of water while CH_3 was found to have decelerated it. This fact is supported by the consideration that hydrogen bonding is important for water intrusion. The presence of CH_3 group specially enhances the methanol flux. The order solvent of permanence: acetone > methanol > water; acetone > water > methanol; acetone > water > methanol for UiO1-CH_3, UiO1-NH_2 and UiO1 composite membrane respectively. This implies that nanopores environment significantly contributed to permeate flux in differential behaviour. The hydrophilicity/hydrophobicity of UiO66-NH_2/UiO66-CH_3 nanoparticles definitely presented different chemical environment as function

of their functional groups, which would specifically account for high/low flux of water because of chemical environment around the nanopores [59-64].

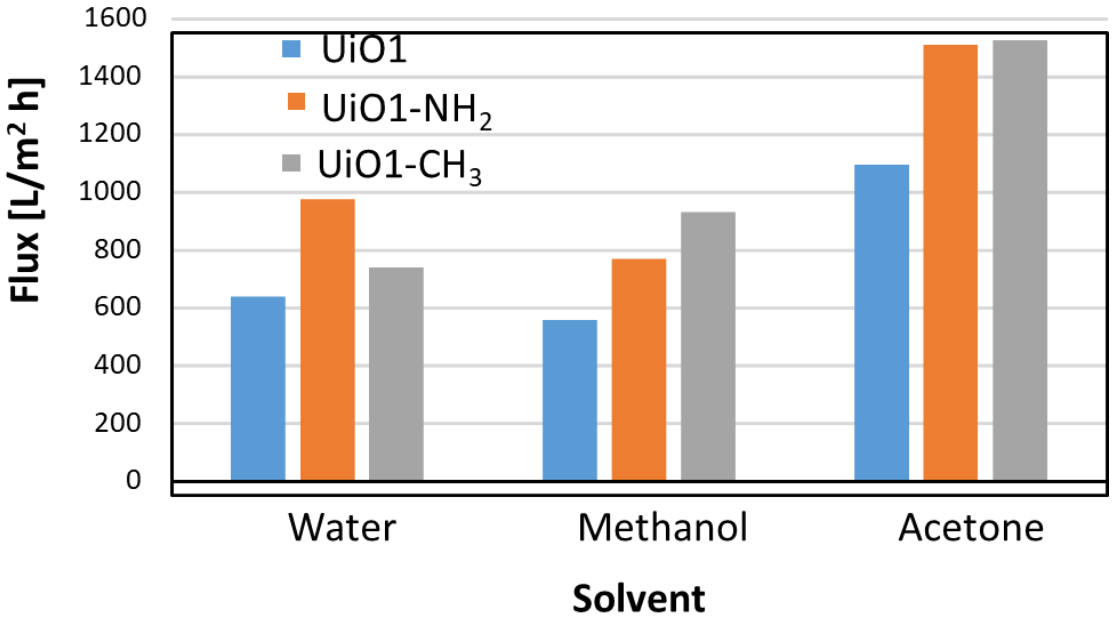

Figure 3-15. Filtration performance: Permeability test of three different composite membrane for solvents.

3.5 Conclusions

Series of ligand modified UiO-66 nanoparticles were synthesized by using water as a modulator. Ligand modification led to formation of polycrystalline and defective particles. The modified UiO-66 gave high flux compared to unmodified UiO-66 nanoparticles. Therefore, it seems polycrystalline nature plays an important role. The ligand modification affects the chemoselectivity in permeation. Pore engineering is a promising approach not only to improve the membrane performance but also to endow chemoselectivity. The synthesis of UiO-66 nanoparticles possessing different functional groups with water as a modulator shows that side functional groups enhances the defect formation as a result of increased bulkiness. These functional groups influence the chemical environment around the pore wall as well as play significant roles in the interaction with different solutes. Thus, the deposition of these nanoparticles not only create an enlarged effective membrane area to minimize voids pathway that circumvent leakage of solutes, but also account for high flux of water as well as the rejection as results of chemical environment around nanopores. Thus, these investigations unlock information for proper understanding and evaluation of the role of chemical environment in UiO-66-CH_3 and UiO-66-NH_2 nanocomposite membranes. In conclusion, the present chapter successfully demonstrates promising aspects of chemical environment around nanopores of engineered UiO-66-based composite membranes for nanofiltration. The composite membranes obtained from the engineered nanoparticles exhibit remarkable filtration performance in a unique manner depending on electrostatic effect/charge of the solute. Thus, pore engineering is a promising approach not only to improve the membrane performance but also to endow chemoselectivity.

3.6 References

[1] Eddaoudi, M.; Kim, J.; Rosi, N.; Vodak, D.; Wachter, J.; O'Keeffe, M.; Yaghi, O. M. Systematic Design of Pore size and Functionality in Isoreticular MOFs and their Application in Methane Storage. Sci. **2002**, 295, 469–472.

[2] Furukawa, H.; Cordova, K. E.; O'Keeffe, M.; Yaghi, O. M. The Chemistry and Applications of Metal-Organic Frameworks. Sci. **2013**, 341, 974.

[3] Zhang, R.; Ji, Wang, S. L.; Wang, N.; Zhang, G.; Li. J. R. Coordination-driven in Situ Self-Assembly Strategy for the Preparation of Metal-Organic Framework Hybrid Membranes. Angew. Chem. Int. Ed. **2014**, 24, 9775–9779.

[4] Guo, Y.; Peng, X. Mass Transport through Metal-Organic Framework Membranes. Reviews. Sci. China Mater. **2018**, 1–18.

[5] Cui, Y.; Liu, X.Y.; Chung, T. S. Ultrathin Polyamide Membranes Fabricated from Freestanding Interfacial Polymerization: Synthesis, Modifications, and Post-Treatment. Ind. Eng. Chem. Res. **2017**, 56, 513–523.

[6] Wang, C.; Liu, X.; Demir, N. K.; Chen, J. P.; Li, K. Applications of Water Stable Metal-Organic Frameworks. Chem. Soc. Rev, **2016**, 45, 5107–5134.

[7] Furukawa, H.; Ko, N.; Go, Y. B.; Aratani, N.; Choi, S. B.; Choi, E.; Yazaydin, A. O.; Snurr, R. Q.; O'Keeffe, M.; Kim, J.; Yaghi, O. M. Ultrahigh Porosity in Metal-Organic Frameworks. Science, **2010**, 424–428.

[8] Wu, F.; Lin, L.; Liu, H.; Wang, H.; Qiu, J.; Zhang, X. Synthesis of Stable UiO-66 Membranes for Pervaporation Separation of Methanol/Methyl Tert-Butyl Ether Mixtures by Secondary Growth. J. Membr. Sci. **2017**, 544, 342–350.

[9] Liu, X.; Demir, N. K.; Wu, Z.; Li, K. Highly Water-Stable Zirconium Metal-Organic Framework UiO-66 Membranes Supported on Alumina Hollow Fibers for Desalination, J. Am. Chem. Soc. **2015**, 137, 6999–7002.

[10] Danchen, M.; Han, G.; Bo Peh.; Chen, S. B. Water-Stable Metal–Organic Framework UiO-66 for Performance Enhancement of Forward Osmosis Membrane. Ind. Eng. Chem. Res. **2017**, 56, 12773–12782.

[11] Kandiah, M.; Nilsen, M. H.; Usseglio, S.; Jakobsen, S.; Olsbye, U.; Tilset, M.; Larabi, C.; Quadrelli, E. A.; Bonino, F.; Lillerud, K. P. Synthesis and Stability of Tagged UiO-66 ZrMOFs. Chem. Mater. **2010**, 22, 6632–6640.

[12] Cheng, X.; Xu, J.; Yanqui, Z.; Cher, H. L.; Zongli, X.; Derrick, N.; Stefan, J. D.; Metthew, R. H.; Lu, S. Building Additional Passageways in Polyamide Membranes with Hydrostable Metal-Organic Frameworks to Recycle and Remove Organic Solutes from Various Solvents. ACS Appl. Mater. Interfaces **2017**, 44, 38877–38886.

[13] Cavka, J. H.; Jakobsen, S.; Olsbye, U.; Guillou, N.; Lamberti, C.; Bordiga, S.; Lillerud, K. P. A New Zirconium Inorganic Building Brick Forming Metal Organic Frameworks with Exceptional Stability. J. Am. Chem. Soc. **2008**, 130, 13850–13851.

[14] Valenzano, L.; Civalleri, B.; Chavan, S.; Bordiga, S.; Nilsen, M. H.; Jakobsen, S.; Lillerud, K. P.; Lamberti, C. Disclosing the Complex Structure of UiO-66 Metal Organic Framework: A Synergic Combination of Experiment and Theory. Chem. Mater. **2011**, 23, 1700–1718.

[15] Tang, X.; Yan, Xiong. Dip-Coating for Fbrous Materials: Mechanism, Methods and Applications. J. Sol-Gel Sc. and Technol. **2017**, 81, 378–404.

[16] Trinh, D. X.; Tran, T. P. N.; Taniike, T. Fabrication of New Composite Membrane Filled with UiO-66 Nanoparticles and Its Application to Nanofiltration. Sep. Purif. Technol. **2017**, 177, 249–256.

[17] Goji. S. Y.; Trinh X. Dai.; Patchanee, C.; Taniike, T. Design of Semi-Continuous Selective Layer Based on UiO-66 Nanoparticles for Nanofiltration. Membr. **2018**, 8, 129.

[18] Wan, L.; Zhou, C.; Xu, K.; Feng, B.; Huang, A. Synthesis of Highly Stable UiO-66-NH_2 Membrane with High Ions Rejection for Seawater Desalination. Micro. and Meso. Mater. **2017,** 252, 207–213.

[19] Liu, J.; Canfield, N.; Liu, W. Preparation and Characterization of a Hydrophobic Metal−Organic Framework Membrane Supported on a Thin Porous Metal Sheet. Ind. Eng. Chem. Res. **2016**, 55, 3823−3832.

[20] Wu, H.; Chua, Y. S.; Krungleviciute.; V.; Tyagi, M.; Chen, P.; Yildirim, T.; Zhou, W. Unusual and Highly Tunable Missing-Linker Defects in Zirconium Metal−Organic Framework UiO-66 and Their Important Effects on Gas Adsorption. J. Am. Chem. Soc. **2013**, 135, 10525–10532.

[20] Kandiah, M.; Usseglio, S.; Svelle, S.; Olsbye, U.; Lillerud, K. P.; Tilset, M. Post-Synthetic Modification of the Metal-Organic Framework Compound UiO-66. J. Mater. Chem. **2010**, 20, 9848–98.

[21] Peterson, G.W.; Destefano, W.R.; Garibay, S. J.; Ploskonka, A.; McEntee, M.; Hall, M.; Karwacki, C. J.; Hupp, J. T; Farha, O. K. Optimizing Toxic Chemical Removal Through Defect-Induced UiO-66-NH_2 Metal-Organic Framework Chem. Eur. J. **2017**, 23, 15918–15916.

[22] Zhu, Y.; Gupta, K. M.; Liu, Q, *et al.* Synthesis and Seawater Desalination of Molecular Sieving Zeolitic Imidazolate Framework Membranes. Desal. **2016**, 385 75–82.

[23] Zhang, L.; Shi, G. Z.; Qiu, S.; Cheng, L. H, Chen, H. L. Preparation of High-Flux Thin Film Nanocomposite Reverse Osmosis Membranes by Incorporating Functionalized Multi-Walled Carbon Nanotubes. Desal. Water Treat. **2011**, 34, 19–24.

[24] Zornoza, B.; Martinez-Joaristi, A.; Serra-Crespo, P.; Tellez, C.; Coronas, J.; Gascon J.; Kapteijn, F. Functionalized Flexible MOFs as Fillers in Mixed Matrix Membranes for Highly Selective Separation of CO_2 from CH_4 at Elevated Pressures. Chem. Commun. **2011**, 47, 9522–9524.

[25] Liu, C. S.; Zhang, Z. H.; Chen, M.; Zhao, H.; Duan, F. H.; Chen, D. M.; Wang, M. H.; Zhang, S.; Du, M. Pore Modulation of Zirconium–Organic Frameworks for High-Efficiency Detection of Trace Proteins. Chem. Commun. **2017**, 53, 3941–3944.

[26] Sharma, R. R.; Chellam, S. Environ. Temperature Effects on the Morphology of Porous Thin Film Composite Nanofiltration Membranes. Sci. Technol. **2005**, 39, 5022–5030.

[27] Nghiem, L. D.; Schafer, A. I.; Elimelech, M. Removal of the Natural Hormones by Nanofiltration Membranes: Measurement, Modeling, and Mechanisms. Environ. Sci. Technol. **2004**, 38, 1888–1896.

[28] Lee, S.; Lueptow, R. M. Membrane Rejection of Nitrogen Compounds. Environ. Sci. Technol. **2001**, 35, 3008–3018.

[29] Deen, W. M. Hindered Transport of Large Molecules in Liquid Filled Pores. AIChE J. **1987**, 33, 1409–1424.

[30] Aimar, P.; Meireles, M.; Sanchez, V. A Contribution to the Translation of Retention Curves into Pore Size Distributions for Sieving Membranes. J. Membr. Sci. **1990**, 54, 321-338.

[31] Van der Bruggen, B.; Schaep, J.; Wilms, D.; Vandecasteele, C. Influence of Molecular size, Polarity and Charge on the Retention of Organic Molecules by Nanofiltration. J. Membr. Sci. 1**999**, 156, 29-41.

[32] Wang, X. L.; Tsuru, T.; Togoh, M.; Nakao, S. I.; Kimura, S. Evaluation of Pore Structure and Electrical Properties of Nanofiltration Membranes. J. Chem. Eng. Jpn. **1995**, 28, 186192.

[31] Le-Clech, P.; Chen, V.; Fane, A. G. Review: Fouling Mechanisms in Membrane Bioreactors Used in Wastewater Treatment. J. Membr. Sci. **2006**, 284, 17–53.

[32] Amy, G. Fundamental Understanding of Organic Matter Fouling of Membranes. Desal. **2008**, 231, 44–51.

[33] Peter-Varbanets, M.; Vital, M.; Hammes, F.; Pronk, W. Stabilization of Flux during Ultra-Low Pressure Ultrafiltration. Water Res. **2010**, 44, 3607–3616.

[34] Huang, Y.; Qin, W.; Li, Z.; Li, Y. Enhanced Stability and CO_2 Affinity of a UiO-66-type Metal–Organic Framework Decorated with Dimethyl Groups. Dalton Trans. **2012,** 41, 9283.

[35] Cliffe, M. J; Wan, W.; Zou, X.; Chater, P. A.; Kleppe, A. K.; Tucker, M. G.; Wilhelm, H.; Funnell, N. P.; Coudert, F.-X.; Goodwin, A. L. Correlated Defect Nanoregions in a Metal-Organic Frameworks. Nat. Commun. **2014**, 5, 4176–4178.

[36] Taddei, M. Review When Defects Turn into Virtues: The Curious Case of Zirconium-Based Metal-Organic Frameworks. Coord. Chem. Rev. **2017**, 343, 1–24.

[37] Nan, J.; Dong, J.; Wang, W.; Jin, W. Formation Mechanism of Metal–Organic Framework Membranes Derived from Reactive Seeding Approach. Micro and Meso. Mater. **2012**, 155, 90–98.

[38] Morris, W.; Wang, S.; Cho, D.; Auyeung, E.; Li, P.; Farha, O. K.; Mirkin, C. A. Role of Modulators in Controlling the Colloidal Stability and Polydispersity of the UiO-66 Metal−Organic Framework. ACS Appl. Mater. Interfaces **2017**, 9, 33413−33418.

[39] Wu, H.; Chua, Y. S.; Krungleviciute, V.; Tyagi, M.; Chen, P.; Yildirim, T.; Zhou, W. Unusual and Highly Tunable Missing-Linker Defects in Zirconium Metal-Organic Framework UiO-66 and Their Important Effects on Gas Adsorption. J. Am. Chem. Soc. **2013**, 135, 10525−10532.

[40] Cliffe, M. J.; Hill, J. A.; Murray, C. A.; Coudert, F. X.; Goodwin, A. L. Defect-Dependent Colossal Negative Thermal Expansion in UiO-66 (Hf) Metal-Organic Framework. Phys. Chem. Chem. Phys. **2015**, 17, 11586−11592.

[41] Ragon, F.; Horcajada, P.; Chevreau, H.; Hwang, Y. K.; Lee, U-H.; Miller, S. R.; Devic, T.; Chang, J. S.; Serre, C. In-Situ Energy-Dispersive X-ray Diffraction for the Synthesis Optimization and Scale-Up of the Porous Zirconium Terephthalate UiO-66. Inorg. Chem. **2014**, 53, 2491−2500.

[42] Diring, S.; Furukawa, S.; Takashima, Y.; Tsuruoka, T.; Kitagawa, S. Controlled Multiscale Synthesis of Porous Coordination Polymer in Nano/Micro Regimes. Chem. Mater. **2010**, 22, 4531−4538.

[43] Oien, S.; Wragg, D.; Reinsch, H.; Svelle, S.; Bordiga, S.; Lamberti, C.; Lillerud, K. P. Detailed Structure Analysis of Atomic Positions and Defects in Zirconium Metal-Organic Frameworks. Cryst. Growth Des. **2014**, 14, 5370−5372.

(44) Bai, Y.; Dou, Y.; Xie, L-H.; Rutledge, W.; Li, J-R.; Zhou, H-C. Zr-Based Metal–Organic Frameworks: Design, Synthesis, Structure, and Applications. Chem. Soc. Rev. **2016**, 45, 2327.

(45) Atzori, C.; Shearer, G. C.; Maschio, L.; Civalleri, B.; Bonino, F.; Lamberti, C.; Svelle, S.; Lillerud, K. P.; Bordiga, S. Effect of Benzoic Acid as a Modulator in the Structure of UiO-66: An Experimental and Computational Study. J. Phys. Chem. C **2017**, 121, 9312−9324.

(45) Gutov, O. V.; Hevia, M. G.; Escudero-Adan, E. C.; Shafir, A. Metal-Organic Framework (MOF) Defects under Control: Insights into the Missing Linker Sites and Their Implication in the Reactivity of Zirconium-Based Frameworks. Inorg. Chem. **2015**, 54, 8396−8400.

(46) Hansch, C.; Leo, A.; Taft, R. W. A Survey of Hammett Substituent Constants and Resonance and Field Parameters. Chem. Rev. **1991**, 91, 165-195.

(47) DeCoste, J. B.; Peterson, G. W.; Jasuja, H.; Grant Glover, T.; You-gui H.; Walton, K. S. Stability and Degradation Mechanisms of Metal–Organic Frameworks Containing the $Zr_6O_4(OH)_4$ Secondary Building Unit. J. Mater. Chem. A. **2013**, 1, 5642–5650.

(48) Kandiah, M.; Nilsen, M. H.; Usseglio, S.; Jakobsen, S.; Olsbye, U.; Tilset, M.; Larabi, C.; Quadrelli, E. A.; Bonino, F.; Lillerud, K. P. Synthesis and Stability of Tagged UiO-66 Zr-MOFs. Chem. Mater. **2010**, 22, 6632−6640.

(49) Liang, W.; Coghlan, C. J.; Ragon, F.; Rubio-Martinez, M.; D'Alessandro, D. M.; Babarao, R. Defect Engineering of UiO-66 for CO_2 and H_2O Uptake-a Combined Experimental and Simulation Study. Dalton Trans. **2016**, 45, 4496−4500.

(50) Fang, Z.; Bueken, B.; De Vos, D. E.; Fischer, R. A. Defect Engineered Metal-Organic Frameworks. Angew. Chem., Int. Ed. **2015**, 54, 7234−7254.

(51) Wu, D.; Yan, W.; Xu, H.; Zhang, E.; Li, Q. Defect Engineering of Mn-Based MOFs with Rod-Shaped Building Units by Organic Linker Fragmentation. Inorg. Chimica. Acta. **2017**, 460, 93−98.

(52) Kozachuk, O.; Luz, I.; Llabrés i Xamena, F. X.; Noei, H.; Kauer, M.; Albada, H. B.; Bloch, E. D.; Marler, B.; Wang, Y.; Muhler, M.; et al. Multifunctional, Defect-Engineered Metal-Organic Frameworks with Ruthenium Centers: Sorption and Catalytic Properties. Angew. Chem. Int. Ed. **2014**, 53, 7058−7062.

(53) Shearer, G. C.; Chavan, S.; Bordiga, S.; Svelle, S.; Olsbye, U.; Lillerud, K. P. Defect Engineering: Tuning the Porosity and Composition of the Metal-Organic Framework UiO-66 via Modulated Synthesis. Chem. Mater. **2016**, 28, 3749−3761.

[54] Liang, W.; Li, L.; Hou, J.; Shepherd, N. D.; Bennett, T. D.; D'Alessandro, D. M.; Chen, V. Linking Defects, Hierarchical Porosity Generation and Desalination Performance in Metal–Organic Frameworks. Chem. Sci. **2018**, 9, 3508–3516.

[55] Mallik, B. S.; Chandra, A. Hydrogen Bond and Residence Dynamics of Ion-Water and Water-Water Pairs in Supercritical Aqueous Ionic Solutions: Dependence on Ion Size and Density. J. Chem. Phys. **2006**, 125, 234502.

[56] Su, J.; Guo, H. Effect of Nanochannel Dimension on the Transport of Water Molecules. J. Phys. Chem. B **2012**, 116, 5925−5932.

[57] Navarro, M.; Benito, J.; Paseta, L.; Gascón, I.; Coronas, J.;Téllez, C. Thin-Film Nanocomposite Membrane with the Minimum Amount of MOF by the Langmuir−Schaefer Technique for Nanofiltration. ACS Appl. Mater. Interfaces **2018**, 10, 1278−1287.

[58] Sorribas, S.; Gorgojo, P.; Téllez.; Coronas, J.; Livingston, A. G. High Flux Thin Film Nanocomposite Membranes Based on Metal− Organic Frameworks for Organic Solvent Nanofiltration. J. Am. Chem. Soc. **2013**, 135, 15201−15208.

[59] Lau, W. J.; Gray, S.; Matsuura, T.; Emadzadeh, D.; Chen, J. P.; Ismail, A. F. A Review on Polyamide Thin Film Nanocomposite (TFN) Membranes: History, Applications, Challenges and Approaches. Water Res. **2015**, 80, 306−324.

[60] Bétard, A.; Fischer, R. A. Metal−Organic Framework Thin Films: From Fundamentals to Applications. Chem. Rev. **2012**, 112, 1055−1083.

[61] Su, J.; Guo, H. Effect of Nanochannel Dimension on the Transport of Water Molecules. J. Phys. Chem. B. **2012**, 116, 5925−5932.

[62] Su, J.; Guo, H. Control of Unidirectional Transport of Single-File Water Molecules through Carbon Nanotubes in an Electric Field. ACS Nano. **2011**, 1, 351–359

[63] Shen, M.; Keten, S.; Lueptow, R. M. Rejection Mechanisms for Contaminants in Polymeric Reverse Osmosis Membranes J. Membr. Sci. **2016**, 509, 36–47.

[64] He, Y.; Tang, Y. P.; Ma, D.; Chun, T. S. UiO-66 Incorporated Thin-Film Nanocomposite Membranes for Efficient Selenium and Arsenic Removal. J. Membr. Sci. **2017**, 541 262–270.

Chapter 4

General Conclusions

4.1 General Summary

This dissertation discusses the synthesis and application of nano-sized Metal-Organic Frameworks for nanofiltration membranes. The results obtained are as summarized below.

In order to lead to the objective of this dissertation, Chapter 1 introduced the following general background information: Metal-Organic Frameworks and synthesis methods, synthesis of nano-sized MOFs, modulators, mechanistic aspect of modulated synthesis, defect engineering, examples of modulated synthesis, applications of MOFs, water purification technologies, membrane filtration processes, problems of utilizing polymeric membrane in water purification, classes of materials for membranes design.

In Chapter 2, series of composite membranes were prepared by depositing UiO-66 nanoparticles onto a regenerated cellulose support, and impacts of the size distribution, loading, as well as combination of these nanoparticles for formation of bimodal membranes were examined. The performance for nanofiltration and resultant selective layer was found to be equipped with best level of the permeability, selectivity and fouling resistance. The designed composite membranes therefore successfully demonstrated promising aspects of the new type of MOF-based composite membranes for nanofiltration, which was realized, based on facile production and easy of optimization through the size distribution of MOF nanoparticles, that can be ex-situ prepared.

Chapter 3 presents an investigation of pore engineering of UiO-66 nanoparticles and applications for nanoparticles with the purpose of exploring the importance of nanoparticles′ chemical environment. This purpose was achieved through series of ligand modified UiO-66 nanoparticles synthesized by using water as modulator. The modification led to the formation of polycrystalline, defective particles and the composite membranes obtained from these nanoparticles gave high flux compared to unmodified UiO-66 nanoparticles as well played an

important role chemoselectivity. This investigations unlocked information for proper understanding and evaluation of the role of chemical environment in UiO-66-CH_3 and UiO-66-NH_2 nanocomposite membranes. Thus, this successfully demonstrated promising aspects of chemical environment around nanopores of engineered UiO-66-based composite membranes for nanofiltration. Thus, pore engineering is a promising approach not only to improve the membrane performance but also to endow chemoselectivity.

4.2 General conclusions

Semi-continuous selective layer based on deposition of UiO-66 nanoparticles for nanofiltration was successfully designed which shows excellent performance. This was obtained because of facile production and easy optimization through the size distribution of MOF nanoparticles that can be ex-situ prepared. Thus, this successfully demonstrated promising aspects of a new type of MOF−based composite membranes for nanofiltration.

Pore engineering was found to be effective to improve the membrane performance as well as to design chemoselectivity. For example, the modified UiO gave higher flux and leakage-tolerance compared to unmodified ones.

Novel composite membrane by the deposition of nanoparticles of engineered porous materials is a promising approach not only to tailor the membrane performance, especially breaking through the bottleneck of the currently used polymeric membranes, but also to study the structure-performance relationship for basic understanding, “how nanochannels contribute to the performance.

Achievements

Publication

S. **Y**. **Goji**., Trinh X. Dai., Patchanee Chammingkwan., and Toshiaki Taniike. Design of semi-continuous selective layer based on deposition of UiO-66 nanoparticles for nanofiltration. *Membranes,* 2018, 8,129.

(ii) **S**. **Y**. **Goji**., Trinh X. Dai., Patchanee Chammingkwan., and Toshiaki Taniike Pore Engineering of UiO-66 Nanoparticles and Applications to Nanofiltration (*In preparation*).

Conferences

(i) S.**Y**. **Goji**., Trinh X. Dai., Patchanee Chammingkwan., Toshiaki Taniike. Design of semi-continuous selective Layer Based on Deposition of UiO-66 Nanoparticles for Nanofiltration. Poster presentation at The 12th SPSJ International Polymer Conference (IPC 2018), Dec 4–7, 2018, Hiroshima, Japan.

(ii) S. **Y**. **Goji**., Trinh X. Dai., Patchanee Chammingkwan., and Toshiaki Taniike. Design of semi-continuous selective layer based on UiO-66 nanoparticles deposition composite membrane. Poster presentation at JAIST World Conference, Feb 26–28, 2018, Japan.